# Female meiosis II and pronuclear fusion require the microtubule transport factor Bicaudal-D

**Paula Vazquez-Pianzola[1*], Dirk Beuchle[1], Gabriella Saro[1], Greco Hernández[2], Giovanna Maldonado[2], Dominique Brunßen[1], Peter Meister[1] and Beat Suter[1*].**

[1]Institute of Cell Biology, University of Bern, 3012 Berne, Switzerland.

[2]Laboratory of Translation and Cancer, Unit of Biomedical Research on Cancer, Instituto Nacional de Cancerología (INCan), Mexico City, Mexico.

[*]Authors for correspondence: (beat.suter@unibe.ch, paula.vazquez@unibe.ch)

keywords: *Drosophila* meiosis, mitosis, spindle assembly, clathrin, Bicaudal-D, BicD, TACC, CH-TOG, microtubule transport, deGradFP.

## ABSTRACT

Bicaudal-D (BicD) is a dynein adaptor that transports different cargoes along microtubules. Reducing the activity of BicD specifically in freshly laid *Drosophila* eggs by acute protein degradation revealed that BicD is needed to produce normal female meiosis II products, to prevent female meiotic products from re-entering the cell cycle, and for pronuclear fusion. As BicD is required to localize the spindle assembly checkpoint (SAC) components Mad2 and BubR1 to the female meiotic products, it appears that BicD functions to localize them to control metaphase arrest of polar bodies. BicD interacts with Clathrin heavy chain (Chc), and both proteins localize to centrosomes, mitotic spindles, and the tandem spindles during female meiosis II. Furthermore, BicD is required to correctly localize clathrin and the microtubule-stabilizing factors, D-TACC and Msps, to the meiosis II spindles, suggesting that failure to localize these proteins may perturb SAC function. Furthermore, right after the establishment of the female pronucleus, *D-TACC* and *C.*

*elegans BicD*, *tacc*, and *Chc* are also needed for pronuclear fusion, pointing to the possibility that the underlying mechanism might be more widely used.

## INTRODUCTION

Encoded by a single gene, the *Drosophila* BicD protein is part of a family of evolutionarily conserved dynein adaptors responsible for the transport of different cargoes along microtubules (Vazquez-Pianzola et al., 2016; Hoogenraad and Akhmanova, 2016; Vazquez-Pianzola and Suter, 2012). The founding member of this protein family, *Drosophila* BicD, was identified because of its essential role during oogenesis and embryo development where it transports mRNAs which control polarity and cell fate (Bullock and Ish-Horowicz, 2001; Suter and Steward, 1991; Suter et al., 1989; Wharton and Struhl, 1989). This process is mediated by its binding to the RNA-binding protein Egalitarian (Egl) (Dienstbier et al., 2009; Mach and Lehmann, 1997). Since then, BicD and its orthologs have been shown to control a diverse group of microtubule transport processes through binding to different cargoes or adaptor proteins (Hoogenraad and Akhmanova, 2016; Vazquez-Pianzola and Suter, 2012).

BicD can alternatively bind to Chc and this interaction facilitates Chc transport of recycling vesicles at the neuromuscular junctions and regulates endocytosis and the assembly of the pole plasm during oogenesis (Li et al., 2010; Vazquez-Pianzola et al., 2014). The best-known function of Chc is in receptor-mediated endocytosis as part of clathrin, a trimeric scaffold protein (called triskelion), composed of three Chc and three Clathrin light chains (Clc) (Brodsky, 2012). Aside from this, clathrin was shown to localize to mitotic spindles in mammalian and *Xenopus* cells (Fu et al., 2010; Royle et al., 2005) and to possess a non-canonical activity by stabilizing the spindle microtubules during mitosis (Royle, 2012). This function depends on clathrin trimerization and its interaction with Aurora A-phosphorylated Transforming Acidic Coiled-Coil protein 3 (TACC3) and the protein product of the colonic hepatic Tumor Overexpressed Gene (ch-TOG) (Booth et al., 2011; Fu et al., 2010; Lin et al., 2010; Royle and Lagnado, 2006; Royle et al., 2005). This heterotrimer forms inter microtubule bridges between Kinetochore-fibers (K-fibers), stabilizing these fibers and

promoting chromosome congression (Booth et al., 2011; Royle et al., 2005). More recently, TACC3 and a mammalian homolog of Chc (CHC17) were shown to control the formation of a new liquid-like spindle domain (LISD) that promotes the assembly of acentrosomal mammalian oocyte spindles (So et al., 2019).

In order to transport its cargos along MTs, BicD interacts with the dynein/dynactin motor complex, a minus-end-directed microtubule motor. This complex is involved in different cellular processes including intracellular trafficking of proteins and RNAs, organelle positioning and microtubule organization, some of them requiring BicD, too. The dynein/dynactin complex plays also essential roles during cell division where it is required for centrosome separation, chromosome movements, spindle organization and positioning, and mitotic checkpoint silencing (Raaijmakers and Medema, 2014).

As *Drosophila* BicD forms complexes with Chc and Dynein, both of which, as described before, perform essential activities during mitosis, we set out to investigate possible *BicD* functions during cell division. Reducing BicD protein levels by specific protein-targeted degradation in freshly laid eggs revealed that BicD is essential for pronuclear fusion. In addition, it is required for metaphase arrest of the female meiotic products after meiosis II completion. This activity seems mediated by BicD's role in localizing the spindle assembly checkpoint (SAC) components. Furthermore, BicD interacts with its cargo protein, Chc, and they both localize to the mitotic spindles and centrosomes and the female tandem meiotic II spindles. In addition, BicD localizes D-TACC, clathrin, and Msps (ch-TOG homolog) to the meiosis II spindles. The failure to properly localize these proteins might also contribute to the SAC function defects observed in embryos with reduced BicD levels. D-TACC and *C. elegans bicd-1*, *tac-1*, and *chc-1* are also needed after fertilization for pronuclear fusion, revealing an evolutionary conserved and essential role of these proteins for early zygote formation and suggesting that their mechanism of action on MTs might be widely used.

## RESULTS

### BicD and its cargo clathrin localize to centrosomes and spindles during mitosis and tandem spindles in meiosis II

Completion of female meiosis and the first mitotic cycles depend on correct spindle formation in the egg and the developing embryo. Inactivation of maternally expressed genes which provide all the proteins that control these first divisions leads either to maternal effect lethality or female sterility. Indeed, *BicD* loss-of-function mutants are female sterile because they do not produce oocytes (Ran et al., 1994) which is an obstacle to studying the role of *BicD* in the maternally controlled early embryonic mitotic divisions. Our laboratory has developed the *BicD*$^{mom}$ females, a method to overcome *BicD* mutant female sterility (Swan and Suter, 1996). *BicD*$^{mom}$ females provide *BicD* from an inducible promoter that can be turned off once oocyte fate is established. Around 3-4 days after shutting down *BicD*, *BicD*$^{mom}$ ovaries contain egg chambers devoid of BicD, and few of them develop into eggs (Swan and Suter, 1996; Vazquez-Pianzola et al., 2014). Using this strategy, we observed that the eggs laid by *BicD*$^{mom}$ females did not develop but were arrested during stage 1 with phenotypes that required a more detailed analysis (see below) (Fig. S1A and SM1-4). These results suggest that *BicD* is also essential downstream of oocyte differentiation to complete meiosis and progress through the early mitotic divisions.

We analyzed BicD localization during mitosis in methanol-fixed embryos. Methanol fixation dissolves the cytosolic pool of BicD, making insoluble pools of the protein more apparent. Surprisingly, during the syncytial divisions, BicD was detected on the centrosomes where it colocalized with the pericentrosomal marker centrosomin (Cnn) and along the mitotic spindles (Fig. 1A,a,b, Fig. S1B). During cellularization, BicD was additionally enriched at the plasma membrane (Fig. 1Ac). We additionally analyzed embryos expressing BicD::GFP. Both staining patterns were highly similar (Fig. S1C), confirming the specificity of the BicD antibody.

The first spindles observed in freshly laid eggs are the female meiotic II tandem spindles. However, assessing BicD localization in these eggs was challenging because of the high levels of BicD in the cytoplasm. A specific BicD signal was observed using anti-BicD antibodies, but its level was the same in the meiotic spindle region as in the cytoplasm (Fig. S1D). Using an anti-GFP antibody in *BicD::GFP, BicD*$^{null}$ eggs detected BicD presence at the meiotic spindle more clearly. BicD::GFP was enriched above cytoplasmic levels on the meiotic tandem spindles and the central aster (Fig. 1B,B', Fig. S1E).

We conclude that BicD associates with the mitotic spindles and the centrosomal region during mitosis and with the tandem spindles and the central aster during female meiosis II. Furthermore, mammalian BicD1 and BicD2 are present at the centrosomes in mammalian cells (Fumoto et al., 2006). Therefore, our data suggest that *BicD* might play a yet unidentified but evolutionarily conserved role at the mitotic/meiotic spindles.

**deGradFP knockdown of BicD::GFP reveals a novel, essential role for BicD during early embryogenesis**

The number of eggs laid by *BicD*$^{mom}$ flies was too small for phenotypic analyses. Thus, we designed a strategy to knock down the BicD protein directly in young embryos (stage 1) using the deGradFP technique (degrade Green Fluorescent Protein), a method to target GFP-fusion proteins for destruction or inactivation (Caussinus et al., 2011). We took advantage of the functional, genomic *BicD::GFP* construct (Paré and Suter, 2000). Additionally, we constructed a deGradFP system specifically active during embryogenesis but not oogenesis. We expressed the deGradFP (NSlmb-vhhGFP4) from a *hunchback* (*hb*) minimal maternal promoter coupled with the *bcd* 3'-UTR (Fig. 2A). The *hb* promoter is active during late oogenesis such that the *deGradFP* mRNA will be loaded into eggs and embryos (Fig. 2A'). The *bcd* 3' UTR promotes mRNA localization to the anterior pole of the oocyte and egg. It also allows translation only upon egg activation in freshly laid eggs, which occurs when Metaphase I (MI) Stage 14 (S14) eggs chambers pass through the oviduct (Berleth et al., 1988; Driever and Nüsslein-Volhard, 1988; Sallés et al., 1994). We refer to this construct

as *hb-deGradFP*. We corroborated the enrichment of the *deGradFP* mRNA in the anterior region of the embryo from egg-laying until before cellularization (Fig. 2B). Immunostaining experiments to detect *hb-deGradFP* expression revealed that the Vhh-GFP was distributed throughout the embryo and did not form an A-P gradient (Fig. 2C). Thus, the deGradFP seems to be stable and can move/diffuse to the rest of the embryo. Therefore, our new *hb-deGradFP* tool should be useful to degrade GFP fusion proteins in entire young embryos.

*BicD::GFP* rescues the sterility phenotype and the embryonic developmental arrest of *BicD* loss-of-function mutants (*BicD::GFP, BicD*$^{null}$ homozygous females) (Paré and Suter, 2000) (Fig. 2D-E). However, when these females expressed two copies of the *hb-deGradFP* construct (*BicD::GFP, BicD*$^{null}$; *hb-deGradFP* homozygous females), 75% of their progeny failed to develop into late embryonic stages and did not hatch into larvae. Instead, eggs and embryos mostly arrest in meiosis or the first mitotic divisions as observed in embryos laid by *BicD*$^{mom}$ females (Fig. 2D,E,H, SM5-7). In the following, we will refer to this progeny and their mothers as *BicD*$^{hb\text{-}deGradFP}$. Most embryos laid by females that expressed two copies of the *hb-deGradFP,* but also a wild-type *BicD*$^{+}$ (*BicD::GFP, BicD*$^{null}$/+(CyO); *hb-deGradFP*), develop normally, indicating that high levels of *hb-deGradFP* expression are not deleterious for development on their own (Fig. 2D-E). *BicD*$^{hb\text{-}deGradFP}$ females have phenotypically wild-type ovaries that express normal BicD::GFP protein levels (Fig. 2F-G), confirming that the *hb-deGradFP* construct is not active during oogenesis. In contrast, in young *BicD*$^{hb\text{-}deGradFP}$ embryos, the BicD::GFP signal was reduced in the entire embryo (Fig. 2H), and BicD::GFP protein levels were downregulated by 50% (Fig. 2I). BicD::GFP is expressed at levels comparable to the wild-type BicD protein (Fig. S2A). However, a 50% reduction in the levels of BicD::GFP protein detected by WB produces already visible phenotypes. In comparison, eggs from heterozygous females (*BicD*$^{null}$/+) that also have a 50% reduction of BicD compared to wild-type embryos (Fig S2A) develop normally (97.3 ±1.03 % embryos hatched into larvae). Although alternative explanations for these differences are possible, we think that the deGradFP might bind BicD::GFP, functionally inactivating the protein before sending it to degradation.

As intended, the deGradFP protein was highly expressed in young embryos, although low protein levels were detected in ovaries (Fig. 2G,I; Fig. S3A). Although we cannot rule out that some S14 oocytes are physically activated during dissection, it is also possible that the *bcd* 3'-UTR sequence is not sufficient to fully control translation in the context of the minimal maternal *hb* promoter and its 5'-UTR. Even though, BicD is also present at the MI spindles in S14 oocytes (Fig. S3B), *BicD*$^{hb\text{-}deGradFP}$ S14 oocytes displayed no evident problems in spindle formation or chromosome alignment in meiotic metaphase I (Fig. S3C-D). This suggests that the early embryonic arrest observed in *BicD*$^{hb\text{-}deGradFP}$ individuals is not due to earlier meiotic defects during late oogenesis.

**_BicD_ is required for the cell cycle arrest of the male and the female meiotic products and for pronuclear fusion**

To learn more about the novel BicD function in the earliest phase of embryonic development and to pinpoint the developmental stage, we collected fully viable control embryos and *BicD*$^{hb\text{-}deGradFP}$ embryos over a 30 min period, let them develop for another 30 min (30-60 min old collections) and analyzed them for developmental defects (Fig. 3A). Twenty-five minutes after eggs laying, control embryos finished the 2$^{nd}$ mitotic division and contained at least four zygotic nuclei. At this early stage, normal zygotic nuclei reside in the interior of the embryo, and the three remaining female meiotic polar body products (mostly fused into one or two rosette-shaped nuclei) reside at the embryonic surface. Indeed, most embryos laid by control mothers (*BicD::GFP*, *BicD*$^{null}$ or *BicD::GFP*, *BicD*$^{null}$ / + (CyO); *hb-deGradFP)* developed normally, displaying more than four zygotic nuclei with wild-type looking mitotic spindles (Fig. 3A-B). However, embryos laid by *BicD*$^{hb\text{-}deGradFP}$ mothers were arrested mostly at earlier stages, displaying abnormal spindle-like structures (Fig. 3A, C). Even though they contained mainly centrally located dividing nuclei, around 25% of these embryos were classified as "arrested with centrosomes" because they were positive for Cnn staining (Fig. 3A, example in Fig 3Ca). In this category, we found embryos that contained at least one spindle displaying clear and sometimes fragmented staining for the centrosomal

marker centrosomin (Cnn) at the spindle poles. Additionally, they frequently displayed "free centrosomes" marked by Cnn signals associated with α-tubulin but without a complete spindle and DNA (Fig. 3Ca1). Embryos showing acentrosomal spindles but containing free centrosomes were also scored into this category. Another 35% of the *BicD*$^{hb\text{-}deGradFP}$ embryos possessed one or more internal acentrosomal spindles that were negative for Cnn staining. These were classified as "arrested, acentrosomal" (Fig. 3A, Cb).

Consistent with the fact that centrosomes are inherited from the father, embryos arrested and classified as "arrested with centrosomes" were mostly marked by the presence of the sperm tail (Fig. S4A-B). In contrast, embryos displaying "acentrosomal"-like spindles and no free centrosomes rarely showed any of these sperm tail markers, indicating that they more likely represent unfertilized eggs with aberrant meiotic products (Fig. S4A-B). We then analyzed the phenotype of arrested fertilized *BicD*$^{hb\text{-}deGradFP}$ eggs in more detail by detecting the presence of the X and Y chromosomes. Male embryos (marked by the presence of the Y) develop only from fertilized eggs. Male embryos from control mothers showed one dot-like signal for the X chromosome and one signal for the Y in each zygotic nucleus, and these nuclei were in the interior of the embryo (Fig. 3D2). The three polar bodies, formed after the two meiotic divisions, normally fused into a single polar body marked by the presence of the 3 X chromosomes (Fig. 3D1). In contrast, all arrested male embryos laid by *BicD*$^{hb\text{-}deGradFP}$ females had at least one internal spindle marked only by the presence of the Y chromosome and no X chromosome signal (Fig. 3E-G). This pattern indicates that pronuclear fusion failed to occur and that a spindle still formed from the paternal pronucleus (Fig. 3E-G). In most of these embryos, the male pronucleus underwent only one additional round of replication since two dots of the Y chromosome signal can be observed in the internal metaphase spindle (70%, Fig. 3E3). Embryos with more than one paternal spindle and many Y chromosome signals were also observed at a lower frequency (30%, Fig 3F2-3,G4-6). Independent of the rounds of replication observed in the parental pronucleus, arrested *BicD*$^{hb\text{-}deGradFP}$ embryos also contained one or several acentrosomal nuclei marked frequently by

several dots of X chromosomal signal (example in Fig. 3E1-2, 3F1, 3G1-4). This suggests that in these *BicD*$^{hb\text{-}deGradFP}$ embryos the female meiotic products did not arrest in metaphase II as they normally do but underwent several cycles of DNA replication instead . These results show that *BicD* is required for the cell cycle arrest of the female and male pronuclei and for pronuclear fusion. Similar phenotypes were observed in eggs laid by females, where *BicD* copies were further reduced by expressing a single copy of the *BicD::GFP* rescue construct (Fig. S5), suggesting that the replication of the meiotic products can take place in the absence of most functional *BicD*. However, these females were unhealthy and died shortly after eclosing or during the first week. During this time, they did not lay sufficient eggs for a complete phenotype analysis. Since the deGradFP only knocks down part of the BicD::GFP pool, the phenotypes we observed in *BicD*$^{hb\text{-}deGradFP}$ embryos and analyzed in detail in this work are likely to resemble a hypomorphic rather than a null condition for *BicD*.

**BicD is needed for replication arrest of the polar bodies and their rosette formation**

To test for a direct role of *BicD* in the female meiosis II, we crossed control and *BicD*$^{hb\text{-}deGradFP}$ females to sterile XO males, causing them to lay unfertilized eggs (Fig. 4). In unfertilized wild-type eggs, egg activation is triggered by passage through the oviduct, and this causes the eggs to complete meiosis II. We observed 1 to 4 rosette-like nuclei in collections of unfertilized control eggs. These represent intermediate stages of the fusion process of the four meiotic products, which ultimately fused to form a single, rosette-shaped nucleus indicating that eggs completed meiosis II. These rosette-shaped nuclei were marked by a total of 4 dots of X-chromosomal signal per egg, which arise from each of the four meiotic products (Fig. 4A, examples in Fig. 4B). In contrast, *BicD*$^{hb\text{-}deGradFP}$ unfertilized eggs contained one to several nuclei forming spindle-like structures, mostly with the appearance of multipolar spindles (Fig. 4A,C). Additionally, their chromosomes did not create a rosette structure that would be typical for a metaphase arrested state. Instead, these nuclei displayed partially decondensed chromatin, an irregular shape, and they lacked the α-tubulin staining

ring surrounding the DNA rosette in control eggs (Fig. 4A,C). Furthermore, the X-chromosomal probe produced more than the usual four signal dots per egg in eggs containing only one meiotic product (Fig. 4Cc) and eggs containing several meiotic products and spindles (Fig. 4Cc'). We also observed eggs with more than four meiotic products (like in Fig. 4Cc'), indicating that *BicD*$^{hb\text{-}deGradFP}$ eggs show over-replication of the meiotic products. The probe used for the FISH experiments recognizes a repetitive region on the X chromosome present along 3 to 3.5 Mb. The fact that this probe detected more than four signals in each *BicD*$^{hb\text{-}deGradFP}$ egg and that these signals showed different brightness and sizes might also suggest that the DNA has become fragmented and/or more decondensed and did not arrest in a metaphase-like state as in the typical rosette structures. This replication, decondensation, and/or fragmentation of the meiotic DNA was not restricted to the sex chromosomes because we observed analogously additional signals when using a probe for the 2nd chromosome (Fig. S6). Altogether, these results indicate that BicD is required for both the replication arrest and the formation of the typical rosette-like structures of the polar bodies.

**Role of BicD in SAC and metaphase arrest of female meiotic products**

After meiosis II completion, *Drosophila* polar bodies remain arrested in a metaphase-like state. In wild-type unfertilized eggs, the four meiotic products fused into a single rosette showed a strong signal for the mitotic marker Phospho-Histone 3 (PH3) along the entire chromosomes indicating that they were arrested in a metaphase-like state (Fig. 4Da-Ea). In contrast, in *BicD*$^{hb\text{-}deGradFP}$ eggs showing one rosette-like structure, indicative of meiosis completion, the PH3 staining was not localized along the entire chromosomes but only enriched at the rosette central region where most of the centromeres are observed (Fig. 4Db-Eb). Moreover, their rosette-like structures showed an increased number of CID-positive dots suggesting that female meiotic products underwent extra rounds of replication/endoreplication (compare Fig. 4Da with 4Db).

Rosette-like structures in *BicD*$^{hb\text{-}deGradFP}$ eggs did not form the typical tubulin ring surrounding the chromosomes observed in wild-type eggs,. Interestingly, DNA extended beyond this tubulin ring and was negative for PH3 staining (Fig. 4Ea, b, c). In the normal situation, Histone H3 phosphorylation starts in pericentromeric heterochromatin regions at the onset of mitosis. It then spreads along the entire length of chromosomal arms, reaching its maximal abundance during metaphase followed by a rapid decrease upon transition to anaphase (Sawicka and Seiser, 2012). Thus, PH3 staining confined to the pericentromeric region in *BicD*$^{hb\text{-}deGradFP}$ polar bodies suggests that these nuclei are not properly arrested or are released from metaphase arrest. Furthermore, *BicD*$^{hb\text{-}deGradFP}$ eggs possessing several meiotic products (Fig. 4Ec,c') showed that not all these nuclei were positive for PH3 staining (Fig. 4Ec2-3,c'), further strengthening the idea that these nuclei are over-replicating due to a failure to arrest in metaphase.

The metaphase arrest of polar bodies depends on the spindle assembly checkpoint (SAC) pathway activation (Défachelles et al., 2015; Fischer et al., 2004; Pérez-Mongiovi et al., 2005). We, therefore, analyzed the localization of two well-conserved orthologs of the SAC pathway, BubR1 and Mad2 (Fig. 5). These proteins associate with unattached kinetochores and, in the case of BubR1, also to kinetochores lacking tension. Because they inhibit the anaphase-promoting complex (APC/C), they are essential to maintain the metaphase arrest. BubR1 was present at polar body kinetochores in the wild-type (100%, n=23) and control BicD::GFP rescued eggs (93%, n=27) (Fig. 5Aa). However, in 43% of the *BicD*$^{hb\text{-}deGradFP}$ eggs, the meiotic products failed to recruit BubR1 to the kinetochores (n=35). The absence of BubR1 from the polar body kinetochores was observed in eggs where polar bodies were fused into a single rosette (Fig. 5Ab) and in eggs showing many additional meiotic products (Fig. 5Ad, d'). The rest of the *BicD*$^{hb\text{-}deGradFP}$ eggs showed either normal BubR1 recruitment (40%) or only a weak signal for kinetochore BubR1 (17%, Fig. 5Ac). Similar results were obtained for Mad2, where 69% of the *BicD*$^{hb\text{-}deGradFP}$ eggs analyzed did not show recruitment of Mad2 to the polar bodies (n=48; Fig. 5B). These data indicate that the failure to activate or maintain the metaphase arrest of polar bodies in the absence of BicD

is probably due to a failure to recruit the SAC components to the kinetochores or maintain their association. That half of the polar bodies still recruited SAC components might also suggest that these nuclei are cycling in and out of the metaphase arrest, duplicating their chromosomes. Altogether, these results suggest that in *BicD*$^{hb\text{-}deGradFP}$ eggs, the meiotic II products do not correctly arrest in metaphase due to a failure to activate or maintain the SAC.

**The BicD cargo and MT-stabilizing factor Chc localizes, like BicD, to centrosomes and mitotic and meiotic spindles**

SAC function is disturb when spindle MT stability is perturbed. Since BicD transports *Drosophila* Chc (Li et al., 2010; Vazquez-Pianzola et al., 2014) and vertebrate orthologs of this protein are needed to stabilize the mitotic MTs (Fu et al., 2010; Royle et al., 2005), we analyzed Chc localization in *Drosophila* embryos. Because available antibodies against Chc do not work well for immunostaining (Li et al., 2010), we analyzed the expression of the Chc using tagged yet functional, Chc fusions (Vazquez-Pianzola et al., 2014). Chc, like BicD, was enriched at the centrosomes and pericentrosomal regions during the entire cell cycle (Fig. 6A-B, S7A-C). During mitosis, Chc associates with the mitotic spindles (Fig. 6A-B, S7B-C). Moreover, similar to BicD, Chc was also enriched during cellularization near the plasma membrane between the nuclei, probably marking the sites where endocytic vesicles start to form (Fig. 6A, S7B) (Sokac and Wieschaus, 2008). *Drosophila* Clathrin light chain (Clc) shows a similar localization pattern during embryogenesis (Fig. S7D). Thus, the Chc/Clc complex localization to the mitotic apparatus appears to be conserved between *Drosophila* and mammalian cells (Royle et al., 2005). Chc was not only present at the mitotic spindles but also localized, like BicD, to the female meiotic II tandem spindles and the central aster (Fig. 6C).

**Proper localization of D-TACC, Msps, and Clc at tandem meiotic spindles requires BicD**

We focused on the early stages of meiosis II in eggs just released from the MI arrest to pinpoint the first meiotic defects. Unfortunately, localization of tagged Chc was irreproducible due to the high cytoplasmic signal. Moreover, overexpressing a tagged Chc in the *BicD*$^{hb\text{-}deGradFP}$ background reduced the flies' viability and fertility, preventing us from collecting enough embryos to analyze the meiotic spindles. Because the Chc partner Clc is also present at the mitotic spindles together with Chc (Fig. S7D), we followed Clc localization during meiosis II. Clc localized to the female MII tandem spindles and the central aster (Fig. 7A). Additionally, we detected an unusual, strong accumulation of Clc at the central aster relative to the levels observed along the MII spindles in *BicD*$^{hb\text{-}deGradFP}$ compared to control spindles (Fig. 7A, A'). We then followed the localization of D-TACC and Msps (Mini spindles) because the spindle localization of their mammalian homologs is interdependent with Chc (Royle, 2012; Royle et al., 2005). In wild-type MII and anaphase II (AII) spindles, D-TACC and Msps were present on tandem spindles and enriched at the central aster (Fig. 7B, C). Additionally, D-TACC is weakly enriched at the spindle equator where the MT plus ends are located during metaphase II and anaphase II (Fig. 7B, arrows). On the other hand, Msps was enriched along both arms of the tandem spindles but stained more strongly the minus ends at the spindle poles (Fig. 7C, arrows). In *BicD*$^{hb\text{-}deGradFP}$ embryos, D-TACC and Msps localization along the tandem spindles was reduced compared to the control spindles (Fig. 7B, C). However, like in control spindles, D-TACC and Msps still showed enrichment at the central aster in *BicD*$^{hb\text{-}deGradFP}$ embryos (Fig. 7B, C). Accordingly, the signal intensity for D-TACC and Msps along the most superficial tandem spindle relative to the signal intensity observed in the central aster was significantly reduced in *BicD*$^{hb\text{-}deGradFP}$ MII spindles (Fig 7B', C').

As a more direct approach to finding out if reduced BicD levels affect Chc localization, we analyzed the spindles of eggs laid by *BicD::GFP, BicD*$^{null}$ females that expressed only one copy of the *hb-deGradFP* construct. In the background of this

combination, which does not produce a phenotype on its own, we overexpressed Chc::mCherry. Eggs produced by such mothers did not develop and showed similar abnormal meiotic products as the ones observed in *BicD*$^{hb\text{-}deGRadFP}$ eggs (see below, Fig. 8D, F). In addition, we detected a mild reduction of the Chc::mCherry signal at the spindle compared to the signal in the central aster (Fig. S8A, A'). These results suggest that BicD is needed to properly localize clathrin, D-TACC, and Msps along the meiotic II spindles.

The central aster is a disk-shaped structure that forms a non-centrosomal microtubule organizing center (ncMTOC) that produces astral MTs and contains several centrosomal proteins. To better understand how the MT polarity at the meiotic tandem spindle relates to the localization of the Clathrin/D-TACC/Msps complex, we stained eggs for minus and plus-end MT markers. These stainings revealed that both plus (Pav, Clip190, EB1) and minus-end (Asp) MT markers are present at the central aster (Fig. S8B-C), suggesting that MTs with different orientations could be present at the central aster. Asp is also enriched at each meiotic spindle's ends (Fig. S8B). The plus end markers were distributed more evenly along the tandem spindle MTs, and only Clip190 was slightly enriched near the DNA region (Fig. S8C). Since TACC and Msps orthologs are MT plus-end tracking proteins (Gutiérrez-Caballero et al., 2015; Lucaj et al., 2015; Nwagbara et al., 2014; Rutherford et al., 2016) and D-TACC is present at the centrosomes (Barros et al., 2005; Lee et al., 2001), this could explain why localization of Clathrin, TACC, Msps is less affected in the central aster. It further suggests that BicD might be needed to stabilize or transport them along the spindles. However, studying the dynamic movement of these proteins along the meiotic tandem spindle is challenging. Chc::mCherry signals, although present all along the spindles, show a diffuse pattern, and we could not detect traceable particles along either the mitotic spindles or the arrested meiotic spindles in *BicD*$^{hb\text{-}deGradFP}$ and control eggs (SM5-7). We could, however, detect Chc::mCherry particles or motile structures that moved along linear tracks resembling MTs during mitosis (Fig S9A. and SM8-9). Although only "escaper" *BicD*$^{hb\text{-}deGradFP}$ eggs make it to the mitotic division of the young embryo (because of the requirement for BicD for pronuclear migration and fusion), the net displacement and velocity of the Chc::mCherry

particles detected in *BicD*$^{hb\text{-}deGradFP}$ embryos was reduced compared to the particles we could track in control embryos (Fig. S9B-D). The Chc particles we detected are rather large and resemble the Chc motile structures reported to move in a *BicD*-dependent manner in synaptic boutons and within the oocyte (Li et al., 2010; Vazquez-Pianzola et al., 2014). Smaller Chc-positive particles may also be subjected to transport along the spindles, but these are below the detection limit. These results suggest that BicD is required to move Chc positive structures in linear tracks during mitosis.

**Chc binds with the same domain to D-TACC and BicD, and D-TACC expression increases the BicD/Chc interaction**

In mammals, Chc interacts directly with TACC3, and the interaction depends on the phosphorylation of Ser$^{552}$ of TACC3 by Aurora A (Fu et al., 2010; Lin et al., 2010). Since D-TACC and clathrin fail to properly localize on *BicD*$^{hb\text{-}deGradFP}$ MII spindles, we investigated whether the *Drosophila* homologs of these proteins can interact with each other and with BicD using a yeast 2-hybrid (Y2H) assay and co-immunoprecipitation experiments (Fig. 8A-B). Indeed, full-length *Drosophila* Chc interacted with D-TACC in both assays.

The minimal region of mammalian isoform Chc22 that interacts with TACC3 spans amino acids 331-542 (Lin et al., 2010). Whereas the corresponding part of *Drosophila* Chc$^{329\text{-}542}$ did not interact with D-TACC in our assays (Fig. 8A), this region with a C-term extension (Chc$^{329\text{-}803}$) interacted with D-TACC almost as strongly as the full-length protein (Fig. 8A). Chc$^{329\text{-}542}$ was also unable to bind BicD (Fig. S10A), but Chc$^{329\text{-}803}$ contains the minimal BicD binding region (Li et al., 2010) (Fig. S10B). Furthermore, chc$^{329\text{-}803}$ interacted in our assays with the BicD CTD (C-terminal domain), a truncated version of BicD that interacts stronger with its cargoes because it does not contain the BicD fold-back domain (Fig. S10B) (Li et al., 2010).

The Chc interaction with D-TACC was not abolished when the conserved Ser residue targeted by the Aurora A kinase was mutated to Alanine ($Ser^{863}$ in D-TACC, corresponds to $Ser^{552}$ of the human protein, Fig. 8A, Fig. S10C). Nevertheless, the phosphomimetic substitution $Ser^{863}$>Asp in D-TACC increased its interaction with full-length Chc (Fig. S10C). These results suggest that phosphorylation of $Ser^{863}$ may not be a prerequisite for the interaction of full-length D-TACC with Chc, at least in the Y2H system. Still, it could enhance the interaction during mitosis and meiosis when the kinase is active.

The interaction of D-TACC with full-length Chc was observed under very stringent Y2H conditions (medium -L, -W, -H, -a; Fig. S10C). In contrast, the interaction between Chc and BicD was only visible under less stringent conditions (medium -L, -W, -H +3 mM 3AT; Fig. S10A, (Cagney et al., 2000)), suggesting that Chc interacts stronger with D-TACC than with BicD in this system. Immunoprecipitation experiments using embryo extracts expressing a Myc::Chc fusion protein aslo supports this hypothesis. Myc::Chc was observed at low levels in BicD Ips. In contrast, the presence of BicD was not detected in the reverse Ips (with anti-Myc antibodies) as previously reported (Fig. 8B) (Vazquez-Pianzola et al., 2014). This result is conceivable due to their weak interaction or the Myc tag interfering with the binding sites. Similarly, BicD antibodies also immunoprecipitated a Flag-tagged version of Chc (Fig. S11). In contrast, D-TACC strongly co-immunoprecipitated with Myc::Chc. On the other hand, no interaction was observed between D-TACC and BicD either by IP or in the Y2H system (Fig. 8B, S10D, S11).

Because we found that D-TACC and BicD bind to the same sequences in the Chc Ankle domain, Chc/BicD, and Chc/D-TACC might only exist as mutually exclusive protein complexes. We then tested if the interaction between BicD-CTD and Chc can be outcompeted in yeast cells by coexpressing D-TACC (Fig 8C). The contrary was the case. The interaction between the BicD-CTD and Chc increased when D-TACC was also co-expressed in yeast cells (Fig 8C). Because Chc acts typically as a triskelion, higher-order complexes of the three Chc molecules could theoretically contain BicD or D-TACC, or both (see models in Fig. 8Cc',c"). The presence of D-TACC might increase the formation or stability of this ternary

complex, bringing additional molecules of BD/AD close together to upregulate the Gal4 promoter in the Y2H system.

**High levels of Chc and D-TACC enhance the embryonic arrest phenotype of *BicD$^{hb\text{-}deGradFP}$* embryos**

*BicD::GFP, BicD$^{null}$* females, expressing only one copy of the *hb-deGradFP* construct *(BicD::GFP, BicD$^{null}$; hb-deGradFP-bcd 3'UTR/+)* laid embryos that showed a reduction of BicD::GFP levels of only 30% on WBs (Fig. S2B-C) and mainly developed normally and hatched into larvae (Fig. 2D-E, 8D). However, when these females expressed an aditional copy of a *Chc* or D-TACC transgene, 80-95% of their progeny failed to hatch as larvae. Instead, they arrested with the same abnormal nuclei phenotype observed in *BicD$^{hb\text{-}deGRadFP}$* embryos (Fig. 8D-G, Fig. S12). Overexpressing Chc or D-TACC alone in females expressing a wild-type copy of *BicD* did not produce visible phenotypes in their embryos, suggesting that high levels of either Chc or D-TACC in a BicD-reduced background are responsible for the phenotypes. Moreover, these embryos showed the same early arrest phenotypes observed in *BicD$^{hb\text{-}deGradFP}$* embryos (Fig. 8E-G, Fig. S12).

**Like BicD, *d-tacc* is required for pronuclear fusion and cell cycle arrest of the male pronucleus and the female meiotic products**

*d-tacc$^{1}$* mutant mothers lay eggs with reduced D-TACC protein levels, and most of these embryos fail to develop (Gergely et al., 2000). Of the male progeny laid by *d-tacc$^{1}$/ Df(3R)110* females, only 25.8% showed signals for the X and Y chromosomes in each zygotic nuclei, indicating that they had performed pronuclear fusion (Fig. S13A). Most of them (74.2%) had at least one internal nucleus marked for the Y chromosome and no X-chromosomal signal (Fig. S13B-D), showing that in *d-tacc$^{1}$* embryos, pronuclear fusion is strongly compromised. Of these embryos that did not perform pronuclear fusion, 30.4% showed normal cell cycle arrest of the female and male meiotic products (Fig. S13B). In 47.85% (Fig. S13C), the paternal pronucleus underwent additional divisions with no over-

replication of the female meiotic products. Only 21.7% *d-tacc1* showed replication of the female meiotic and male derived nuclei (Fig. S13D). The lower penetrance of this female meiosis phenotype than the one observed in *BicD*$^{hb\text{-}deGRadFP}$ eggs (70% of the arrested eggs) could be because *d-tacc*$^{1}$ embryos produce sufficient levels of D-TACC to rescue the female meiosis phenotype (Gergely et al., 2000). Therefore, BicD and D-TACC are required for pronuclear fusion and metaphase arrest of the male pronucleus and the female meiotic products. We also observed abnormal meiosis with delayed polar body extrusion in eggs from *C. elegans* worms fed with bacteria expressing dsRNA against *tac-1* (Fig. 9). Moreover, pointing to a conserved role for these proteins in pronuclear fusion, we found that eggs from worms fed with dsRNA against *bicd-1, chc-1,* and *tac-1* did not undergo pronuclear fusion either (Fig. 9).

## DISCUSSION

### A useful strategy to study the effect of lethal or female sterile mutations in early embryogenesis reveals that *BicD* is required for meiosis II and pronuclear fusion

We found that BicD localizes to the female tandem spindles and the central aster during meiosis II. After fertilization, BicD also localizes to the mitotic spindles and the centrosomes. *BicD*$^{null}$ mutants rarely survive and are sterile, but we generated embryos with reduced levels of BicD at the beginning of embryogenesis (*BicD*$^{hb\text{-}deGradFP}$ embryos) by setting up a strategy based on the deGDradFP technique. Consistent with BicD localization at the female meiotic II spindles, we discovered that *BicD*$^{hb\text{-}deGradFP}$ embryos arrest development displaying aberrant meiotic products and no pronuclear fusion. Especially if combined with the CRIPSP-Cas9 strategy first to produce functional GFP tagged proteins of interest, the construct designed in this paper could be helpful to study the role of female-sterile and lethal mutations during very early embryonic development (Nag et al., 2018).

**Connecting BicD to the SAC pathway**

In unfertilized *BicD*$^{hb\text{-}deGradFP}$ eggs, the female meiotic products were not arrested in metaphase as it normally happens. Instead, they underwent additional rounds of replication. They failed to recruit or maintain the recruitment of the SAC pathway components BubR1 and Mad2, which are normally present at the kinetochores in the wild-type female meiotic polar bodies. Interestingly, in *Drosophila* mutants for *Rod, mps1*, and *BubR1*, well-conserved orthologs of the SAC pathway, the polar bodies cannot remain in a SAC-dependent metaphase-like state and decondense their chromatin, too (Défachelles et al., 2015; Fischer et al., 2004; Pérez-Mongiovi et al., 2005). Furthermore, in these mutants, the polar bodies cycle in and out of M-phase, replicating their chromosomes similarly to those in *BicD*$^{hb\text{-}deGradFP}$ eggs. Thus, it appears that BicD functions to localize the SAC components to induce and/or maintain the metaphase arrest of the polar bodies. Several mechanisms could explain the failure to maintain SAC activation observed in *BicD*$^{hb\text{-}deGradFP}$ embryos. BicD might be needed to recruit the SAC components to kinetochores directly. On the other hand, during mitosis, the RZZ complex (Rod–Zw10–Zwilch) binds to the outer kinetochore region and recruits Mad2, Spindly, and the dynactin complex. Spindly and dynactin act cooperatively to recruit dynein, which then transports the SAC components along the microtubules away from kinetochores as a mechanism to trigger checkpoint silencing and anaphase onset (Basto et al., 2004; Howell et al., 2001; Wojcik et al., 2001; Griffis et al., 2007). Since BicD N-terminal domain binds Dynein and dynactin and promotes their interaction (Splinter et al., 2012), it is also possible that BicD helps to move the SAC components away from the kinetochores. If this does not happen, the SAC remains persistently activated. We also find that BicD activity in *BicD*$^{hb\text{-}deGradFP}$ embryos is insufficient to localize clathrin, TACC, and Msps efficiently along the MTs of the spindle. During mitosis, impairment of MT motors, such as dynein, and treatments that prevent the TACC/ clathrin complex from binding to the mitotic spindles and affecting K-fiber stability, persistently activate the SAC, too (Rieder and Maiato, 2004; Royle et al., 2005). Thus, reduced levels of BicD in *BicD*$^{hb\text{-}deGradFP}$ embryos could additionally trigger SAC hyperactivation through its role in stabilizing the K-fibers. Although our data

strongly suggest that the lack of BicD contributes to SAC defects through its role in localizing Clathrin, D-TACC, and Msps, further work is needed to elucidate if BicD also acts more directly by biding to and localizing the SAC components, or indirectly by affecting the function of dynein.

Whereas persistent SAC activation leads to metaphase arrest and delayed meiosis (D-Meiosis), at least during mitosis, this delay is known to be rarely permanent. Most cells that cannot satisfy the SAC ultimately escape D-mitosis and enter G1 as tetraploid cells by a poorly understood mechanism (Rieder and Maiato, 2004). It is possible that in *BicD*$^{hb\text{-}deGradFP}$, the SAC pathway is constantly activated, delaying meiosis. However, at one point, the nuclei might escape the metaphase II arrest, cycling in and out of M-phase, thereby replicating their chromosomes and de-condensing their chromatin. The fact that female meiotic products overreplicate in *BicD*$^{hb\text{-}deGradFP}$ eggs show no or only pericentromeric PH3 staining supports the notion that these nuclei are on an in-out metaphase arrest phase. The meiotic products in about half of the *BicD*$^{hb\text{-}deGradFP}$ embryos failed to stain for the SAC components BubR1 and Mad2 support this hypothesis.

**Connecting BicD to the D-TACC/Msps/clathrin complex**

Chc, its partner Clc, and BicD are enriched at mitotic spindles and centrosomes. Furthermore, these proteins and the clathrin-interacting partners D-TACC and Msps localize to the tandem spindles and the central aster of the female meiotic II apparatus. The interaction of *Drosophila* Chc with D-TACC is conserved, and Chc interacts through the same protein domain directly with D-TACC and BicD (Fu et al., 2010; Lin et al., 2010). Moreover, BicD is needed for localizing D-TACC, Msps, and clathrin throughout the meiotic II tandem spindles. The TACC3/Chc interaction was proposed to form a domain in tandem to bind spindle MTs (Hood et al., 2013). We hypothesize that BicD could help recruit Chc to the microtubules by association with dynein. Because Chc usually acts as a trimer with Clc (triskelion), potentially each Chc might interact with either BicD or D-TACC. Thus, a mixed complex could be formed, and BicD might help to move, recruit, or stabilize Chc and D-TACC along the

spindles via the interaction of BicD/Chc in the same trimer (model in Fig. 8Cc"). The fact that expression of D-TACC enhances the Chc/BicD interaction and that overexpression of *Chc* and *D-TACC* arrested early development in a background where BicD is reduced to levels that do not produce visible phenotypes on their own, supports this model. Our results suggest that with respect to BicD, the levels of D-TACC and Chc should be tightly balanced for these proteins to perform their normal function in early development, as has been shown previously for other BicD transport processes (Vazquez-Pianzola et al., 2014).

**Role of BicD in pronuclear fusion**

BicD performed a role in pronuclear fusion that is conserved during evolution since *C. elegans* eggs depleted for *bicd-1* also failed to undergo pronuclear fusion. Moreover, *Drosophila D-TACC* and *C. elegans chc-1* and *tac-1* are also needed for pronuclear fusion. These genes might be required indirectly through their role in meiosis since preliminary data suggest that meiosis II is also compromised in *bicd-1* and *chc-1 dsRNA-fed* worms (Fig. S14). Alternatively, they might play a more direct role in pronuclear migration, which depends on Dynein and MTs in bovine, primate, and *C. elegans* embryos (Gönczy et al., 1999; Payne et al., 2003). This would then suggest that the underlying mechanism may be used to correctly build or stabilize different kinds of MTs. Figuring out their precise mechanistic involvement in pronuclear fusion is an interesting question for further studies.

## MATERIALS AND METHODS

***Drosophila* stocks**

*P{matα4-GAL-VP16}, Nos-Gal4:Vp16 , UAS-Clc::GFP, Histone::RFP*, C(1;Y)1, y1w: y+/0 and *C(1)RM, y1 v1/0* stocks were obtained from the Bloomington *Drosophila* Stock Center (NIH P400D018537), Flies containing the genome rescue transgenes p*CHC3+* (Bazinet et al., 1993) and *4C-CHC* (Kasprowicz et al., 2008), were kindly provided by C. Bazinet and P. Verstreken, respectively. *D-tacc*$^{1}$ and *Df 3R(110),* covering the *tacc* locus, were provided by

J. Raff (Gergely et al., 2000). S. Bullock provided the *UAS-Chc::eGFP* and *UAS-Chc::mCherry flies (Li et al., 2010)*. Transgenic flies *pUASP-Chc-V5-K10-AttB* and *pUASP-myc-chc-K10-AttB* were described previously (Vazquez-Pianzola et al., 2014). *Df(2L)Exel7068* (Exelixis) was used as *BicD* deficiency (*BicDDf*). The $BicD^{null}$ allele, *BicDr5*, the *BicD::GFP* flies and the method to generate $BicD^{mom}$ females were described (Paré and Suter, 2000; Ran et al., 1994; Swan and Suter, 1996; Vazquez-Pianzola et al., 2014). *White (w)* flies were used as controls.

To produce unfertilized eggs, virgin *w* females were crossed to *C(1;Y)1, y1w: y+/0* males to generate XO males that are phenotypically normal but sterile. XO males were then crossed to virgin females of the desired phenotype. Eggs laid by these females were not fertilized.

**DNA constructs and generation of transgenic flies**

The generation of the flies expressing the *hb-deGRadFP* construct was as follows. First, we cloned the NSlmb-vhhGFP4 sequence (that comprises the F-box domain contained in the N-terminal region of the *Drosophila* supernumerary limbs (Slmb) protein fused to the GFP-binding nanobody VhhGFP4 sequence) described by Caussinus and colleagues (Caussinus et al., 2011). Then, the NSlmb-vhhGFP4 was cloned under the *hunchback* (*hb*) minimal maternal promoter containing the 5'-UTR leader of the maternal 3.2 Kb *hb* transcript and combined with the *bcd* 3'-UTR, following the strategy used by Schulz and Tautz. They used it to induce an artificial Hb gradient in embryos (Schulz and Tautz, 1995). The *Nslmb-vhhGFP4* sequence was PCR-amplified with specific primers bearing *BamHI* and *KpnI* sites using the plasmid pUAS-Nslmb-vhhGFP4 as the template (Caussinus et al., 2011).

Primer sequences were the following ones. Nano-GFP-sense-BamHI (GGATCCATGATGAAAATGGAGACTGACAAAAT) and Nano-GFP-anti-Kpn (GGTACCTTAGCTGGAGACGGTGACCTGGGTG). PCR products were subcloned into the same sites of the pCaSper-AttB vector to create the plasmid pCasper-AttB-Nslmb-vhhGFP4 (or pw+GFP nanobody). A 1.5 Kbp fragment of the *bicoid* 3'-UTR genomic region (Berleth et al., 1988) was amplified from a genomic library using specific primers containing

KpnI and NotI restrictions sites. Primers were: bcd 3'UTR sense-Kpn I (GGTACCACGCGTAGAAAGTTAGGTCTAGTCC) and bcd 3'UTR anti-Not I (GCGGCCGCGCTAGTGCTGCCTGTACAGTGTCT). The insert was cloned by T-end ligation into the pCR2.1 TOPO vector and later subcloned into the KpnI/ NotI sites of pCasper-AttB-Nslmb-vhhGFP4 to generate the pCasper-AttB-Nslmb-vhhGFP4-bcd 3'-UTR construct (or pw+ GFP nanobody-bcd 3'-UTR). The minimal maternal *hunchback (hb)* promoter region together with the 5'-UTR leader of the maternal 3.2 Kb *hb* transcript were amplified using as template the Lac8.0 construct already described (Margolis et al., 1994) and kindly provided by Jim Posakony. Primers for this amplification contained flanking BglII and BamHI sites and were the following ones. Hb-pr-sense–BglII (AGATCTTCCGGATCAGCGGCGCTGATCCTGC), and Hb-pr-Anti-BamHI (GGATCCCTTGGCGGCTCTAGACGGCTTGCGGACAGTCCAAGTGCAATTC). Inserts were further cloned into the *BamHI* of Nslmb-vhhGFP4-bcd 3'-UTR to generate Hb-Nslmb-vhhGFP4-bcd 3'UTR (or pw+ Hb-GFP nanobody-bcd3'UTR). This final plasmid was injected into embryos containing the ZH-attP-14/3R-86F landing platform to generate flies expressing the *hb-deGradFP* construct.

The *don Juan (Dj)::mCherry* construct to produce transgenic flies was generated as follows. First, the mCherry region was PCR-amplified with primers containing BamHI and HindIII sites using pC4-SqhP-mCherry plasmid as the template (a gift from Romain Levayer). Next, the reverse primer added a GS-rich region as a linker and removed the stop codon. Then , the amplified fragment was further subcloned into the BamHI/HindIII sites of the plasmid *pw+SnattB* (Koch et al., 2009) to generate the plasmid *pw+attB*-mCherry. Next, the genomic region containing the minimal promoter, the 5'-UTR, and the ORF of *Dj* gene was PCR-amplified from genomic fly DNA using primers containing EcoRI and BamHI sites and cloned into the same sites of *pw+attB*-mCherry to generate the final construct *pw+attB – Don Juan (Dj)::mCherry*. Finally, this construct was further injected into flies containing the ZH-attP-52 / 3L-64A landing platform for transgenesis.

**Hatching rate determination and embryo development**

Hatching rates were scored as follows. First, Virgin females of the desired genotype were crossed to control *white* males. Females were allowed to lay eggs on agar plates for several hours or overnight. Around 100-200 embryos were marked in the plate and further developed for 48 h at 25$^{o}$C. After 48 h, embryos that did not hatch were counted. 30 min to 60 min or 2- to 5h old embryos were collected for scoring embryo development. Embryos were then fixed and stained to detect both α-tubulin and DNA to score the development stage.

**Western blots**

The preparation of ovaries for Western blots was as follows. Seven pairs of ovaries were collected in 20 µl of SDS-sample buffer, boiled for 2 min., vortexed for 15 sec., and cooked for another 8 min. Finally, they were loaded onto an SDS –PAGE. Western blots were performed using mouse monoclonal anti-BicD antibodies (a mixture of 1B11 and 4C2, 1:10 dilution, (Suter and Steward, 1991)), mouse anti-α-tubulin (1:2,000 dilution of the cell culture´s supernatant, Developmental Studies Hybridoma Bank (DSHB)), rabbit anti-mammalian Chc (1:500 dilution, (Hirst et al., 2009)), rabbit anti-GFP (1:3,000 dilution, Immunokontact, 210-PS-1GFP), rabbit anti-Clc (1:3,000, (Heerssen et al., 2008)), mouse monoclonal anti-Myc 9E10 (1:5 cell culture supernatant, DSHB), rabbit anti-D-TACC (1:10,000 dilution, (Kao and Megraw, 2009)), rabbit anti-D-TACC (1:500) and rabbit anti-Flag (1:320, Sigma F7423). Primary antibodies were detected using horseradish peroxidase-conjugated secondary antibodies (GE Healthcare, NA934V, LNA931V/AH). To detect the deGRadFP expressed from the *hb-deGRadFP* construct, anti-llama IgG-heavy and light chain antibodies (1:500 dilution, Bethyl, A160-100A) were used and developed using anti-goat IgG (H+L)-HRP conjugated antibodies (1:500 dilution, Invitrogen, A15999). We found that, although the *hb-deGRadFP* construct expresses a fusion protein between the Fbox and the Vhh (and not the whole Immunoglobulin) of a Llama nanobody that recognized GFP, these Vhh can still be recognized by the commercially available anti-Llama serum made in rabbits

from Bethyl. Indeed, others have reported that rabbit immunoglobulins purified from the same serum could recognize different nanobodies (Haddad et al., 2016)

**Immunoprecipitations (Ips)**

Ips were done essentially as previously described (Vazquez-Pianzola et al., 2011). 30 µl of protein-G Sepharose beads (Amersham) and 1 ml of embryo extracts were used per IP. Extracts were prepared from 0-20 h old embryos expressing a Chc::Myc fusion protein under a maternal Tubulin promoter. Extracts from wild-type embryos (OreR) were also prepared as a negative control. For each IP, 1 ml of cell culture supernatant of monoclonal anti-BicD 1B11, anti-BicD 4C2, or anti-Myc 9E10 antibodies were bound to the beads. To IP TACC, a solution containing 2 µl of the polyclonal anti-TACC UT316 antibody (Kao and Megraw, 2009) diluted in 1 ml of PBS was used to bind to the protein-G beads. Beads were resuspended in 30 µl of sample buffer, and 7 to 15 µl per well was analyzed by Western blot.

**Immunostainings**

Immunostainings of embryos were done using the following primary antibodies: mouse anti-BicD (a mix of 1B11 and 4C2, 1:10 dilution), mouse anti-Myc 9E10 (dilution 1:5, DSHB), mouse anti-V5 (1:200, Invitrogen, R960-25), rabbit anti-Cnn (1:500 (Heuer et al., 1995)), rabbit anti Clc (1:500 (Heerssen et al., 2008)),

mouse monoclonal anti-α-tubulin DM1A (1:500, Sigma, T9026 or T6199), rabbit anti-α-tubulin (1:500, Abcam, ab18251), guinea pig anti-α-tubulin (1:1000, AA345, Geneva Antibody Facility), rabbit anti-GFP (1:300, previously preabsorbed on embryos, Immunokontakt), rabbit anti D-TACC UT316 (1:1,000 (Kao and Megraw, 2009)), rabbit anti D-TACC (1:500 (Gergely et al., 2000)), mouse anti D-TACC (1:200, (Chou et al., 2020), rabbit anti Pav (1:200, (Lie-Jensen et al., 2019), rabbit anti Asp (1:250, Ito and Goshima, 2015), rabbit anti-Msps (1:500 (Cullen et al., 1999)), mouse anti-Flag M2 (1:200, Sigma, F3165), rabbit anti CID (1:400 (Buster et al., 2013)), rabbit anti p-Histone H3 (S10) (1:200,

Cell Signalling, 9701L), mouse anti p-Histone H3 6G3 (1:200, Cell Signalling, 9706), rabbit anti BubR1 (1:2,000 (Logarinho et al., 2004)), rabbit anti Mad2 (1/1,000 (Logarinho et al., 2004)), rabbit anti EB1 (1:500, Rogers et al., 2002) and rabbit anti-Clip190 (1:50, Lantz and Miller, 1998). To detect the hb-deGRadFP construct, anti-llama IgG-heavy and light chain (1:500 dilution, Bethyl, A160-100A) was developed donkey anti-goat Alexa Fluor 680 (H+L) (Ivitrogen, A21084 ). Secondary antibodies used were Cy3-conjugated goat anti-mouse (Jackson Immunoresearch, 115-165-146), Alexa Fluor 647-conjugated goat anti-mouse (Jackson Immunoresearch, 115-606-146), DyLight 649-conjugated or anti-rabbit antibodies (Jackson Immunoresearch, 111-495-144), A488-conjugated goat anti-rabbit (Molecular Probes, A-11034), Oregon Green 488 conjugated goat anti-mouse (Invitrogen, O11033), donkey anti-mouse AF488 (Life Technologies, A21202), AF568 conjugated donkey anti-mouse (Life Technologies, A100037) and AF488 conjugated donkey anti-rabbit A488 (Molecular Probes, A21206). Nuclei were visualized by staining DNA with 2.5 µg/ml Hoechst 33258 (Molecular Probes) for 40 minutes during the final wash or incubated overnight when early meiosis in embryos was analyzed. Control immunostainings using only secondary antibodies were performed to detect unspecific binding of the secondary antibodies. For co-localization studies, control samples using only one of the primary antibodies and both secondary antibodies were prepared to detect bleed through to the other channel. When detecting tagged proteins, samples of wild-type specimens were used to control for unspecific binding of the anti-tag antibody. As indicated, embryos were either fixed with 4% paraformaldehyde (PFA) or with methanol. Methanol fixation was mainly used to preserve the cytoskeleton structure and reduce the cytoplasmic levels in BicD staining. Methanol fixation was done as previously described (Kellogg et al., 1988). When antigens were not well preserved in methanol fixations (for example, this was observed for the Chc fusion proteins), fixation with 4% paraformaldehyde (PFA) was used. To detect endogenous BicD::GFP in ovaries, ovaries were fixed with 4% PFA. For preserving the endogenous Clc::GFP signal, embryos were hand-devitellinized and fixed in a mixture of Heptane saturated with PFA for 15 min. For preserving the Dj:mCherry and Chc::mCherry signal, the

embryos were fixed with MetOH. Stage 14 oocytes for immunostainings were prepared as previously described (Radford and McKim, 2016).

Images were analyzed with a Leica TCS-SP8 confocal microscope. Most of the spindle pictures represent Z-stack maximal intensity projections along the frames. MII and Anaphase II images were acquired such that the central aster signal was highest, but bellow saturation. Due to the strong Clc signal in the cytoplasm, the spindle perpendicular position to the surface and the depth of the sample, it was not possible to analyze Clc localization at the different regions of the meiotic spindles by directly analyzing the Z-stack of maximal confocal projection images. The high cytoplasmic signal in the first planes masked the localization at the spindle in the deeper planes. Thus, to detect the presence of Clc along the tandem meiosis spindles, Z-stack images were processed to correct for depth and bleaching in Image J. All stacks were processed the same way. First, a crop area corresponding to the spindle of the same size was cropped in each image. Channels were then split and subjected to corrections separately. Each channel was smooth with a median filter radius of 1 to decrease the noise. The channel corresponding to the Clc staining had the most robust signal intensity loss through the sample´s depth. This channel was subject to bleach correction with a simple ratio fit to compensate for intensity attenuation in the image´s deeper stacks. Channels corresponding to α-tubulin and DNA staining did not lose much intensity with the sample´s depth. They were subjected to an attenuation correction using an ImageJ plugin already described (Biot et al., 2008). After intensity correction, the final image was created by merging the channels previously subjected to maximal intensity Z-stack projection.

**Live imaging in *Drosophila* embryos**

To analyze the localization of Chc during the cell cycle, embryos expressing the corresponding fluorescent proteins (Chc::mCherry or Chc::GFP) were imaged with the resonance scanner of a Leica Sp8 confocal microscope. To analyze Chc particle movements, Chc::mCherry embryos were imaged with a Nikon W1 LIPSI spinning disk microscope.

Images were taken every 0.5 seconds with a 100x immersion objective. Since the embryos moved during the cell cycle, we analyzed the particle movement during a total of 150 frames corresponding to 75 seconds. The particles were detected and tracked using the TrackMate plugin in Fiji (Tinevez et al., 2017). The following settings were used: blob diameter: 0.75 mm, threshold: 2, linking maximal distance: 0.75 mm, gap closing maximal distance, and frame gap: 0.

**Fluorescent *in situ* hybridization (FISH)**

Sinthesis of RNA probes and hybridization experiments for mRNA FISH, were performed as previously described (Vazquez-Pianzola et al., 2017). To detect the deGRadFP mRNA, the *VhhGFP4* region of the *hb-deGRadFP* transgene was first amplified by PCR with primers containing T3 and T7 promoter sequences, and the plasmid pUAS-Nslmb-vhhGFP4 as a template (Caussinus et al., 2011). Primer sequences were the following ones. The sense primer containing the T3 promoter was:

GGGGGGAATTAACCCTCACTAAAGGGAGAATGGATCAAGTCCAACTGGTGGAGT

and the antisense primer containing the T7 promoter was:

GGGGGGTAATACGACTCACTATAGGGAGATTAGCTGGAGACGGTGACCTGGGTG.

Antisense and sense probes were generated using T7 and T3 RNA polymerase, respectively. A sense probe was used to detect unspecific background.

DNA FISH to *Drosophila* chromosomes was done mainly according to (Dernburg, 2000). DNA oligos hybridizing to repetitive regions of the Y (AATAC)6 and the 2nd chromosome (AACAC)7 modified with Cy3 and Cy5 fluorophores at their 5' end, respectively, were ordered from Microsynth. The sequences were already described (Dernburg, 2000). The sequence used to detect the X chromosome by hybridizing to TTT-TCC-AAA-TTT-CGG-TCA-TCA-AAT-AAT-CAT recognizes the 359-bp satellite block on the *D. melanogaster* X chromosome as well as minor variants on chromosome 3 was described by (Ferree and Barbash, 2009). A 5' end Cy5 fluorophore-labeled probe was used. Embryos were fixed with methanol for DNA FISH. Probes were used at a final concentration of 5 ng/µl in hybridization

buffer. The blocking buffer used (before adding the first antibody for detection of the desired proteins) was: 2x SSC, 0.5% BSA (molecular grade BSA from Biolabs or Acetylated BSA from Ambion) and Tween-20 at 0.1%. Donkey fluorescent-conjugated secondary antibodies were used as described in the immunofluorescence experiments.

**Yeast two-hybrid experiments**

Two-hybrid plasmids containing the *Drosophila Egl* (Egl; CG4051) full-length (pEgl-AD and pEgl-BD), *BicD* full-length (pBicD-AD and pBicD-BD), and the *BicD* carboxy-terminal domain (CTD; amino acids 535–782) (pBicD(535–782)-BD and pBicD (535–782)-AD) were previously described (Rashpa et al., 2017). *D-TACC* (CG9765) full-length; and *Chc* (CG9012) full-length, a fragment containing amino acids 329-803, and another one bearing amino acids 329–542 were cloned into the pOAD and or pOBD2 vectors (Cagney et al., 2000) in-frame either with the activator domain (AD) or the DNA-binding domain (BD) sequence of GAL4, respectively, to create the "prey" plasmids, pD-TACC-AD, pChc-AD, pChc (329–803)-AD, and pChc(329–542)-AD, as well as the "bait" plasmids pChc-BD, pChc (329–803)-BD and pChc (329–542)-BD. To produce the constructs D-TACC-Ala and D-TACC-Asp, D-TACC Ser$^{863}$ was mutated to alanine and aspartic acid codon, respectively, by site-directed mutagenesis. Changes were verified by sequencing.

TACC was cloned onto the vector pYX122 (Westermann et al. 2000; Addgene plasmid #45048; a kind gift of Prof. María Soledad Funes, Instituto de Fisiología Celular, UNAM, Mexico) lacking the GFP reporter cistron, to generate the construct pTACC-YX22 and which expresses TACC under the constitutive TPI promoter. pYX122 contains the auxotrophic gene marker *His3*. Interactions between "bait" and "prey" proteins were detected following a yeast interaction-mating method using the strains PJ69-4a and PJ69-4alpha (Cagney et al., 2000). For all cases, diploid cells containing both AD and BD constructs were selected in media lacking tryptophan and leucine (–(L,W), *Growth test*). To test for possible interactions, cells were further replica-plated in media lacking leucine, tryptophan, and adenine (–(L, W, a), media lacking leucine, tryptophan, histidine, and adenine (-(L,W,H,a), or media lacking

leucine, tryptophan, and histidine, and containing the indicated amounts of 3-Amino-1,2,4-triazole (3AT), (-(*Interaction test*). To analyze the effect of TACC on the BicD CTD and Chc interaction in the yeast two-hybrid system, diploid cells containing both bait Chc-BD and pray BicD CTD-AD plasmids were grown on the auxotrophic medium –(Leu, Trp), further cotransformed with either pYX122 empty vector or pTACC-YX22 and platted onto the auxotrophic media –(Leu, Trp, His). The interaction was detected in serial dilutions plated onto –(Leu, Trp, His, ade). For each test, ten-fold serial dilutions are presented. Growth was scored after 4-5 days of growth at 30°C.

### *C. elegans* strains, RNAi, and imaging

N2, JDU233 (*H2B::mCherry;α-tubulin::GFP*), VJ512, *chc-1(tm2866)III/hT2[bli-4(e937) let-?(q782) qIs48](I;III)*. Worms were fed with dsRNA on NGM plates containing 1mM IPTG and carbenicillin using clones from the Ahringer RNAi library (Kamath and Ahringer, 2003). For non-lethal phenotypes, the progeny was imaged after 60 hours of feeding of gravid adults at 20°C. For lethal phenotypes, L3/L4 larvae were transferred onto RNAi plates and fed 12 h at room temperature to obtain gravid adults. The empty vector L4440 was used as a control. Embryo dissections were performed as previously described (Bellanger et al., 2007), and embryos were imaged immediately on an agar pad using an AxioVision (Zeiss) microscope with a 100x NA 1.4 oil objective with a GFP and a mCherry filter set. One plane was acquired every 10 seconds using Visiview, and images were processed using ImageJ and Photoshop.


## ACKNOWLEDGEMENTS

We thank S. Bullock, C. Bazinet, J. Hirst**,** J. Raff, T. Melgraw, H. Ohkura, G. Rogers, C. Sunkel, M. Affolter, E. Caussinus, D. Van Vactor, K. Haglund, G. Goshima, J. Dumont, the Bloomington *Drosophila* Stock Center (NIH P400D018537), and the Developmental Studies Hybridoma Bank (created by the NICHD of the NIH and maintained at The University of Iowa, Department of Biology, Iowa City, IA 52242) for constructs, fly or worms stocks and antibodies. We thank FlyBase (U41HG000739) for the *Drosophila* genomic resources. We

thank Andrew Swan for his scientific advice on how to study female meiosis and Yury Belyaev for his help with image processing.

This work was supported by funding's from the Swiss National Science Foundation (SNF, project grant 31003A_173188; www.snf.ch) and the University of Bern (www.unibe.ch) to BS, an SNF grant (project grant IZCOZ0_189884/31003A_176226) to P.M. and an Equal Opportunity grant from the Phil.-Nat. faculty to P.V.P. (www.unibe.ch).

**Competing interests.** The authors declare no competing financial interests.

**Author contributions.** P.V.P., D. B., G.S., G. H., G. M., and D. H performed experiments. P.V.P., G. S., P.M., and G.H. analyzed data. P.V. P. and B.S. conceived the studies. G.S. and P. M. contributed to writing the results of the *C. elegans* experiments. P.V.P and B.S. wrote the manuscript.

## REFERENCES

**Basto, R., Scaerou, F., Mische, S., Wojcik, E., Lefebvre, C., Gomes, R., Hays, T. and Karess, R.** (2004). In vivo dynamics of the rough deal checkpoint protein during *Drosophila* mitosis. *Curr. Biol.* **14**, 56–61.

**Bazinet, C., Katzen, A. L., Morgan, M., Mahowald, A. P. and Lemmon, S. K.** (1993). The *Drosophila* clathrin heavy chain gene: clathrin function is essential in a multicellular organism. *Genetics* **134**, 1119–1134.

**Bellanger, J.-M., Carter, J. C., Phillips, J. B., Canard, C., Bowerman, B. and Gönczy, P.** (2007). ZYG-9, TAC-1 and ZYG-8 together ensure correct microtubule function throughout the cell cycle of *C. elegans* embryos. *Journal of Cell Science* **120**, 2963–2973.

**Berleth, T., Burri, M., Thoma, G., Bopp, D., Richstein, S., Frigerio, G., Noll, M. and Nüsslein-Volhard, C.** (1988). The role of localization of *bicoid* RNA in organizing the anterior pattern of the *Drosophila* embryo. *EMBO J.* **7**, 1749–1756.

**Biot E, Crowell E, Höfte H, Maurin Y, Vernhettes S & Andrey P**. (2008). A new filter for spot extraction in *N*-dimensional biological imaging. In *Fifth IEEE International Symposium on Biomedical Imaging (ISBI'08): From Nano to Macro*, pp. 975-978.

**Booth, D. G., Hood, F. E., Prior, I. A. and Royle, S. J.** (2011). A TACC3/ch-TOG/clathrin complex stabilises kinetochore fibres by inter-microtubule bridging. *EMBO J.* **30**, 906–919.

**Brodsky, F. M.** (2012). Diversity of clathrin function: new tricks for an old protein. *Annu. Rev. Cell Dev. Biol.* **28**, 309–336.

**Bullock, S. L. and Ish-Horowicz, D.** (2001). Conserved signals and machinery for RNA transport in *Drosophila* oogenesis and embryogenesis. *Nature* **414**, 611–616.

**Buster, D. W., Daniel, S. G., Nguyen, H. Q., Windler, S. L., Skwarek, L. C., Peterson, M., Roberts, M., Meserve, J. H., Hartl, T., Klebba, J. E., et al.** (2013). SCFSlimb ubiquitin ligase suppresses condensin II-mediated nuclear reorganization by degrading Cap-H2. *J Cell Biol* **201**, 49–63.

**Cagney, G., Uetz, P. and Fields, S.** (2000). High-throughput screening for protein-protein interactions using two-hybrid assay. *Meth. Enzymol.* **328**, 3–14.

**Caussinus, E., Kanca, O. and Affolter, M.** (2011). Fluorescent fusion protein knockout mediated by anti-GFP nanobody. *Nature Publishing Group* **19**, 117–121.

**Chou, V. T., Johnson, S., Long, J., Vounatsos, M. and Vactor, D. V**. (2020). dTACC restricts bouton addition and regulates microtubule organization at the Drosophila neuromuscular junction. *Cytoskeleton (Hoboken)* 77, 4–15.

**Cullen, C. F., Deák, P., Glover, D. M. and Ohkura, H.** (1999). *mini spindles*: A gene encoding a conserved microtubule-associated protein required for the integrity of the mitotic spindle in *Drosophila. J Cell Biol* **146**, 1005–1018.

**Défachelles, L., Hainline, S. G., Menant, A., Lee, L. A. and Karess, R. E.** (2015). A maternal effect *rough deal* mutation suggests that multiple pathways regulate *Drosophila* RZZ kinetochore recruitment. *Journal of Cell Science* **128**, 1204–1216.

**Dernburg A. F.** (2000) *In Situ* hybridization to somatic chromosomes. In: *Drosophila* Protocols (ed. W. Sullivan, M. Ashburner and R. S. Hawley), pp. 24–55. Cold Spring Harbor, New York, USA: Cold Spring Harbor Laboratory Press.

**Dienstbier, M., Boehl, F., Li, X. and Bullock, S. L.** (2009). Egalitarian is a selective RNA-binding protein linking mRNA localization signals to the dynein motor. *Genes Dev.* **23**, 1546–1558.

**Driever, W. and Nüsslein-Volhard, C.** (1988). A gradient of bicoid protein in *Drosophila* embryos. *Cell* **54**, 83–93.

**Ferree, P. M. and Barbash, D. A.** (2009). Species-specific heterochromatin prevents mitotic chromosome segregation to cause hybrid lethality in *Drosophila*. *PLoS Biol.* **7**, e1000234.

**Fischer, M. G., Heeger, S., Häcker, U. and Lehner, C. F.** (2004). The mitotic arrest in response to hypoxia and of polar bodies during early embryogenesis requires *Drosophila Mps1*. *Curr. Biol.* **14**, 2019–2024.

**Fu, W., Tao, W., Zheng, P., Fu, J., Bian, M., Jiang, Q., Clarke, P. R. and Zhang, C.** (2010). Clathrin recruits phosphorylated TACC3 to spindle poles for bipolar spindle assembly and chromosome alignment. *Journal of Cell Science* **123**, 3645–3651.

**Fumoto, K., Hoogenraad, C. C. and Kikuchi, A.** (2006). GSK-3beta-regulated interaction of BICD with dynein is involved in microtubule anchorage at centrosome. *EMBO J.* **25**, 5670–5682.

**Gergely, F., Kidd, D., Jeffers, K., Wakefield, J. G. and Raff, J. W.** (2000). D-TACC: a novel centrosomal protein required for normal spindle function in the early *Drosophila* embryo. *EMBO J.* **19**, 241–252.

**Gönczy, P., Pichler, S., Kirkham, M. and Hyman, A. A.** (1999). Cytoplasmic dynein is required for distinct aspects of MTOC positioning, including centrosome separation, in the one cell stage *Caenorhabditis elegans* embryo. *J Cell Biol* **147**, 135–150.

**Griffis, E. R., Stuurman, N. and Vale, R. D. (2007).** Spindly, a novel protein essential for silencing the spindle assembly checkpoint, recruits dynein to the kinetochore. *J Cell Biol* 17.

**Haddad M., Soukkarieh C., Khalaf H.E. and Abbady A. Q. (2016).** Purification of polyclonal IgG specific for Camelid's antibodies and their recombinant nanobodies. Open Life Sciences. https://doi.org/10.1515/biol-2016-0001

**Heerssen, H., Fetter, R. D. and Davis, G. W.** (2008). Clathrin dependence of synaptic-vesicle formation at the *Drosophila* neuromuscular junction. *Curr. Biol.* **18**, 401–409.

**Heuer, J. G., Li, K. and Kaufman, T. C.** (1995). The *Drosophila* homeotic target gene *centrosomin (cnn)* encodes a novel centrosomal protein with leucine zippers and maps to a genomic region required for midgut morphogenesis. *Development* **121**, 3861–3876.

**Hirst, J., Sahlender, D. A., Choma, M., Sinka, R., Harbour, M. E., Parkinson, M. and Robinson, M. S.** (2009). Spatial and functional relationship of GGAs and AP-1 in Drosophila and HeLa cells. *Traffic* **10**, 1696–1710.

**Hood, F. E., Williams, S. J., Burgess, S. G., Richards, M. W., Roth, D., Straube, A., Pfuhl, M., Bayliss, R. and Royle, S. J.** (2013). Coordination of adjacent domains mediates TACC3–ch-TOG–clathrin assembly and mitotic spindle binding. *J Cell Biol* 202, 463–478.

**Hoogenraad, C. C. and Akhmanova, A.** (2016). Bicaudal D Family of Motor Adaptors: Linking Dynein Motility to Cargo Binding. *Trends Cell Biol.* **26**, 327–340.

**Howell, B. J., McEwen, B. F., Canman, J. C., Hoffman, D. B., Farrar, E. M., Rieder, C. L. and Salmon, E. D.** (2001). Cytoplasmic dynein/dynactin drives kinetochore protein transport to the spindle poles and has a role in mitotic spindle checkpoint inactivation. *J Cell Biol* **155**, 1159–1172.

**Ito, A. and Goshima, G. (2015).** Microcephaly protein Asp focuses the minus ends of spindle microtubules at the pole and within the spindle. *J Cell Biol* 211, 999–1009.

**Kamath, R. S. and Ahringer, J.** (2003). Genome-wide RNAi screening in Caenorhabditis elegans. *Methods* **30**, 313–321.

**Kao, L.-R. and Megraw, T. L.** (2009). Centrocortin Cooperates with Centrosomin to Organize *Drosophila* Embryonic Cleavage Furrows. *Curr. Biol.* **19**, 937–942.

**Kasprowicz, J., Kuenen, S., Miskiewicz, K., Habets, R. L. P., Smitz, L. and Verstreken, P.** (2008). Inactivation of clathrin heavy chain inhibits synaptic recycling but allows bulk membrane uptake. *J Cell Biol* **182**, 1007–1016.

**Kellogg, D. R., Mitchison, T. J. and Alberts, B. M.** (1988). Behaviour of microtubules and actin filaments in living *Drosophila* embryos. *Development* **103**, 675–686.

**Koch, R., Ledermann, R., Urwyler, O., Heller, M. and Suter, B.** (2009). Systematic functional analysis of Bicaudal-D serine phosphorylation and intragenic suppression of a female sterile allele of *BicD*. *PLoS ONE* **4**, e4552.

**Lantz, V. A. and Miller, K. G. (1998).** A class VI unconventional myosin is associated with a homologue of a microtubule-binding protein, cytoplasmic linker protein-170, in neurons and at the posterior pole of Drosophila embryos. *J Cell Biol* 140, 897–910.

**Li, X., Kuromi, H., Briggs, L., Green, D. B., Rocha, J. A. O. J., Sweeney, S. T. and Bullock, S. L.** (2010). Bicaudal-D binds clathrin heavy chain to promote its transport and augments synaptic vesicle recycling. *EMBO J.* **29**, 992–1006.

**Lie-Jensen, A., Ivanauskiene, K., Malerød, L., Jain, A., Tan, K. W., Laerdahl, J. K., Liestøl, K., Stenmark, H. and Haglund, K.** (2019). Centralspindlin Recruits ALIX to the Midbody during Cytokinetic Abscission in Drosophila via a Mechanism Analogous to Virus Budding. *Curr. Biol.* 29, 3538-3548.e7.

**Lin, C.-H., Hu, C.-K. and Shih, H.-M.** (2010). Clathrin heavy chain mediates TACC3 targeting to mitotic spindles to ensure spindle stability. *J Cell Biol* **189**, 1097–1105.

**Logarinho, E., Bousbaa, H., Dias, J. M., Lopes, C., Amorim, I., Antunes-Martins, A. and Sunkel, C. E.** (2004). Different spindle checkpoint proteins monitor microtubule attachment and tension at kinetochores in *Drosophila* cells. *Journal of Cell Science* **117**, 1757–1771.

**Mach, J. M. and Lehmann, R.** (1997). An Egalitarian-BicaudalD complex is essential for oocyte specification and axis determination in *Drosophila*. *Genes Dev.* **11**, 423–435.

**Margolis, J. S., Borowsky, M., Shim, C. W. and Posakony, J. W.** (1994). A small region surrounding the distal promoter of the *hunchback* gene directs maternal expression. *Dev. Biol.* **163**, 381–388.

**Nag, R. N., Niggli, S., Sousa-Guimarães, S., Vazquez-Pianzola, P. and Suter, B.** (2018). *Mms19* is a mitotic gene that permits Cdk7 to be fully active as a Cdk-activating kinase. *Development* **145**, dev156802.

**Paré, C. and Suter, B.** (2000). Subcellular localization of Bic-D::GFP is linked to an asymmetric oocyte nucleus. *Journal of Cell Science* **113 ( Pt 12)**, 2119–2127.

**Payne, C., Rawe, V., Ramalho-Santos, J., Simerly, C. and Schatten, G.** (2003). Preferentially localized dynein and perinuclear dynactin associate with nuclear pore complex proteins to mediate genomic union during mammalian fertilization. *Journal of Cell Science* **116**, 4727–4738.

**Pérez-Mongiovi, D., Malmanche, N., Bousbaa, H. and Sunkel, C.** (2005). Maternal expression of the checkpoint protein BubR1 is required for synchrony of syncytial nuclear divisions and polar body arrest in *Drosophila melanogaster*. *Development* **132**, 4509–4520.

**Raaijmakers, J. A. and Medema, R. H. (2014).** Function and regulation of dynein in mitotic chromosome segregation. *Chromosoma* 123, 407–422.

**Radford, S. J. and McKim, K. S.** (2016). Techniques for Imaging Prometaphase and Metaphase of Meiosis I in Fixed *Drosophila* Oocytes. *J Vis Exp* e54666.

**Ran, B., Bopp, R. and Suter, B.** (1994). Null alleles reveal novel requirements for *Bic-D* during *Drosophila* oogenesis and zygotic development. *Development* **120**, 1233–1242.

**Rashpa, R., Vazquez-Pianzola, P., Colombo, M., Hernandez, G., Beuchle, D., Berger, F., Peischl, S., Bruggmann, R. and Suter, B.** (2017). *Cbp80* is needed for the expression of piRNA components and piRNAs. *PLoS ONE* **12**, e0181743.

**Rieder, C. L. and Maiato, H.** (2004). Stuck in division or passing through: what happens when cells cannot satisfy the spindle assembly checkpoint. *Dev. Cell* **7**, 637–651.

**Royle, S. J.** (2012). The role of clathrin in mitotic spindle organisation. *Journal of Cell Science* **125**, 19–28.

**Royle, S. J. and Lagnado, L.** (2006). Trimerisation is important for the function of clathrin at the mitotic spindle. *Journal of Cell Science* **119**, 4071–4078.

**Royle, S. J., Bright, N. A. and Lagnado, L.** (2005). Clathrin is required for the function of the mitotic spindle. *Nature* **434**, 1152–1157.

**Sallés, F. J., Lieberfarb, M. E., Wreden, C., Gergen, J. P. and Strickland, S.** (1994). Coordinate initiation of *Drosophila* development by regulated polyadenylation of maternal messenger RNAs. *Science* **266**, 1996–1999.

**Sawicka, A. and Seiser, C.** (2012). Histone H3 phosphorylation - a versatile chromatin modification for different occasions. *Biochimie* **94**, 2193–2201.

**Schulz, C. and Tautz, D.** (1995). Zygotic *caudal* regulation by *hunchback* and its role in abdominal segment formation of the *Drosophila* embryo. *Development* **121**, 1023–1028.

**So, C., Seres, K. B., Steyer, A. M., Mönnich, E., Clift, D., Pejkovska, A., Möbius, W. and Schuh, M.** (2019). A liquid-like spindle domain promotes acentrosomal spindle assembly in mammalian oocytes. *Science* **364**, eaat9557.

**Sokac, A. M. and Wieschaus, E.** (2008). Local actin-dependent endocytosis is zygotically controlled to initiate *Drosophila* cellularization. *Dev. Cell* **14**, 775–786.

**Splinter, D., Razafsky, D. S., Schlager, M. A., Serra-Marques, A., Grigoriev, I., Demmers, J., Keijzer, N., Jiang, K., Poser, I., Hyman, A. A., et al.** (2012). BICD2, dynactin, and LIS1 cooperate in regulating dynein recruitment to cellular structures. *Mol. Biol. Cell* 23, 4226–4241.

**Suter, B. and Steward, R.** (1991). Requirement for phosphorylation and localization of the Bicaudal-D protein in *Drosophila* oocyte differentiation. *Cell* **67**, 917–926.

**Suter, B., Romberg, L. M. and Steward, R.** (1989). *Bicaudal-D*, a *Drosophila* gene involved in developmental asymmetry: localized transcript accumulation in ovaries and sequence similarity to myosin heavy chain tail domains. *Genes Dev.* **3**, 1957–1968.

**Swan, A. and Suter, B.** (1996). Role of *Bicaudal-D* in patterning the *Drosophila* egg chamber in mid-oogenesis. *Development* **122**, 3577–3586.

**Tinevez, J.-Y., Perry, N., Schindelin, J., Hoopes, G. M., Reynolds, G. D., Laplantine, E., Bednarek, S. Y., Shorte, S. L. and Eliceiri, K. W.** (2017). TrackMate: An open and extensible platform for single-particle tracking. *Methods* 115, 80–90.

**Vazquez-Pianzola, P. and Suter, B.** (2012). Conservation of the RNA Transport Machineries and Their Coupling to Translation Control across Eukaryotes. *Comp. Funct. Genomics* **2012**, 287852–13.

**Vazquez-Pianzola, P., Adam, J., Haldemann, D., Hain, D., Urlaub, H. and Suter, B.** (2014). Clathrin heavy chain plays multiple roles in polarizing the *Drosophila* oocyte downstream of *Bic-D. Development* **141**, 1915–1926.

**Vazquez-Pianzola P., Suter B., Hernández G.** (2016) Evolution of the Molecules Coupling mRNA Transport with Translational Control in Metazoans. In: Evolution of the Protein Synthesis Machinery and Its Regulation (ed. G.Hernández R. Jagus), pp. 531-546. New York.

**Vazquez-Pianzola, P., Schaller, B., Colombo, M., Beuchle, D., Neuenschwander, S., Marcil, A., Bruggmann, R. and Suter, B.** (2017). The mRNA transportome of the BicD/Egl transport machinery. *RNA Biol* **14**, 73–89.

**Vazquez-Pianzola, P., Urlaub, H. and Suter, B.** (2011). Pabp binds to the *osk* 3'UTR and specifically contributes to *osk* mRNA stability and oocyte accumulation. *Dev. Biol.* **357**, 404–418.

**Westermann, B. and Neupert W.** (2000). Mitochondria-targeted green fluorescent proteins: convenient tools for the study of organelle biogenesis in *Saccharomyces cerevisiae*. *Yeast* 16(15): 1421-1427.

**Wharton, R. P. and Struhl, G.** (1989). Structure of the *Drosophila* BicaudalD protein and its role in localizing the posterior determinant *nanos. Cell* **59**, 881–892.

**Wojcik, E., Basto, R., Serr, M., Scaërou, F., Karess, R. and Hays, T.** (2001). Kinetochore dynein: its dynamics and role in the transport of the Rough deal checkpoint protein. *Nat. Cell Biol.* **3**, 1001–1007.

# Figures

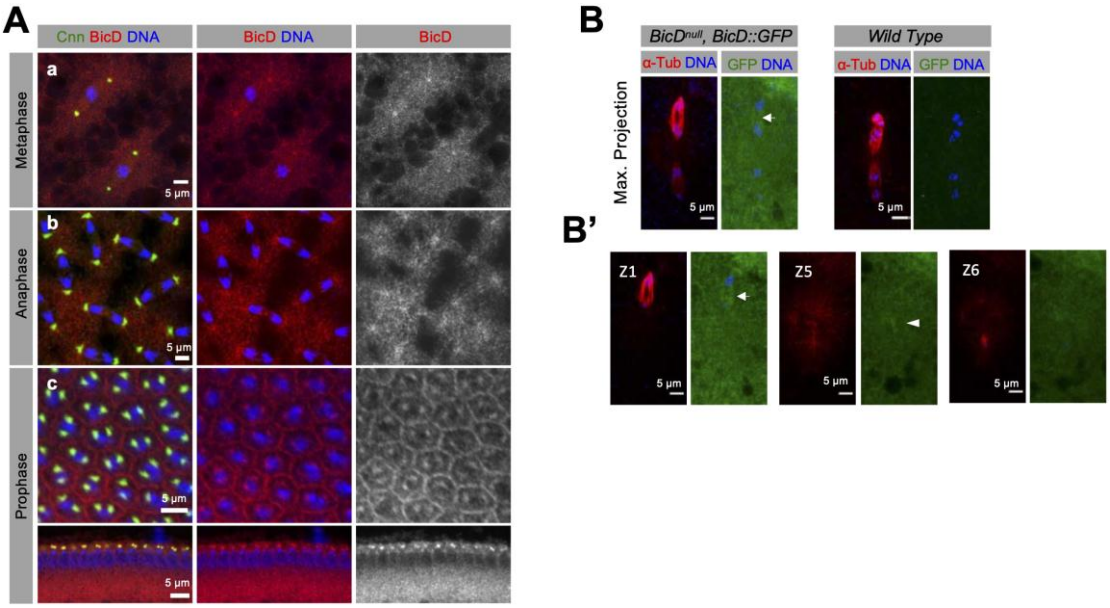


**Figure 1. BicD localizes to mitotic spindles and centrosomes, and the female meiotic II spindles. (A)** BicD (red) is present at metaphase spindles and colocalized with the pericentrosomal marker Cnn (green). Wild-type embryos in nuclear cycle 10 (NC10) (a), NC12 (b) and during cellularization (NC14) (c ) are shown. **(B, B')** A AII tandem spindle is shown. BicD::GFP (detected with anti-GFP antibodies) is enriched in the region of the tandem spindles (arrow marks the most superficial spindle) and the central aster (arrowhead) above cytoplasmic levels. Embryos were also stained for anti-α-tubulin (red). Enrichment at the most superficial spindle is only detected in the maximum projection image due to the high cytoplasmic levels of BicD::GFP in the upper frames. BicD::GFP signal at the central aster becomes more evident when the deeper Z-planes are analyzed (**B'**; see Z5, Z6; arrowhead). Hoechst (blue) shows the DNA in all embryos.

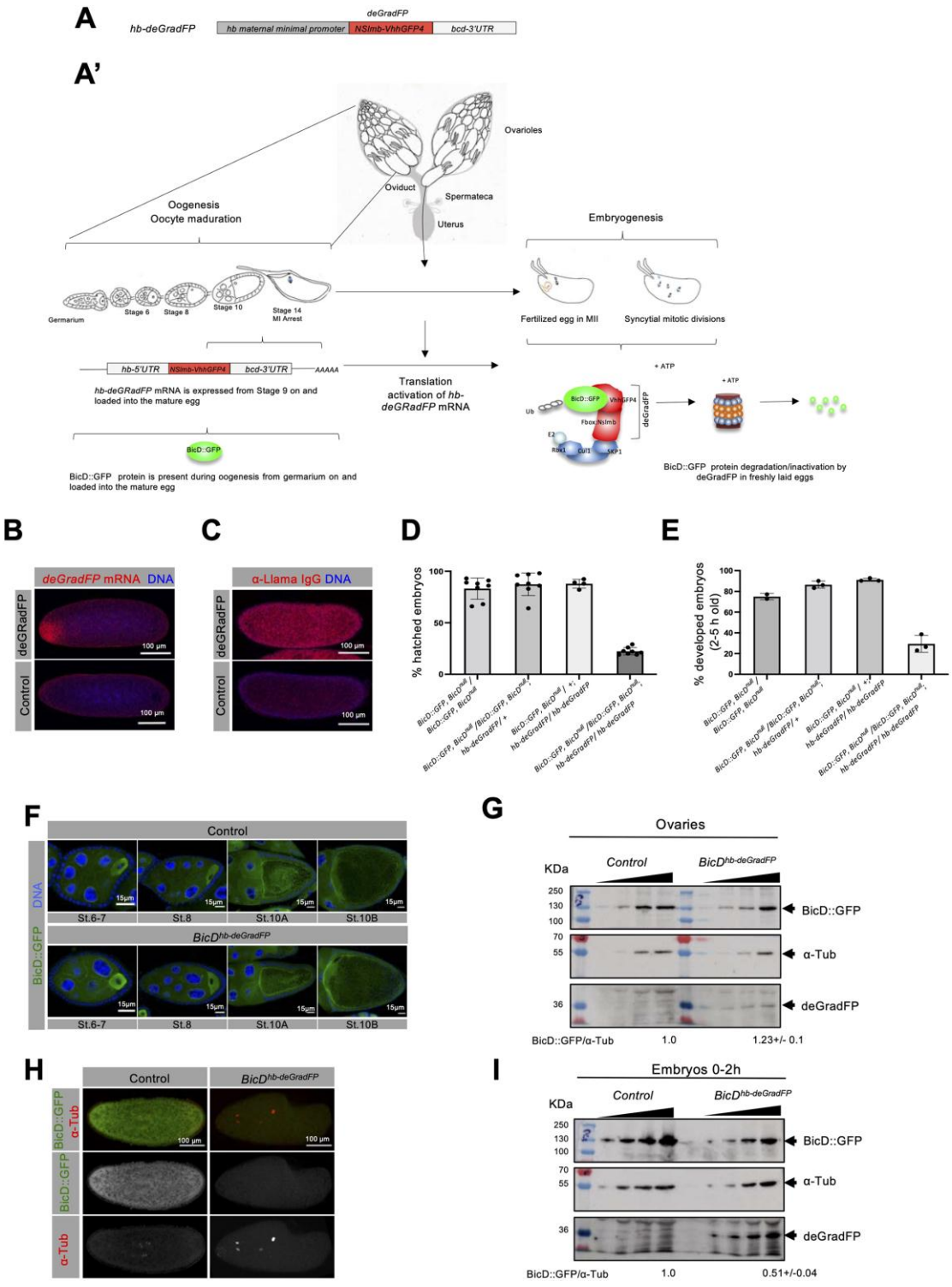


**Figure 2. *hb-deGradFP* degrades BicD::GFP specifically in freshly laid eggs, causing early developmental arrest. (A)** Scheme depicting the construct expressed in flies. **(A')** Model of its mechanism of action**. (B)** RNA FISH detects the *deGradFP* mRNA (red) enriched in the anterior region of freshly laid embryos. **(C)** The deGradFP construct (red

signal) is ubiquitously present in young embryos. Wild-type embryos without the *deGradFP* transgene were used as negative controls in B and C. **(D)** Percentage of embryos of the depicted maternal genotype that hatched as larvae. **(E)** Percentage of normally developed embryos laid by the indicated mothers. **(F-I)** Ovaries and embryos produced from control (*BicD::GFP*, $BicD^{null}$) and $BicD^{hb\text{-}deGradFP}$ females were used. **(F)** Shows BicD::GFP fluorescence signal (green). **(H)** BicD::GFP was detected using anti-GFP antibodies (green). Embryos were staged by anti-α-tubulin staining (red). **(G, I)** Western blots showing BicD::GFP and deGradFP levels in ovaries **(H)** and 0-2h old embryos **(I)**. Increasing amounts of cytoplasmic extracts were loaded for each sample (loading control: α-tubulin). Relative abundance of BicD::GFP/α-tubulin, normalized to the control, was calculated for the last 2 lanes. Hoechst (blue) shows the DNA in IF experiments. The deGradFP expression was detected using an anti-Llama serum that recognizes the Vhh GFP expressed from this construct.

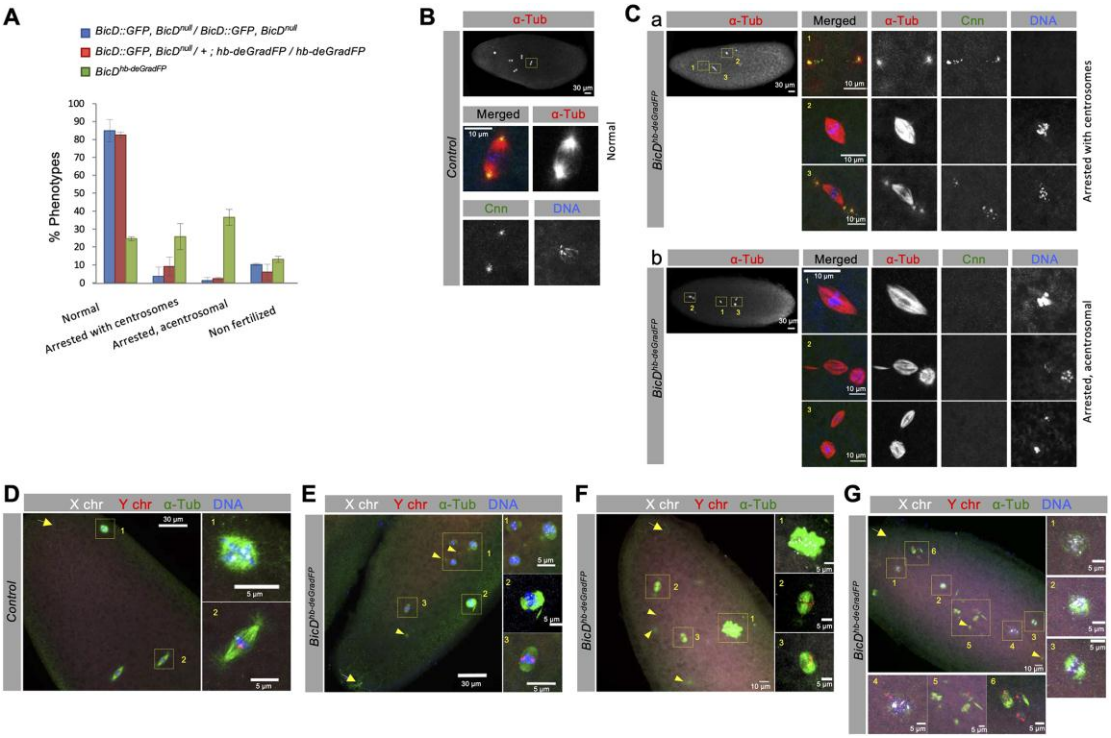


**Figure 3. Fertilized *BicD*$^{hb\text{-}deGradFP}$ embryos arrest at the start of embryogenesis with abnormal spindles, over-replicated female meiotic products, and without pronuclear fusion. (A-C)** 30-60 min old embryos with the indicated maternal genotypes stained for α-tubulin (red), Cnn (green), and DNA (blue). **A)** Percentage of embryos displaying the different phenotypes. The genotypes of their mothers are indicated. Embryos were characterized as unfertilized when no internal nuclei were seen and the 4 polar bodies, arranged in rosette-like structures (mostly fused into a single one), were observed at the surface of the embryo. Two independent collections (n1 and n2) were analyzed**.** Error bars show the SD. For *BicD::GFP, BicD*$^{null}$*/BicD::GFP, BicD*$^{null}$ *n1=84, n2=82.* For *BicD::GFP, BicD*$^{null}$*/+; hb-deGradFP/hb-deGradFP n1=55, n2=70.* And for *BicD*$^{hb\text{-}deGradFP}$ *n1=42, n2=63.* (**B-C***)* Examples of the observed phenotypes**. (B)** Normal nuclear divisions in a control embryo (from a *BicD::GFP, BicD*$^{null}$ mother)**. (C)** Overview of the spindles seen in *BicD*$^{hb\text{-}deGradFP}$ embryos classified as "arrested with centrosomes" (a) or as "arrested, acentrosomal" (b). **(D-G)** DNA FISH with X (white) and Y (red) chromosomal probes and stained for α-tubulin (green) and DNA (blue). Arrows mark the sperm tails and arrowheads

free centrosomes. **(D)** Example of a control wild-type male embryo in the 2nd mitotic metaphase. **(E-G)** Examples of arrested *BicD*$^{hb\text{-}deGradFP}$ male embryos. Images are z-stack projections through the nuclei and yellow boxes mark the corresponding magnified nuclei.

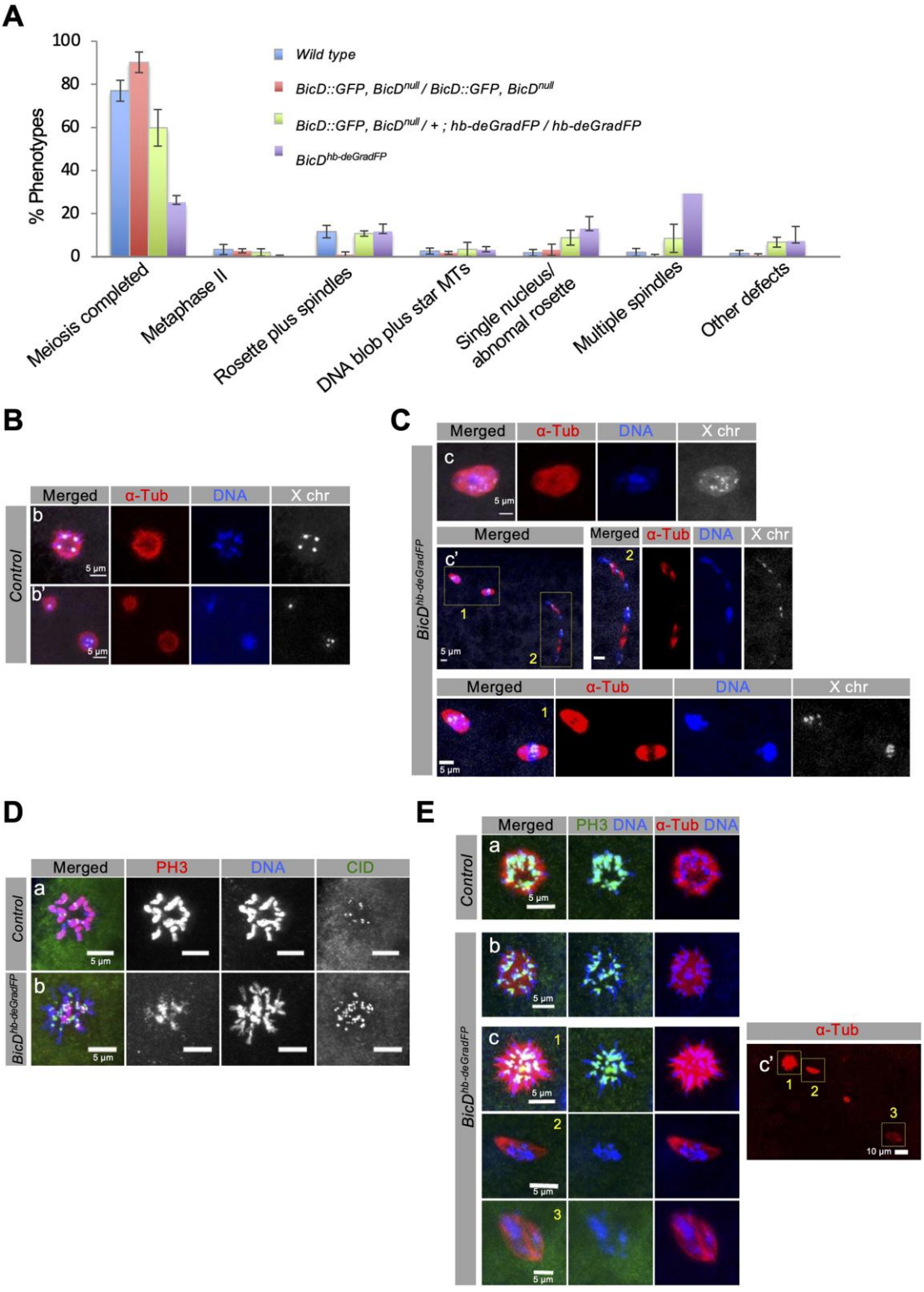

**Figure 4. Female meiotic products fail to arrest in metaphase and undergo extra rounds of replication in unfertilized *BicD*$^{hb\text{-}deGradFP}$ eggs.**

**(A)** 0-1 h old unfertilized eggs from the depicted mothers stained for α-tubulin (red) and DNA (blue) and classified as follows. 1) eggs that apparently completed meiosis normally (up to four rosette like structures that normally fuse into one single rosette); 2) eggs displaying a normal metaphase II tandem spindle; 3) eggs presenting 1-2 rosette like structures plus 1-2 spindles (probably representing normal meiosis intermediate products); 4) eggs with a big DNA blob surrounded by a star of microtubules (MT); 5) eggs containing one single nucleus/ abnormal rosette; 6) eggs containing several spindles; 7) eggs with other defects. Error bars show the SD of three to four independent egg collections (n1 to n4). For *Wild type*, n1= 145, n2=95, n3=67; for *BicD::GFP*, *BicD*$^{null}$*/BicD::GFP*, n1=92, n2=72, n3=147*;* for *BicD*$^{null}$, *BicD::GFP/ +; hb-deGradFP /hb-deGradFP*, n1=68, n2=46, n3= 69, n4=67*;* for *BicD*$^{hb\text{-}deGradFP}$, *n1=29, n2=45, n3=32* were scored. **(B-C)** Eggs from the same parents as in A) subjected to FISH to detect the X chromosome (white) and stained for α-tubulin (red) and DNA (blue). **(B)** Meiotic products in control eggs (*BicD::GFP*, *BicD*$^{null}$), fused into a single **(b)** or two rosette-like structures **(b'). (C) (c)** *BicD*$^{hb\text{-}deGradFP}$ egg with a single abnormal rosette-like structure. **(c')** *BicD*$^{hb\text{-}deGradFP}$ egg with more than four meiotic products. **(D)** Unfertilized wild-type and *BicD*$^{hb\text{-}deGradFP}$ eggs stained for CID (green, marking centromeres), PH3 (red) and DNA (blue). 100% (12/12 confocal images) of the single fused rosette nuclei in control eggs showed strong PH3 staining along the entire chromosomes. In 90,9 % (10/11) of these structures in *BicD*$^{hb\text{-}deGradFP}$ the signal was only enriched at the rosette central region. 86% (6/7 confocal images) of the single fused rosette-like nuclei in control eggs showed normal CID staining. In contrast, 63.7 % (7/11) of these structures in *BicD*$^{hb\text{-}deGradFP}$ eggs showed an increased number of CID-positive dots. **(E)** Eggs were stained for α-tubulin (red), PH3 (green), and DNA (blue). Images are z-stack projections through the nuclei and yellow boxes mark the corresponding magnified nuclei.

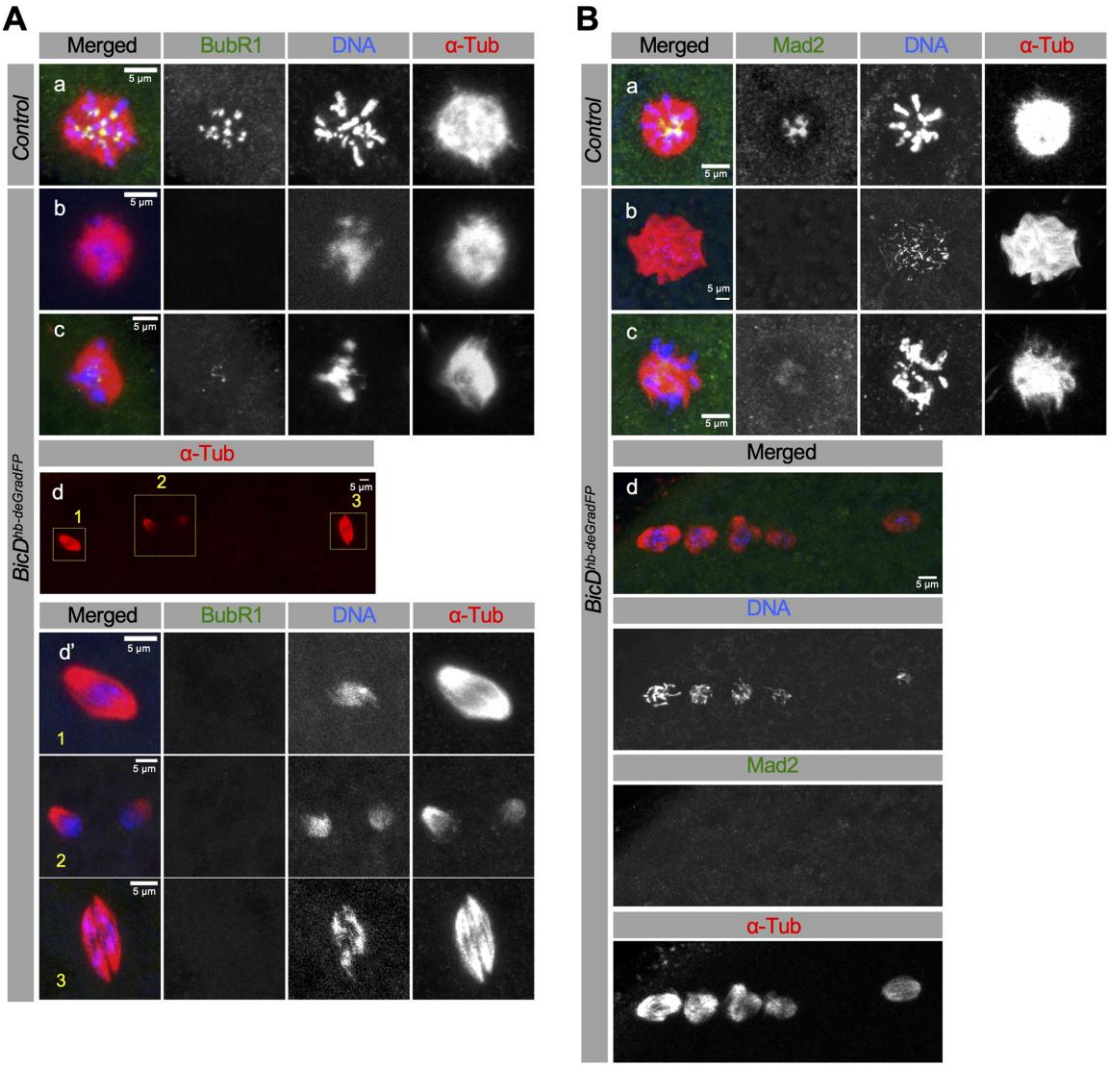


**Figure 5. BicD contributes to the recruitment of the SAC components BubR1 and Mad2 to the female meiotic products.** 0-1 h old unfertilized eggs stained for α-tubulin (red), DNA (blue) and BubR1 **(A)** or Mad2 **(B)** (green). Control meiotic products (either from wild-type (in Aa) or *BicD::GFP, BicD*$^{null}$ (in Ba) eggs) fused into a single rosette showed BubR1**(Aa)** and Mad2 **(Ba)** staining at the kinetochores. *BicD*$^{hb\text{-}deGradFP}$ egg containing a unique rosette-like polar body without BubR1 **(Ab)** or Mad2 **(Bb)** signals. *BicD*$^{hb\text{-}deGradFP}$ egg with only one polar body that stains only weakly for BubR1 **(Ac)** or Mad2 **(Bc).** *BicD*$^{hb\text{-}deGradFP}$ eggs where the female meiotic products have replicated and don't stain for BubR1 **(Ad,d')** or Mad2 **(Bd).** (**Ad'**) magnified images of the indicated nuclei in Ad. Images are z-stack projections through the nuclei.

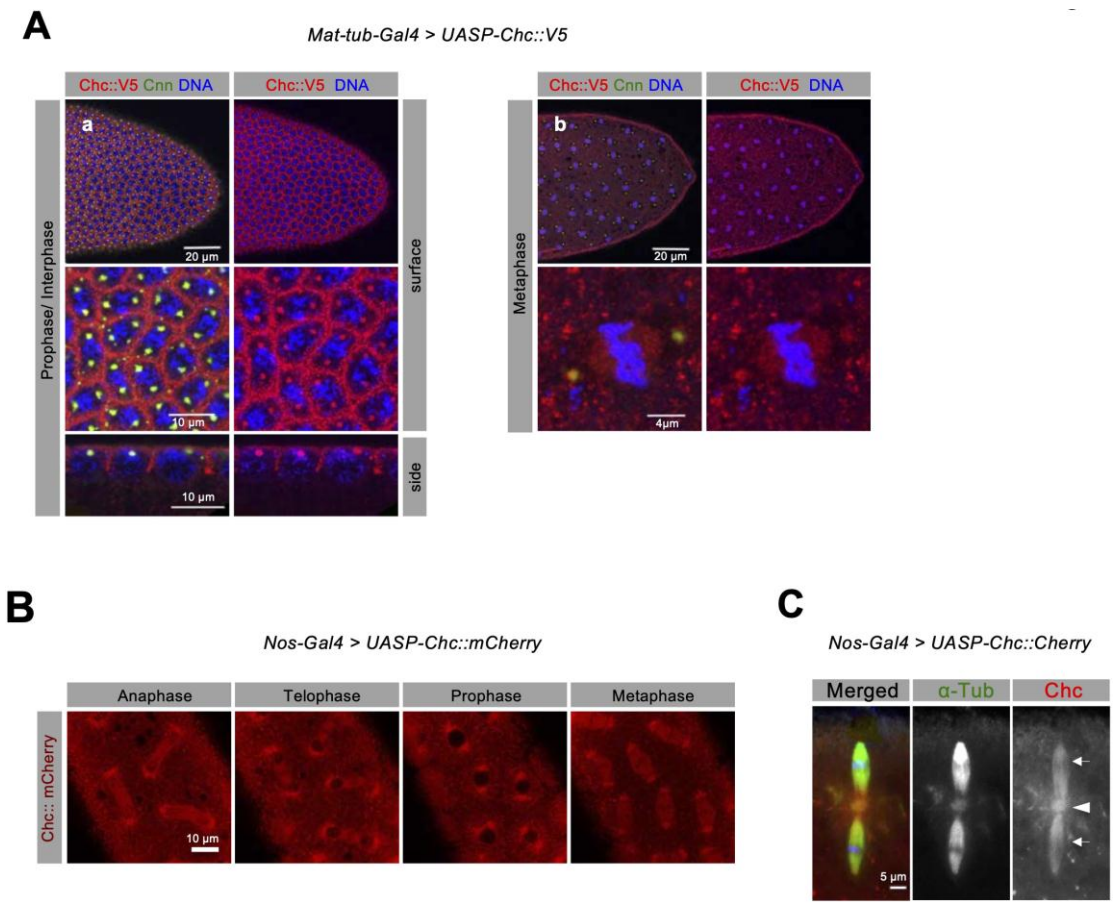


**Figure 6. Chc localizes to centrosomes and spindles during mitosis, and to meiotic II spindles. (A)** Chc::V5 expressing embryos stained for V5 (red) and Cnn (green). A cellular blastoderm (a) and an embryo in metaphase of NC13 are shown (b). **(B)** Live imaging of Chc::mCherry expressing embryos. **(C)** Chc::mCherry, detected with anti-mCherry antibodies (red), is present along both MII tandem spindles (arrows) and at the central aster (arrowhead).

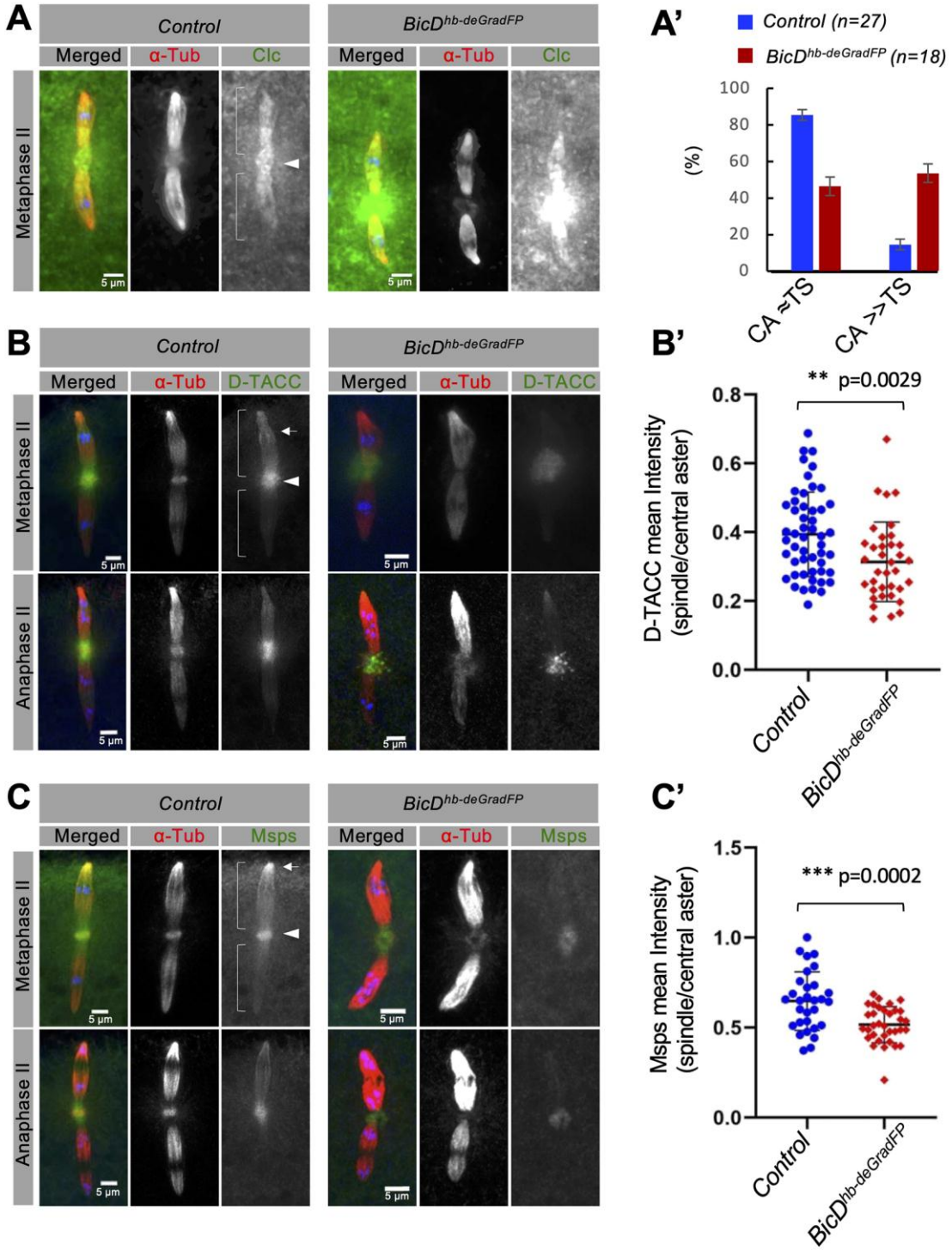


**Figure 7. Proper localization of D-TACC, Msps, and clathrin at MII tandem spindles requires BicD.**

Controls (laid by wild-type mothers for (A) or homozygous *BicD::GFP*, *BicD*$^{null}$ (B-C)) and *BicD*$^{hb\text{-}deGradFP}$ embryos stained for α-tubulin (red) and either Clc **(A),** D-TACC **(B)** or Msps

**(C)** (green). DNA is shown in blue. The tandem spindles (brackets), spindle minus (arrow in C) and plus-ends (arrow in B) and the central aster (arrowheads) are indicated. **(A)** Maximum intensity projection images subjected to depth correction (see Methods) are shown. Clc hyper-accumulates at the central aster *in* $BicD^{hb\text{-}deGradFP}$eggs. (A') Percentage of embryos showing similar signal intensity along the tandem spindles (TS) and the central aster (CA) (CA ≈TS), and embryos with hyper-accumulation of Clc at the central aster (CA>>TS) is shown for both genotypes. n= sum of embryos scored for each genotype. Control: n1=16, n2=18, $BicD^{hb\text{-}deGradFP}$: n1=14, n2=10; 2 experiments. Two independent researchers performed the qualitative scoring blindly. **(B-C)** Maximum intensity projection images are shown. The signal on the most superficial spindle (image top) is often stronger than the signal from the inner spindle due to the depth of the sample and antibody penetration issues. The signal in the inner spindle is also often masked by the cytoplasmic signal above. Compared to the signal intensity in the central aster, D-TACC and Msps signals on the $BicD^{hb\text{-}deGradFP}$ spindles are reduced. **(B', C')** The mean fluorescent signal intensity ratio (signal in the most superficial spindle vs signal in central aster) for D-TACC (B') and Msps (C') was quantified for each imaged MII and AII spindle. Data are presented as mean ± SD. Statistical significance and p values were determined by the Student's unpaired test. (B') Control: n=51, $BicD^{hb\text{-}deGradFP}$: n=36; 3 experiments. (C') Control: n=30, $BicD^{hb\text{-}deGradFP}$: n=34; 2 experiments.

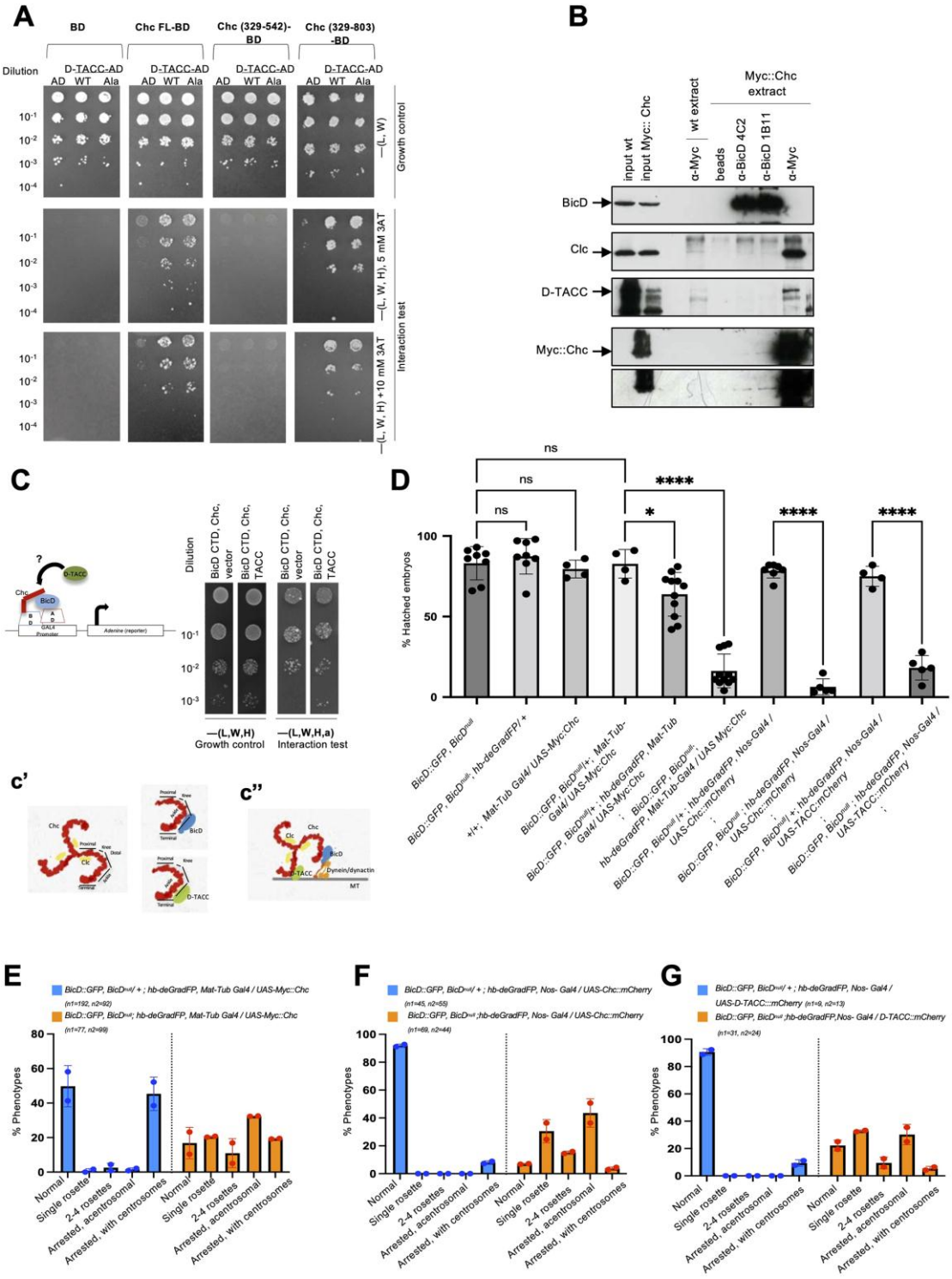


**Figure 8.** ***Drosophila*** **Chc binds to D-TACC through the same domain it interacts with BicD, and** ***BicD*** **and** ***Chc*** **genetically interact in embryos. (A)** Yeast two-hybrid interaction tests (Y2H). Full-length (FL) and partial Chc fragments (Chc$^{329\text{-}542}$ and Chc$^{329\text{-}803}$), respectively, were fused to the DNA binding domain (BD). Full-length D-TACC wild-type

(WT) and *D-TACC*$^{S863A}$ were fused to the activator domain (AD). Empty vectors served as negative controls. **(B)** IP of total embryo extracts expressing a Myc-tagged Chc fusion protein (Myc::Chc). Antibodies used for the IPs are indicated on top. Beads alone and anti-Myc pull-downs in wild-type (wt) embryo extracts were done as negative controls. Western blots of the IP material tested for the presence of BicD, Clc, D-TACC and Myc::Chc. Input represents 0.15% of the cytoplasmic extract used for each IP. Bottom panel shows a longer exposure of the Myc::Chc blot. **(C)** Interaction between BicD CTD-AD and Chc full length fused to the BD was tested in the presence of either empty vector or a vector expressing D-TACC. A diagram of interaction tested is shown and serial dilutions are presented. The co-expression of TACC increases the BicD-CTD/Chc interaction. (c') Models depicting the interactions between Chc, Clc, BicD and D-TACC. Chc is known to form trimers with Clc (triskelion). BicD and D-TACC bind both to the Ankle region of Chc. (c'') Model for the formation of putative ternary complexes on the MT is shown. **(D)** Percentage of embryos that hatched into larvae (their maternal genotypes are indicated). Note that an increase of the number of embryos arrested in embryogenesis was even observed in embryos expressing a wild-type copy of *BicD* when Chc was expressed under the strong maternal tubulin promoter.

Error bars show the SD. 50 to 200 eggs were counted for each replicate. Statistical significance and p values were determined by one-way Anova test. **(E-G)** 30-60 min old embryos with the indicated maternal genotypes stained for α-tubulin (red), Cnn (green), and DNA (blue). Percentage of embryos displaying the different phenotypes. Although the ratio of the number of eggs arrested with centrosomes compared to the ones without vary in the different genotypes (since overexpression of Chc and D-TACC increased the frequency of unfertilized eggs), the eggs show a similar early arrest phenotype as observed in *BicD*$^{hb\text{-}deGradFP}$. Two independent collections were analyzed**.** Error bars show the SD.

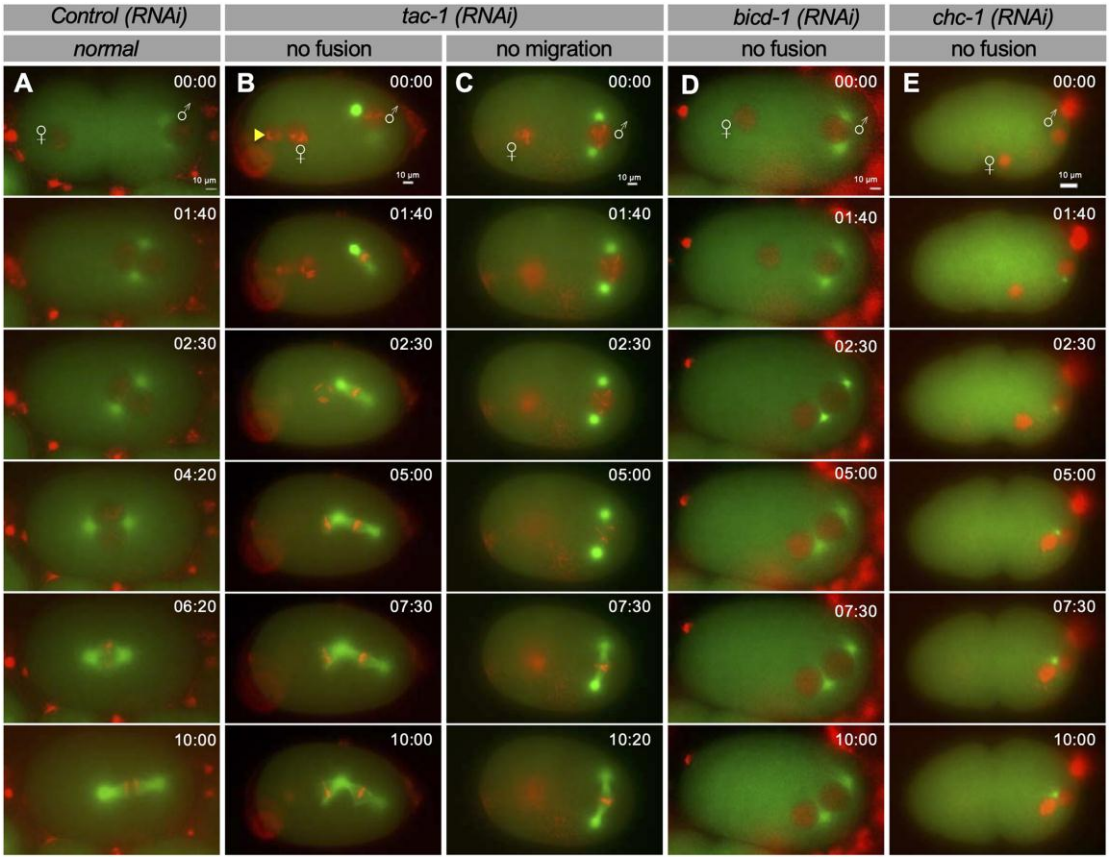


**Figure 9. *C. elegans chc-1, bicd-1* and *tac-1* are required for pronuclear fusion.**

Time-lapse images of embryos expressing *H2B::mCherry* and *α-tubulin::GFP*. Female and male pronuclei and the elapsed time (in minutes and seconds) from the start of the movie are indicated. **(A)** Control embryos grown on either regular food (6/6) or control empty vector RNAi food (14/15) progress normally from meiosis to the formation of the first mitotic spindle. The female pronucleus at the embryo anterior (left) and the male pronucleus and its two associated centrioles at the posterior (right) are indicated. The female pronucleus moves towards the posterior pole and the male pronucleus and both meet at the posterior. After centration and rotation the pronuclei fused to form the first mitotic spindle at the center of the zygote along the A-P axis. **(B-C)** *tac-1(RNAi)* embryos show meiosis and pronuclear fusion defects as previously described using DIC microscopy (Bellanger J. M. et al. 2007). **(B)** *tac-1(RNAi)* embryo showing abnormal meiosis with delayed polar body extrusion (arrowhead) and no pronuclear fusion (2/5 analyzed). The male pronucleus formed a spindle on its own at

the posterior pole, and both pronuclei met at the posterior pole forming a common spindle without pronuclear fusion. **(C)** *tac-1(RNAi)* embryo with normal meiosis but defective female pronuclear migration and no pronuclear fusion (2/5 embryos). The male pronucleus formed a spindle at the posterior pole. **(D)** Delayed female pronuclear migration was observed in a fraction of the *bicd-1(RNAi)* embryos (3/10). Although both pronuclei ultimately met at the posterior, they neither fused nor moved towards the center of the embryo. **(E)** Animals fed with *chc-1* dsRNA food looked sick and carried few progenies in the uterus. The few living *chc-1(RNAi)* embryos showed delayed female pronuclear migration, no pronuclear fusion and lack of centration (2/4 embryos). Additional phenotypes observed are described in Fig S14.

Supplementary Fig. S1

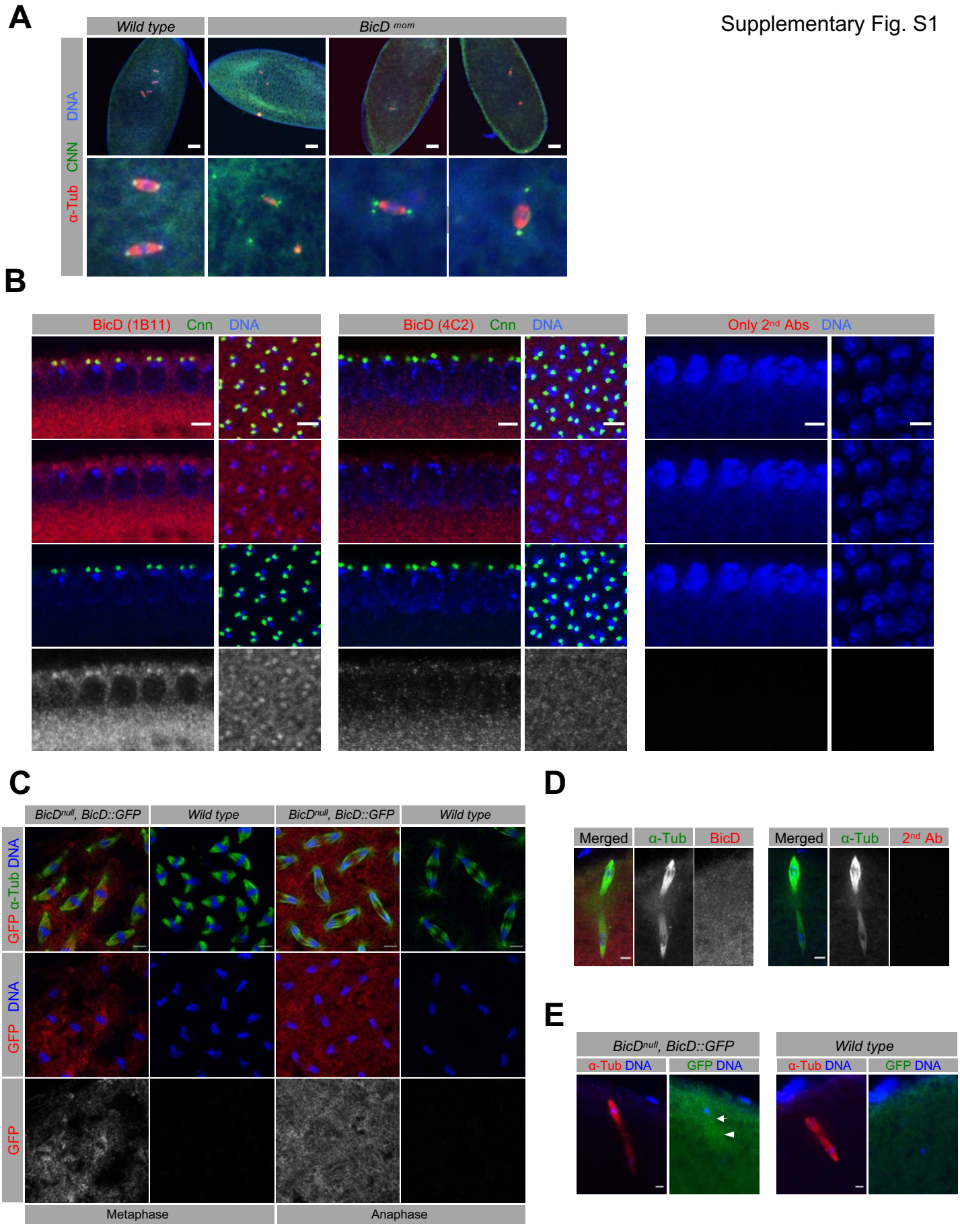

**Fig. S1. BicD localizes to mitotic spindles and centrosomes, and to meiotic II spindles. *BicD*$^{mom}$ embryos arrest during meiosis or the first mitotic divisions**. **(A)** Embryos laid by *BicD*$^{mom}$ females were fixed and subjected to immunostaining to detect α-tubulin (red), Cnn (green), and DNA (blue). Wild-type embryos were used as control. *BicD*$^{mom}$ embryos arrested in early embryogenesis displaying few spindles and rosette structures. Abnormal spindles with detached and multiple centrosomes were observed as well as centrosomes not associated with any DNA. Scale bars are 20 μm. **(B)** Wild-type embryos were stained using anti-BicD (either 1B11 or 4C2, red) and anti-Cnn antibodies (green). Embryos were also incubated without primary antibodies to control for unspecific binding of the secondary antibodies (2$^{nd}$ Ab control, right panels). BicD was detected specifically on centrosomes using the 1B11 antibody. Embryos in nuclear cycle 14 (NC14) are shown. Scale bars are 10 μm. **(C)** BicD::GFP expressing embryos were stained using anti-GFP (red) and anti-α-tubulin (green) antibodies. To control for unspecific binding of the antibodies, wild-type embryos were also stained. BicD::GFP is detected at centrosomes and spindles in syncytial blastoderm embryos. Scale bars are 5 μm. Embryos in NC11-12 are shown. **(D)** 0-5 min embryos were subjected to immunofluorescence to detect BicD, using the BicD 1B11 monoclonal antibodies. Incubation with the first antibody was omitted to control for the un-specific binding of the second antibody (2nd Ab control, right panels). In wild-type embryos, BicD (red) was detected in the cytoplasm but neither excluded from nor enriched at the meiotic spindles (anti-α-tubulin, green). **(E)** *BicD::GFP, BicD*$^{null}$ embryos were stained with anti-GFP (green) and anti-α-tubulin (red) antibodies. To control for unspecific binding of the antibodies, wild-type embryos were also stained. Maximum Z-projection of a meiotic metaphase MII tandem spindle is shown. BicD::GFP was detected on tandem spindles (arrow) and the central aster (arrowhead). Only enrichment at the most superficial spindle is detected in the maximum projection image due to the high cytoplasmic levels of BicD::GFP in the upper frames that mask the enrichment at the central aster and the internal spindle. Scale bars are 5 μm.

Supplementary Fig. S2

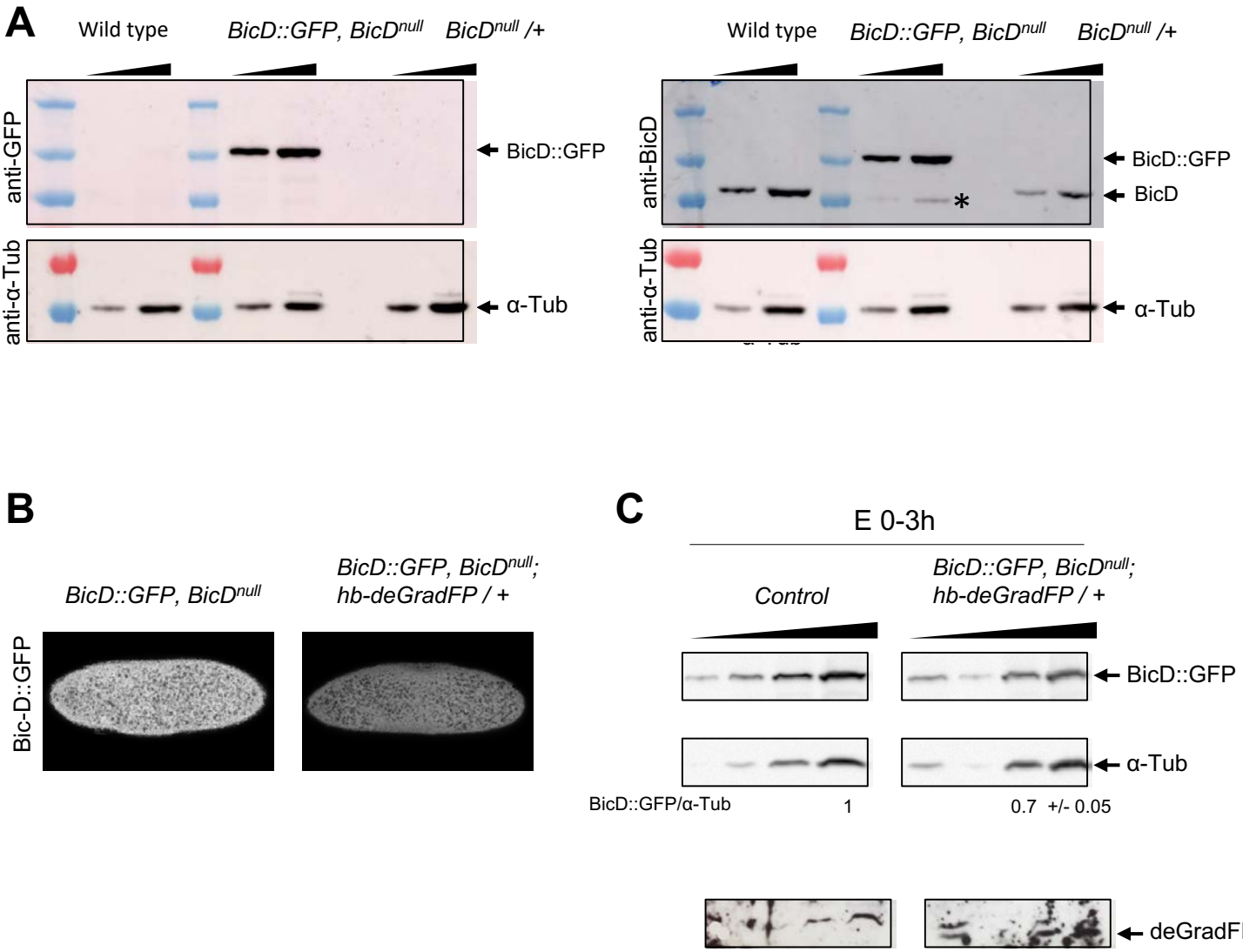

**Fig. S2. *BicD::GFP, BicD$^{null}$* females expressing only one copy of the hb-deGradFP construct produce embryos that develop normally and hatch into larvae. (A)** Western blots showing BicD and BicD::GFP levels in 0-2 h old embryos laid by mothers of the depicted genotypes using anti-BicD and anti-GFP antibodies, respectively. Increasing amounts of cytoplasmic extracts were loaded for each sample (loading control: α-tubulin). BicD::GFP is expressed at similar levels as wt BicD. *) Note that the band recognized by the BicD antibody in *BicD::GFP, BicD$^{null}$* extracts has a lower apparent molecular weight than wt BicD and may represent a degradation product of BicD::GFP that is cleaved at the C-terminal region since it is not recognized by the anti-GFP antibody. **(B)** Embryos laid by control (*BicD::GFP, BicD$^{null}$*) and rescued *BicD::GFP, BicD$^{null}$* females expressing only one copy of the hb-deGradFP construct (*BicD::GFP, BicD$^{null}$*; *hb-deGradFP*/+) were immunostained with anti-GFP antibodies. The ubiquitously reduced levels of GFP signal suggests ubiquitous degradation of the BicD::GFP protein in *BicD$^{hb\text{-}deGradFP}$* embryos. **(C)** Western blots showing BicD::GFP and deGradFP levels in 0-2 h old embryos using anti-GFP and anti-llama IgG antibodies, respectively. Increasing amounts of cytoplasmic extracts were loaded for each sample (loading control: α-tubulin). Relative abundance of BicD::GFP/α-tubulin was normalized to the control and calculated for the last 2 lanes. BicD levels in *BicD$^{hb\text{-}deGradFP}$* embryos were reduced by around 30% compared to control embryos and these embryos showed no developmental defects (Fig. 2 D-E).

Supplementary Fig. S3

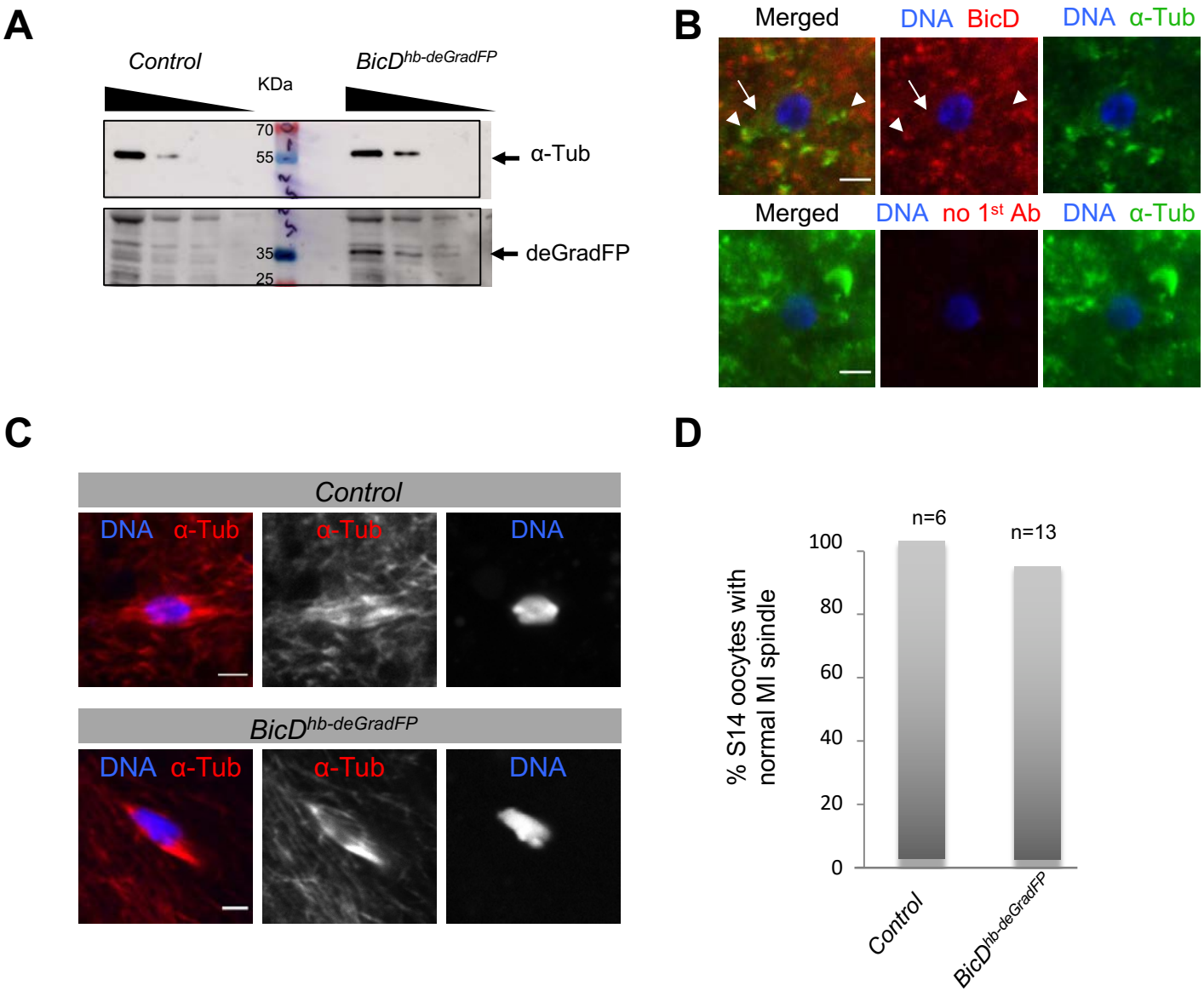

**Fig. S3. Although low levels of deGradFP protein are detected in ovaries of *BicD*$^{hb\text{-}deGradFP}$ females, *BicD*$^{hb\text{-}deGradFP}$ stage 14 oocytes show no apparent meiosis I defects. (A)** Ovaries from control (homozygous *BicD::GFP, BicD*$^{null}$) and *BicD*$^{hb\text{-}deGradFP}$ females were dissected in Robbs medium to prevent oocyte activation. They were then subjected to Western blotting using anti-llama IgG antibodies to detect the deGradFP fusion protein. α-tubulin was used as the loading control. **(B)** Wild-type stage 14 oocytes stained to detect α-tubulin (green), BicD (red), and DNA (blue). To control for unspecific binding of the secondary antibody, the anti-BicD antibody was omitted (lower panels). BicD was present in the cytoplasm, but it was also detected at metaphase I oocyte spindles (arrow) and anastral poles of the spindles (arrowheads). **(C)** Stage 14 oocytes from control (homozygous *BicD::GFP, BicD*$^{null}$) and *BicD*$^{hb\text{-}deGradFP}$ females were prepared and stained to detect α-tubulin (red) and DNA (blue). Metaphase I oocyte spindles were imaged. **(D)** Percentage of normally looking spindles for the depicted genotypes. Spindles were classified as normal, when they showed a normal bipolar appearance or as abnormal when multipolar spindles were observed. Images are confocal z-stack projections. Scale bars are 2 μm.

Supplementary Fig. S4

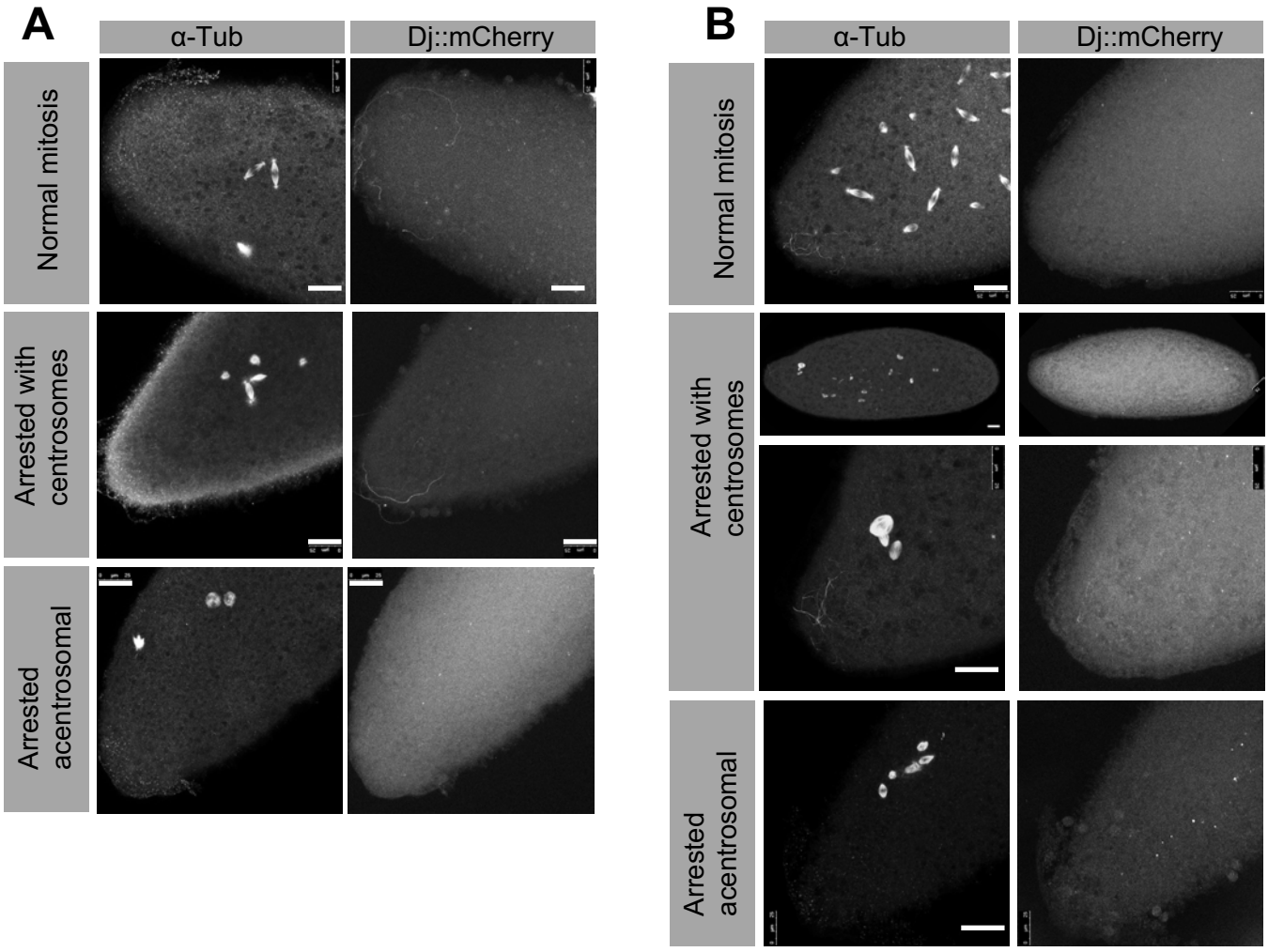


**Fig. S4. Arrested fertilized *BicD*$^{hb\text{-}deGradFP}$ eggs show abnormal spindles with centrosomes whereas non-fertilized *BicD*$^{hb\text{-}deGradFP}$ eggs have acentrosomal spindles. (A-B)** Virgin *BicD*$^{hb\text{-}deGradFP}$ females were crossed to males that expressed a fusion protein between Don Juan and mCherry (Dj::mCherry) under the control of the endogenous *Dj* promoter. Dj associates with sperm tails, and the fertilizing sperm tail ends up in the cytoplasm of the *Drosophila* egg (Santel et al., 1997). Embryos laid by these females were collected and stained to detect α-tubulin, too. mCherry fluorescence was preserved with MetOH fixation. **(A)** Dj::mCherry can be detected on the sperm tail only in young embryos (with few zygotic nuclei). **(B)** After Dj::mCherry is shed from the sperm tail during the early mitotic divisions, the presence of the sperm tail could still be followed for some time during the late syncytial divisions with α-tubulin staining. Images are confocal z-stack projections. Scale bars represent 25 μm.

Supplementary Fig. S5

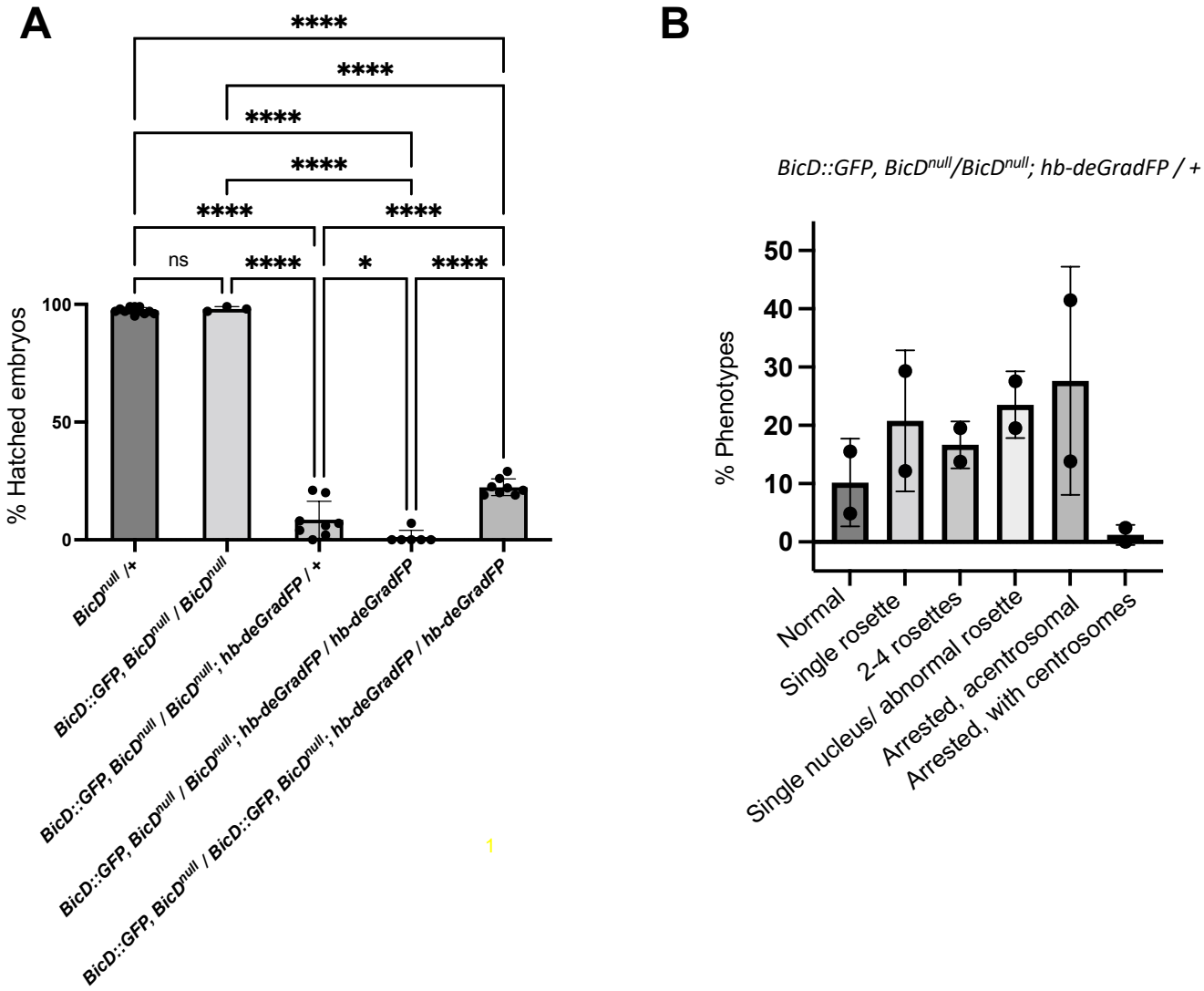


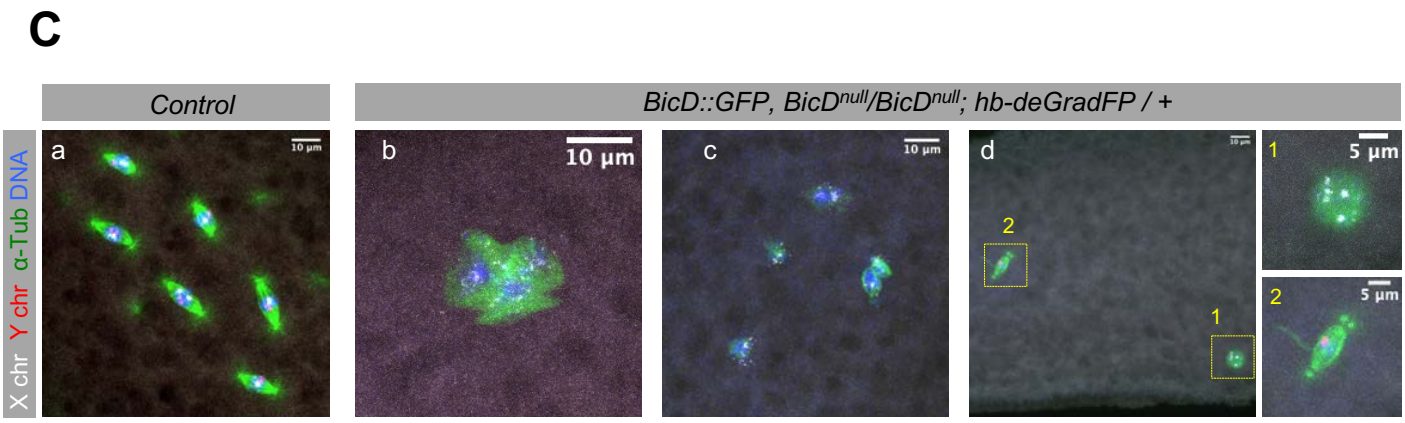

**Fig. S5. Eggs from females that express the *hb-deGradFP* in a rescue background with a single rescuing copy of *BicD::GFP* (to further reduce the BicD levels) show abnormal meiotic products and no pronuclear fusion, like *BicD*$^{hb\text{-}deGradFP}$ eggs. (A)** Percentage of embryos of the depicted maternal genotype that hatched as larvae. Females that express 2 copies of the *hb-deGradFP* and only one copy of the (*BicD*$^{null}$*, BicD::GFP/BicD*$^{null}$*; hb-deGradFP/hb-deGradFP* females) are mainly not viable. The few that do survive till adulthood, are unhealthy and most of them died shortly after eclosing, having too little time to lay sufficient eggs for an analysis of the phenotype. Almost all embryos laid by these females failed to hatch. Embryos laid by mothers with a single *hb-deGradFP* in the same *BicD* background (*BicD*$^{null}$*, BicD::GFP/BicD*$^{null}$*; hb-deGradFP/+)* hatched also at lower rates than *BicD*$^{hb\text{-}deGradFP}$ embryos (that expressed 2 copies of the rescue *BicD::GFP* and 2 *hb-deGradFP* copies). These females, too, seemed to have neurological problems, which probably affected their mating behavior since they laid mainly unfertilized eggs that arrested with abnormal spindles without centrosomes (see B). Error bars show the SD. 80 to 200 eggs were counted for each replicate for all genotypes except for *BicD*$^{null}$*/BicD*$^{null}$*, hb-deGradFP/ hb-deGradFP* were a total of 61 eggs from 6 overnight collection were analyzed. **(B)** 30 -60 min old embryos from *BicD::GFP, BicD*$^{null}$*/BicD*$^{null}$*; hb-deGradFP* / + mothers were stained for α-tubulin (red), the centrosome marker Cnn (green), and DNA (blue). Percentage of embryos displaying the different phenotypes. Two independent collections (n1= 41 and n2=58) were analyzed**.** Error bars show the SD. (**C***)* DNA FISH with X (white) and Y (red) chromosomal probes and stained for α-tubulin (green) and DNA (blue). Examples of the observed phenotypes**. (a)** Normal nuclear divisions in a control embryo (from a *BicD::GFP, BicD*$^{null}$ mother)**. (b-d)** Overview of the spindles seen in the *BicD::GFP, BicD*$^{null}$*/BicD*$^{null}$*; hb-deGradFP/+* embryos. **(b)** An egg classified as single "nucleus/ abnormal rosette" showing many signals for the X-Chromosome, indicating that this represents an unfertilized embryo where the meiotic products fused into a single nucleus and underwent replication/fragmentation. **(c)** Shows an egg classified as "arrested, acentrosomal", with 5 meiotic products that also had replicated and/or became fragmented. The evidence for this is that they have in total more than 4 X-chromosomal signals. **(d)** An example of an embryo "arrested with centrosomes" that did not undergo pronuclear fusion. Images are z-stack projections through the nuclei and yellow boxes mark the corresponding magnified nuclei.

Supplementary Fig. S6

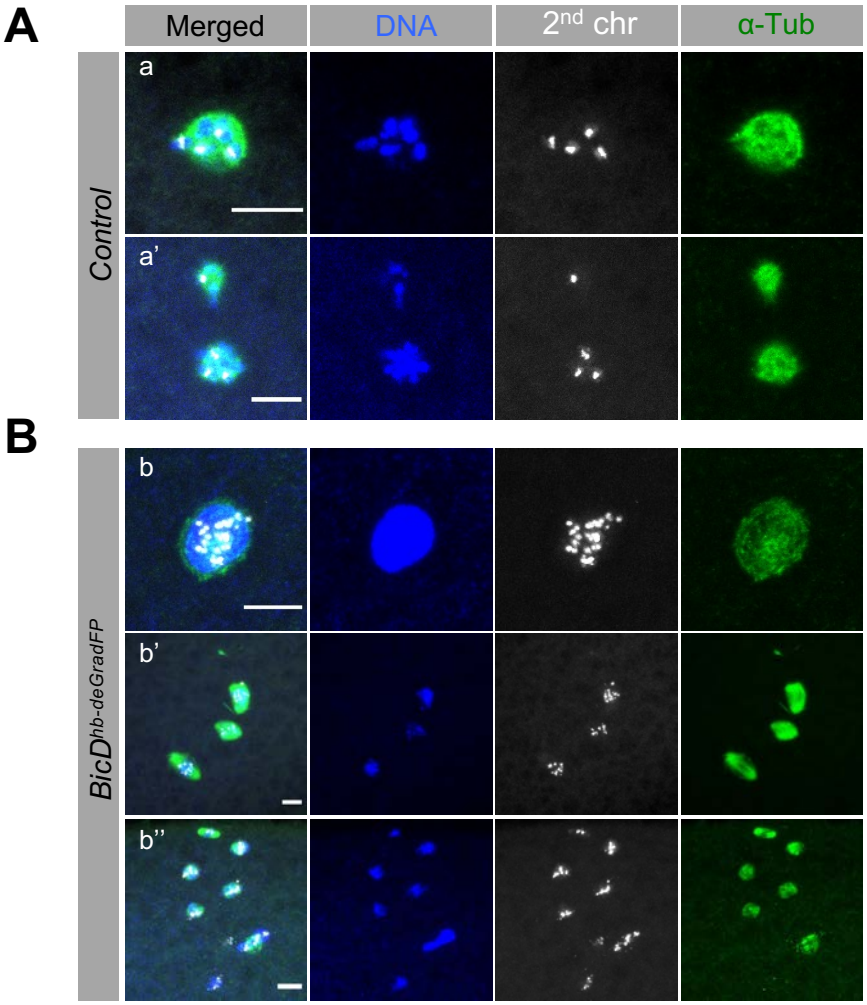

**Fig. S6. Unfertilized *BicD*$^{hb\text{-}deGradFP}$ eggs produce abnormal meiotic products that undergo extra rounds of replication.**

Control (homozygous *BicD::GFP, BicD*$^{null}$) and *BicD*$^{hb\text{-}deGradFP}$ virgin females were crossed to XO males to collect unfertilized eggs. Eggs were subjected to DNA *in situ* hybridization coupled to immunofluorescence to detect the presence of the 2$^{nd}$ chromosome (white), α-tubulin (green), and DNA (blue). **(A)** Eggs in control samples show normal completion of meiosis. Magnified pictures of the meiotic products observed in two different eggs are shown (a, a'). In a), the four meiotic products have fused into a single polar body with a rosette shape. In the egg depicted in a', the meiotic products have fused into two rosette-like structures. The polar bodies in each egg contain in total four dots of signal for the 2nd chromosome, corresponding to the four meiotic products that are produced after normal completion of meiosis II. **(B)** (b) Example of a *BicD*$^{hb\text{-}deGradFP}$ egg showing the presence of a single big nucleus without the typical rosette-like structure. The chromatin appears de-condensed with many signals for the 2$^{nd}$ chromosome. (b') A *BicD*$^{hb\text{-}deGradFP}$ egg that has three meiotic products without the typical rosette-like appearance. In all nuclei, the 2$^{nd}$ chromosome probe generates many dots. (b") Egg with many meiotic products marked with numerous 2$^{nd}$ chromosome signals. Images are confocal z-stack projections. Scale bars represent 10 μm.

Supplementary Fig. S7

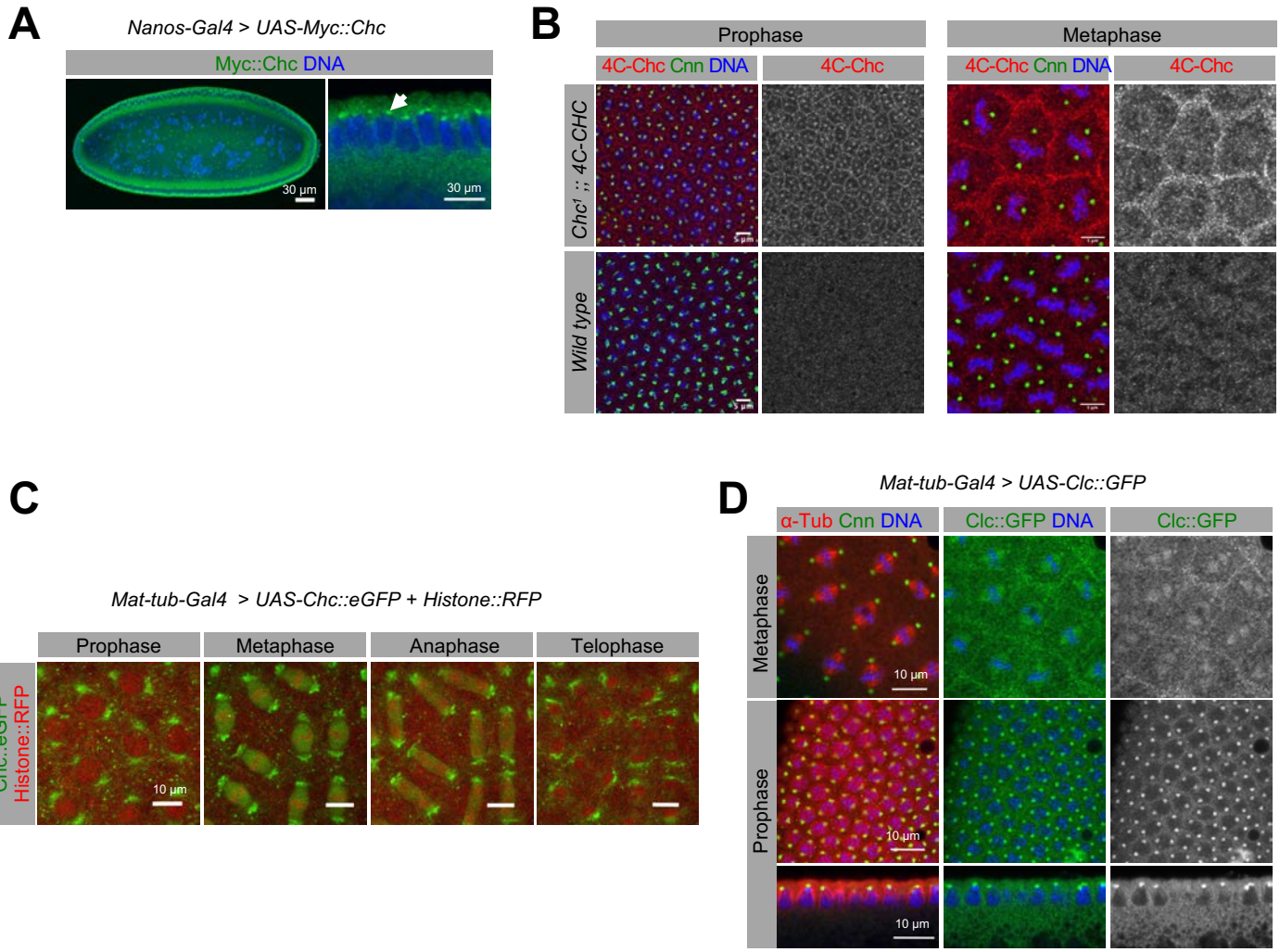

**Fig. S7. Chc and Clc localize to mitotic spindles and centrosomes throughout the cell cycle in syncytial *Drosophila* embryos. (A)** Localization of a Myc-tagged Chc fusion protein (green) in embryos laid by *Nanos-Gal4 > pUASP-Myc::Chc* females. Chc is enriched apically where it further accumulates in a single strong dot above each blastoderm nucleus (arrow) resembling the centrosome localization. Embryo in NC14 is shown. **(B)** Chc localization at the mitotic spindles and centrosomes, was not an overexpression artifact, because Flag-tagged Chc expressed under its own promoter in a *Chc* $^{null}$ background, showed the same localization pattern. Embryos laid by mothers homozygous for a lethal allele of *Chc (Chc*$^{1}$*),* but rescued with two copies of the Flag-tagged Chc (expressed from the 4C-CHC construct), were stained to detect Chc and the pericentrosomal marker Cnn using anti-Flag antibodies (red) and anti-Cnn antibodies (green), respectively. DNA is shown in blue. Both proteins co-localized at the centrosomes. Embryos in prophase of NC11 and metaphase embryos in NC9 (*wild type*) and NC8 (*Chc*$^{1}$, *4C-CHC*) are shown. **(C)** Live imaging of embryos expressing Chc::mCherry (upper panels) or embryos expressing a Chc::eGFP fusion protein (green) and histone-RFP (red; to visualize the chromosomes, lower panels). Chc::mCherry and Chc::eGFP localized to the centrosomes and spindles throughout the cell cycle. **(D)** Embryos from mothers expressing a Clathrin light chain (Clc) fused to GFP (Clc::GFP) under the maternal-Tubulin promoter were devitellinized by hand to preserve the Clc::GFP signal. They were then subjected to immunostaining to detect α-tubulin and Cnn. A magnified picture of a region of an embryo in metaphase of NC12 and another in prophase of NC14 are shown. Left panels show an overlay of the signals for α-tubulin (red), Cnn (green), and DNA (blue). Middle panels show the signal for DNA (blue) and Clc::GFP (green). Right panels show the signal for Clc::GFP in gray. Like Chc, Clc is localized to the mitotic spindles and centrosomes throughout the cell cycle. It is also enriched near the plasma membrane between the nuclei. The side view reveals an apical enrichment as well.

Supplementary Fig. S8

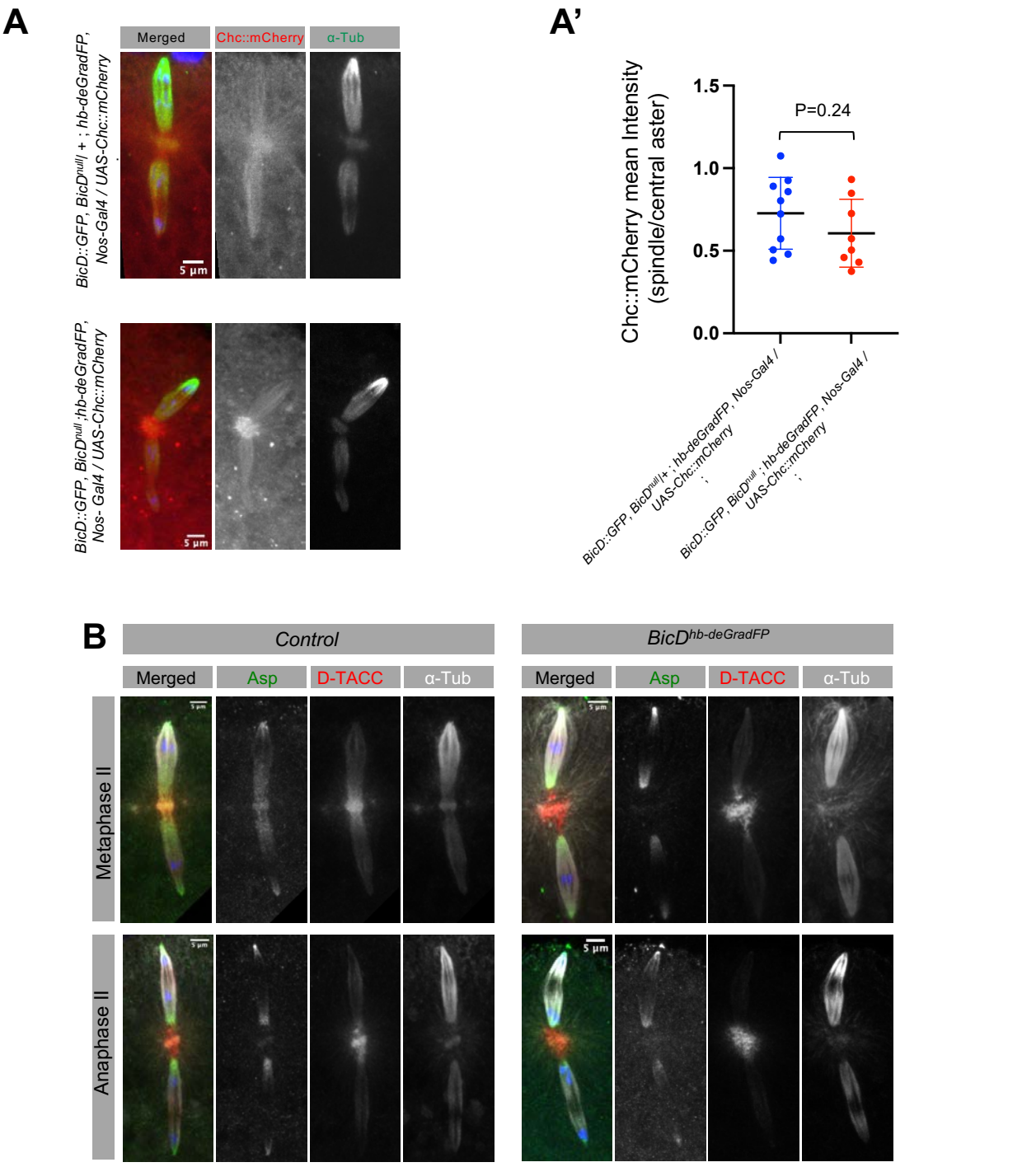

**Fig. S8. Proper localization of Chc at the meiosis II tandem spindles requires BicD. MT polarity is not affected in eggs with reduced BicD.**

**(A)** 5 min egg collections of controls (laid by *BicD::GFP, BicD* $^{null}$/ + ; *hb-deGradFP, Nos-Gal4/UAS-Chc::mCherry)* and *BicD::GFP, BicD*$^{null}$*; hb-deGradFP, Nos-Gal4/UAS-Chc::mCherry,* stained for α-tubulin (green). mCherry signal in red. Chc::mCherry localized to the tandem spindles and to the central aster. Compared to the signal intensity in the central aster, Chc::mCherry signals on the spindles in a *BicD::GFP, BicD*$^{null}$ background are reduced compared to the signals observed in eggs that have a wild-type copy of BicD which cannot be degraded by *hb-deGradFP* expression. **(A')** The mean fluorescent signal intensity ratio (signal in the most superficial spindle vs signal in central aster) for Chc::mCherry was quantified for each imaged MII and AII spindle. Data are presented as mean ± SD.

**(B)** 5 min egg collections of controls (laid by wild-type mothers and *BicD*$^{hb\text{-}deGradFP}$ embryos stained for α-tubulin (white), D-TACC (red) and the minus end MT marker Asp (green). **(C)** 5 min egg collections of wild-type embryos stained for α-tubulin (red) and either Pav, Clip190 or EB1 used as plus end MT markers (green). Maximum intensity projection images and DNA (blue) are shown in all pictures.

Supplementary Fig. S9

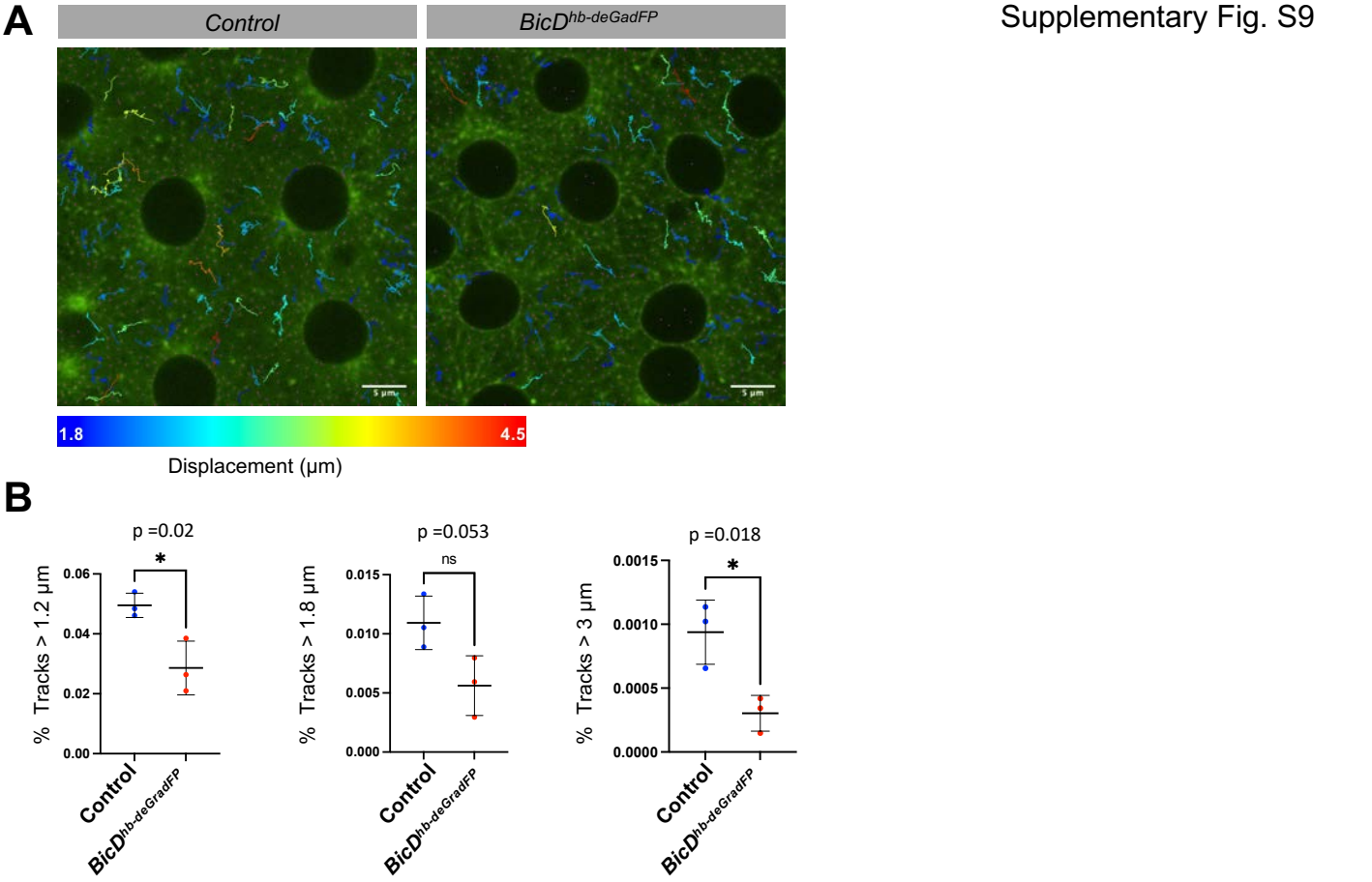


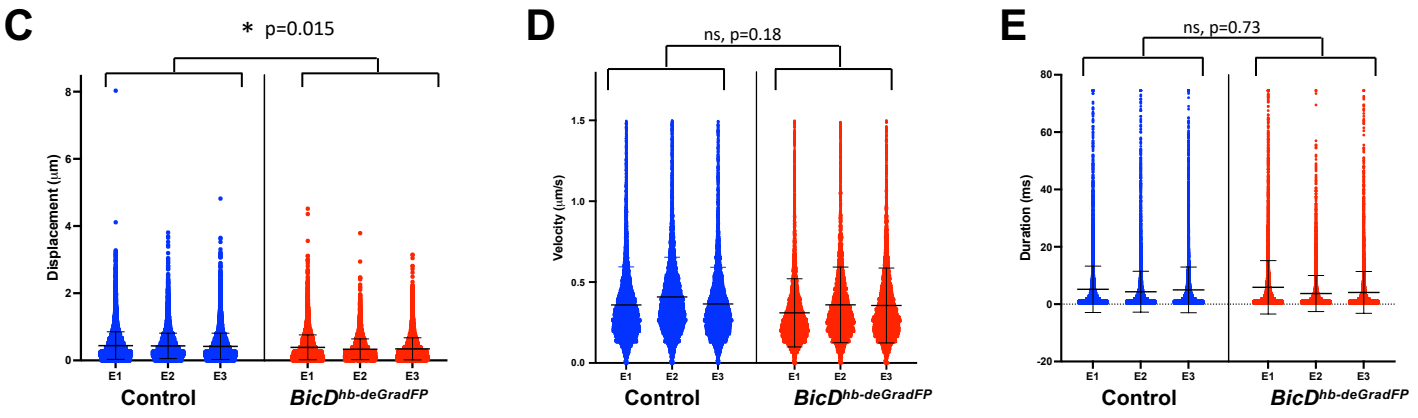


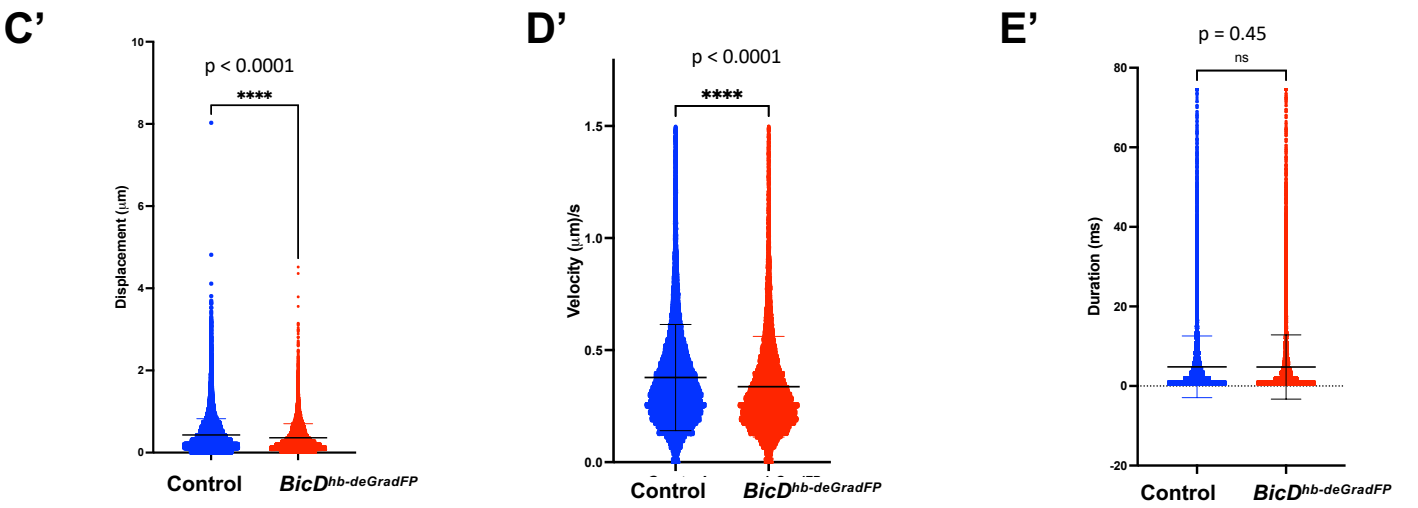

**Fig. S9. Chc::mCherry particle movement depends on *BicD*.**

Live imaging of embryos expressing a Chc::mCherry fusion protein. *Nanos-Gal4Vp16* drives the expression of a *UASP-Chc:mCherry* construct either in $BicD^{hb\text{-}deGradFP}$ background (embryos laid by *BicD::GFP,* $BicD^{null}$*/BicD::GFP,* $BicD^{null}$*; hb-deGradFP, UASP-Chc::mCherry/hb-deGradFP, Nanos-Gal4Vp16)* or females that express a wild-type copy of *BicD* that cannot be targeted by the *hb-deGradFP* construct *(BicD::GFP,* $BicD^{null}$*/ + ; hb-deGradFP, UASP-Chc::mCherry/hb-deGradFP, Nanos-Gal4Vp16).* Most $BicD^{hb\text{-}deGradFP}$ are arrested in or soon after meiosis II. The embryos imaged here escaped this arrest and thus might still have some functional BicD. Chc::mCherry particles were imaged during the mitotic cycles and were detected and tracked using the TrackMate plugin in Fiji. 3 embryos were analyzed per genotype (E1-3). **(A)** Shows an individual time frame of a movie that shows all the tracks detected for 75 seconds that have a displacement of more than 1.8 µm. **(B)** Number of tracks showing the indicated net displacements in each embryo. $BicD^{hb\text{-}deGradFP}$ embryos showed a significantly smaller number of particles with the threshold net displacement. The displacement **(C),** velocity **(D)** and duration **(E)** of all the Chc::mCherry particles that moved more than 1.2 µm in 75 sec was plotted for each imaged embryo. Chc::mCherry particles in $BicD^{hb\text{-}deGradFP}$ embryos showed a significantly reduced net displacement compared to the particles tracked in control embryos. The mean velocity is also reduced. However, the running time of the identified tracks was not affected, indicating that we can detect particles that can be followed for the same amount of time and that these particles are more static in $BicD^{hb\text{-}deGradFP}$ embryos. Data are presented as mean ± SD. Statistical significance and p values were determined by the Nested t test**. (C', D', E')** All the corresponding tracks detected in C, D and E were grouped for each genotype and statistical significance and p values were determined by the Student's unpaired test.

Supplementary Fig. S10

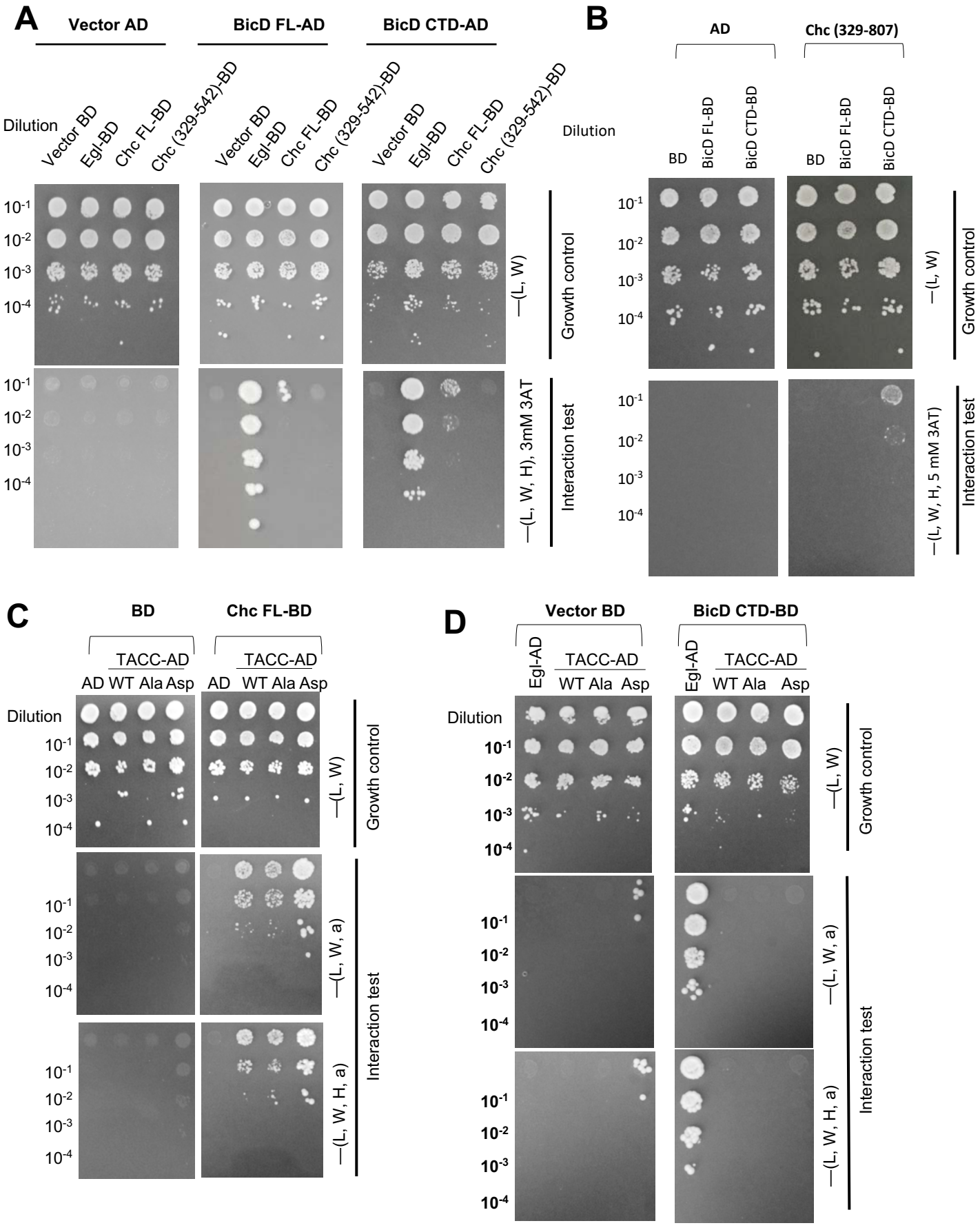

**Fig. S10. *Drosophila* Chc interacts through the same region with both BicD and D-TACC in the yeast two-hybrid system**. **(A)** Interaction test of full-length and BicD C-terminal Domain (CTD) fused to the DNA activation domain (AD) with Chc full-length (FL) or a $Chc^{329-542}$ fused to the DNA binding domain (BD). Full-length Egl was used as a positive control for the BicD interaction. BicD FL and BicD CTD interact with full-length Chc but not with the short $Chc^{329-542}$ fragment. **(B)** Interaction test of the Chc fragment with a C-terminally extended region ($Chc^{329-807}$) fused to the AD with BicD FL and BicD CTD in the BD. The extended $Chc^{329-807}$ fragment interacts with the BicD CTD. **(C)** Interaction test between Chc FL with D-TACC wild type (WT), D-$TACC^{S863A}$, and D-$TACC^{S863D}$. Chc interacts with all D-TACC variants, but the interaction is stronger with D-$TACC^{S863D}$. **(D)** Interaction test of the BicD CTD in the BD with the same versions of D-TACC used in C. No interaction between BicD and D-TACC was observed. Egl was used as a positive control for BicD interaction. Empty vectors were used as negative controls.

Supplementary Fig. S11

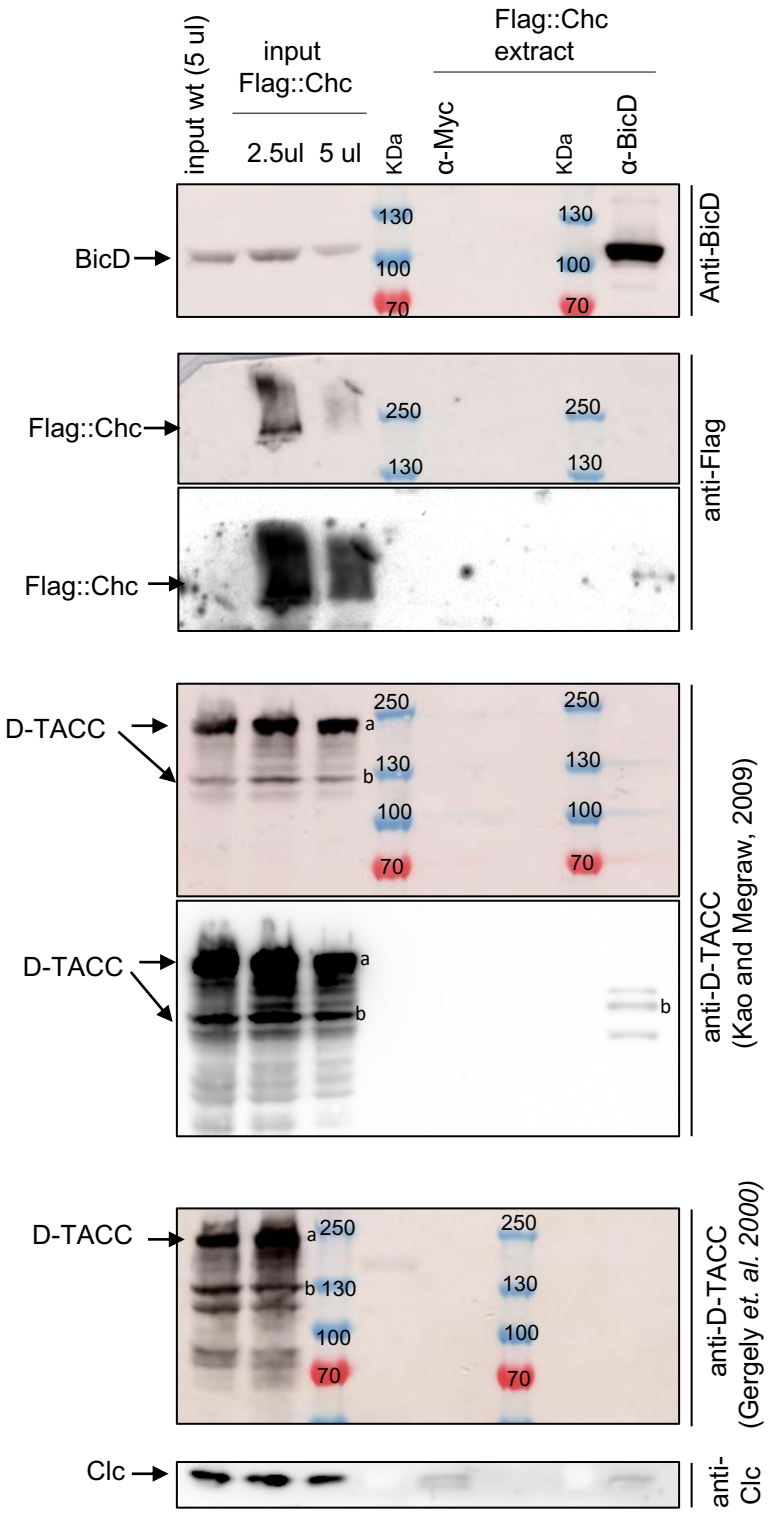

**Fig. S11. BicD interacts with Chc.**

IP of total embryo extracts expressing a Flag-tagged Chc fusion protein (Flag::Chc). Anti-BicD 1B11 antibody was used to IP BicD and anti-Myc was used as a negative control. Western blots of the precipitated material were tested for the presence of Flag::Chc, BicD, Clc and D-TACC. D-TACC was detected with two different antibodies that recognized different regions of D-TACC. Chc::Flag was present in the BicD IP in low amounts. Although at longer exposure times we could detect bands recognized by the D-TACC antibody described by (Kao and Megraw, 2009), these bands were of lower molecular weight than expected and no additional bands were detected when probing the BicD IP with the anti D-TACC antibody described in Gergely *et. al. 2000.* This suggest that BicD interacts directly with Chc, but probably not with D-TACC. 0.125% and 0.25 % of the cytoplasmic extract used for each IP was loaded as input. Duplicated panels show longer exposure times.

Supplementary Fig. S12

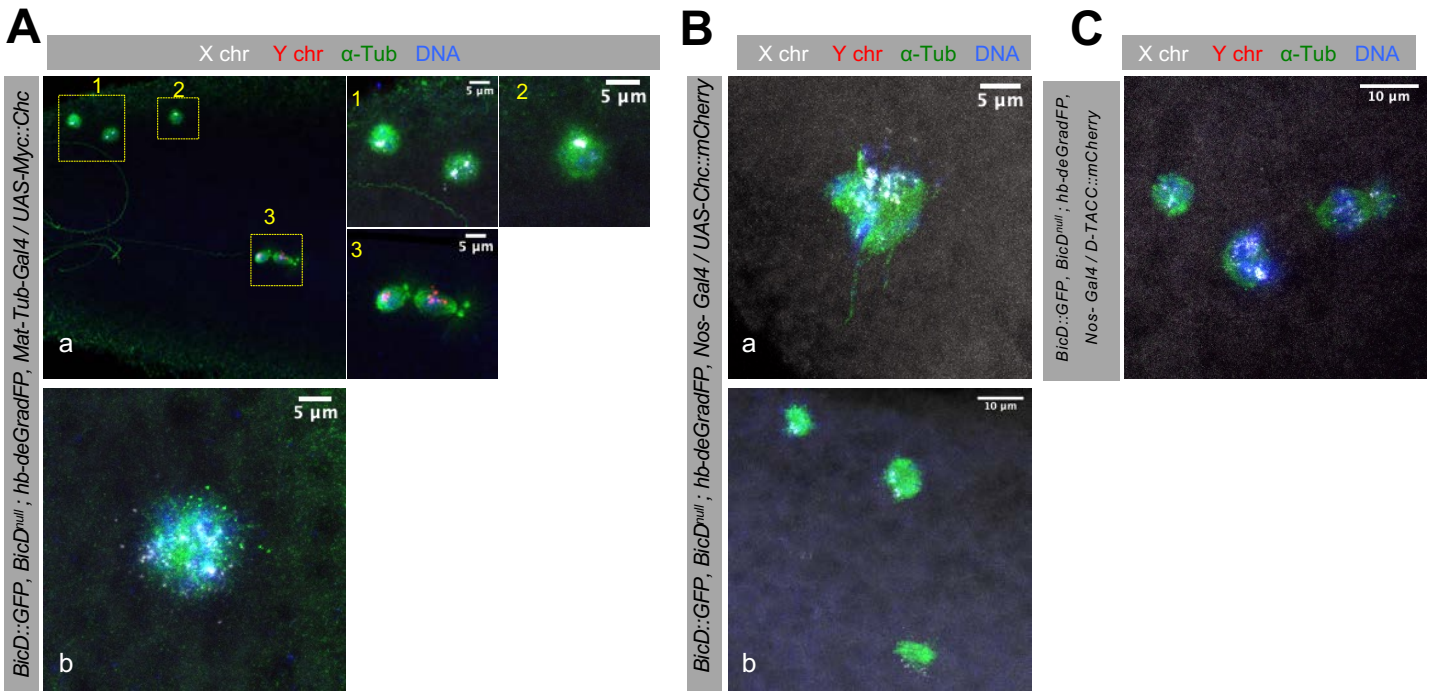


**Fig. S12. Eggs overexpressing Chc and D-TACC in the background of reduced levels of BicD that do not produce phenotypes on their own. This genetic interaction showed similar phenotypes as the ones observed in *BicD*$^{hb\text{-}deGradFP}$ eggs.** 30-60 min old eggs with the indicated maternal genotypes were collected and subjected to FISH to detect the X (white) and Y (red) chromosomes. The eggs were also stained for α-tubulin (red) and DNA (blue). (A-C) Examples of phenotypes observed in eggs expressing either an additional copy of Chc (Chc::myc in A and Chc::mCherry in B) under the strong Mat-tub-Gal4 driver (A) or a medium strength Nos-Gal4 driver (B), or expressing an additional copy of D-TACC (C) in the background of reduced levels of BicD (one single copy of the *hb-deGradFP* construct in a *BicD*$^{null}$ background rescued with 2 copies of BicD::GFP). (Aa) Example of an egg that did not undergo pronuclear fusion. Although the maternal meiotic (magnified in 1,2) products did not replicate, the maternal pronucleus did not fuse to the paternal pro-nucleus as expected (magnified in 3). The paternal pronucleus has replicated (Ab-Ba) Example of eggs where the maternal meiotic products had fused to form an abnormal single rosette. Several signals for the X-Chromosome are observed, indicating that the meiotic products had replicated/fragmented/ uncondensed DNA. (Ba-C) Example of eggs showing several maternal meiotic products that did not fuse into a single meiotic product and had replicated/fragmented/uncondensed DNA as judged from the appearance of more than 4 X-chromosomal signals.

Supplementary Fig. S13

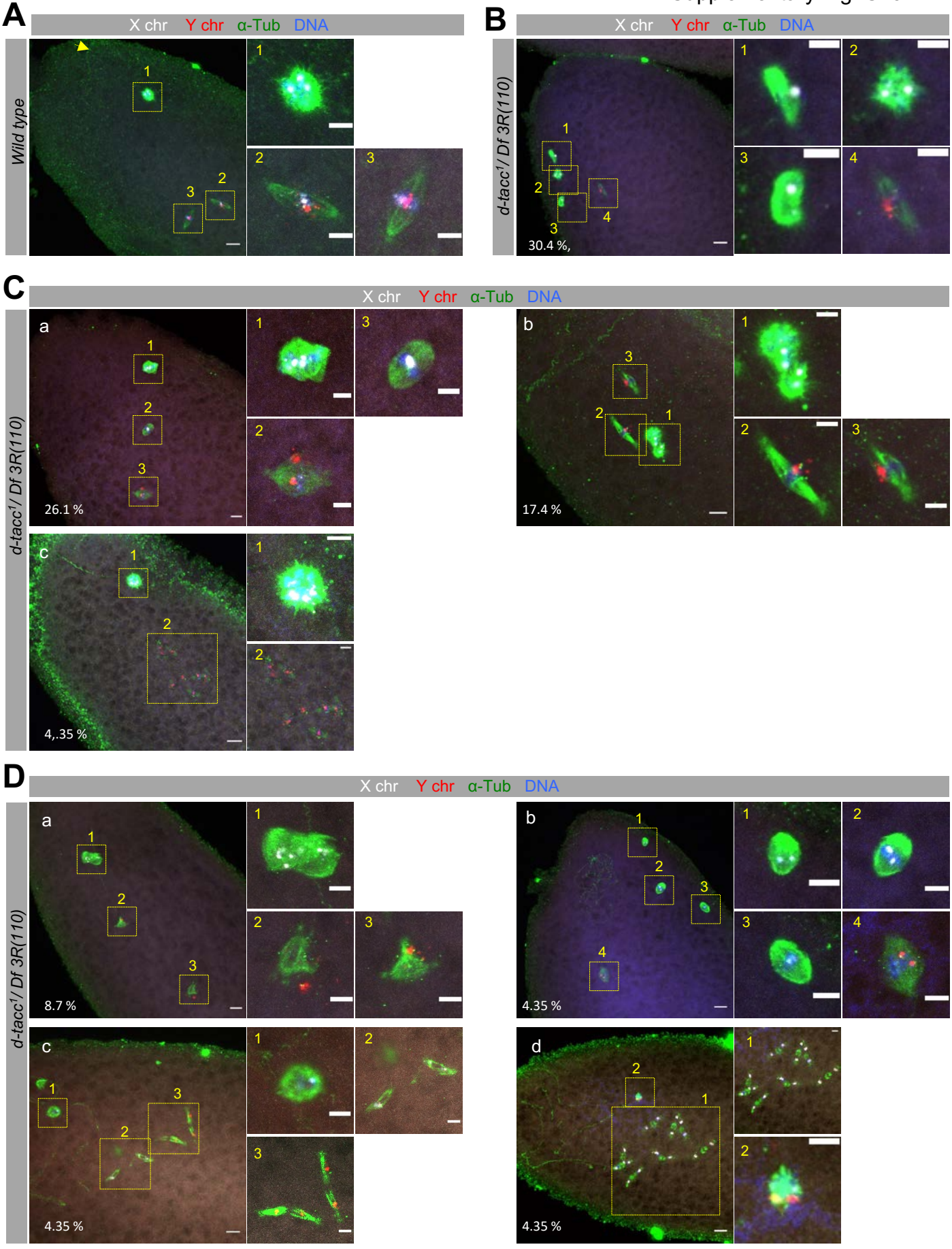

**Fig. S13. Maternal *d-tacc* is needed for pronuclear fusion and cell cycle arrest of the paternal pronucleus and the female meiotic products.** Male embryos (0-1h old collections) from *wild type* (A) and *d-tacc*$^{1}$ */Df3R(110*) (B-D) mothers were subjected to *in situ* hybridizations with probes detecting the X chromosome (white) and the Y chromosome (red) and stained for α-tubulin (green) and DNA (blue). **(A)** Example of an embryo that had undergone normal pronuclear fusion. A wild-type embryo in the second mitotic cycle is shown. The zygotic internal nuclei contain one signal for the X and one for the Y chromosome indicating normal pronuclear fusion (magnified in 2,3). The remaining polar body contains 3 clear signals for the X chromosome (magnified in 1). 100 % of wild-type embryos undergo normal pronuclear fusion. **(B-D)** 74.2 % of *d-tacc*$^{1}$ embryos show zygotic internal nuclei marked only by the presence of the Y chromosome, indicating a problem in pronuclear fusion. The remaining polar bodies have only signals for the X chromosome. **(B)** 30.4% of the *d-tacc*$^{1}$ embryos that did not undergo pronuclear fusion neither showed replication of the paternal pronuclei (only one signal for the Y chromosome, magnified in 4) nor of the female products (a total number of 4 signals for the X chromosome, magnified in 1 to 3). **(C)** 47.8 % of the embryos with no pronuclear fusion showed additionally, replication of the paternal pronuclei but not of the female meiotic products. Most of these embryos (26.1%) contained a single paternal nucleus with 2 signals for the Y chromosome (Ca, magnified in 2). However, embryos, where the paternal nucleus had undergone several additional replications, were also observed at a lower frequency (b,c). **(D)** 21.75 % of the embryos that did not perform pronuclear fusion showed replication of the female meiotic products and the paternal pronuclei. In this category, embryos showed multiple signals for the X chromosome (more than 3 in total) and variable replication rounds of the paternal pronuclei. (a) A *d-tacc*$^{1}$ embryo where the paternal pronucleus and the female meiotic products had undergone one round of replication. It has two paternal nuclei, each marked by one signal for the Y chromosome (magnified in 2-3), and the polar bodies had fused into one rosette structure containing 8 signals for the X chromosome. (b) *d-tacc*$^{1}$ embryos with one paternal nucleus that had replicated its chromosomes (magnified in 4) and

3 polar bodies with a total of 6 X chromosome signals (magnified in 1-3). (c) In this *d-tacc*$^{1}$ embryo the paternal nucleus had divided twice (4 signals for the Y chromosome in two nuclei) and the polar bodies showed a total number of 5 X chromosomal signals (magnified in 1-2). (d) *d-tacc*$^{1}$ embryo, where the female meiotic products divided many times (magnified in 1) and the paternal pronucleus only once (2 Y chromosomal signals, magnified in 2). Wild type (n= 23) and *d-tacc*$^{1}$ (n=29) z-stack projections through all the nuclei are shown and were analyzed to quantify the different phenotypes observed. In wild-type embryos, most polar bodies (83%) were arranged into one single rosette containing 3 signals for the X chromosome. We only rarely detected a clear replication of the polar bodies (4.3%, in 1 out of 23 embryos analyzed).

Supplementary Fig. S14

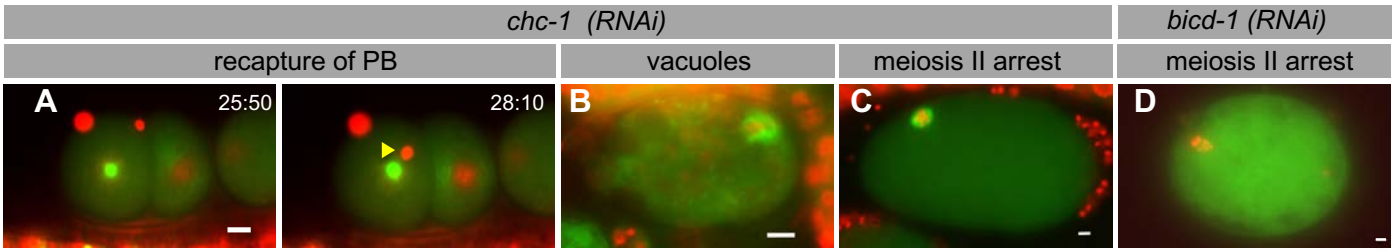


**Fig. S14. *C. elegans chc-1*, *bicd-1* are required for normal completion of meiosis and early zygotic development.**

Fluorescent microscopy time lapse images (A) or a single plane pictures from *chc-1(RNAi)* (A-C) or *bicd-1*(*RNAi)* (D) embryos expressing *H2B::mCherry* and *α-tubulin::GFP* are shown. Pictures are oriented anterior to the left. The additional phenotypes observed from the ones depicted in Fig. 8 are shown here. (A) Elapsed time (in minutes and seconds) from the start of the movie is indicated. One out of 4 of the living *chc-1(RNAi)* embryos imaged showed a recapture of the polar body (arrowhead) by the mitotic spindle followed by its nuclear fusion to the anterior blastomere of the 2-cell stage. The remaining embryo showed normal development. (B-C) Animals fed with *chc-1* dsRNA food looked sick and carried few progenies in the uterus. They arrested development. **(B)** Example of a dying *chc-1(RNAi)* embryo with vacuoles. **(C)** Example of a *chc-1(RNAi)* egg arrested in meiosis II. (D) *C. elegans bicd-1* deletion led to embryonic development issues (8/10 *bicd-1(tm3421*) homozygous embryos did not hatch). This is consistent with *bicd-1* being an essential gene. Moreover, 20% of hatched animals died at the adult stage without progeny, suggesting again that the maternal contribution rescued their embryonic development. Consistent with this, we also observed eggs arrested in meiosis II from *bicd-1(RNAi)fed* worms (D). Scale bars are 10 µm.

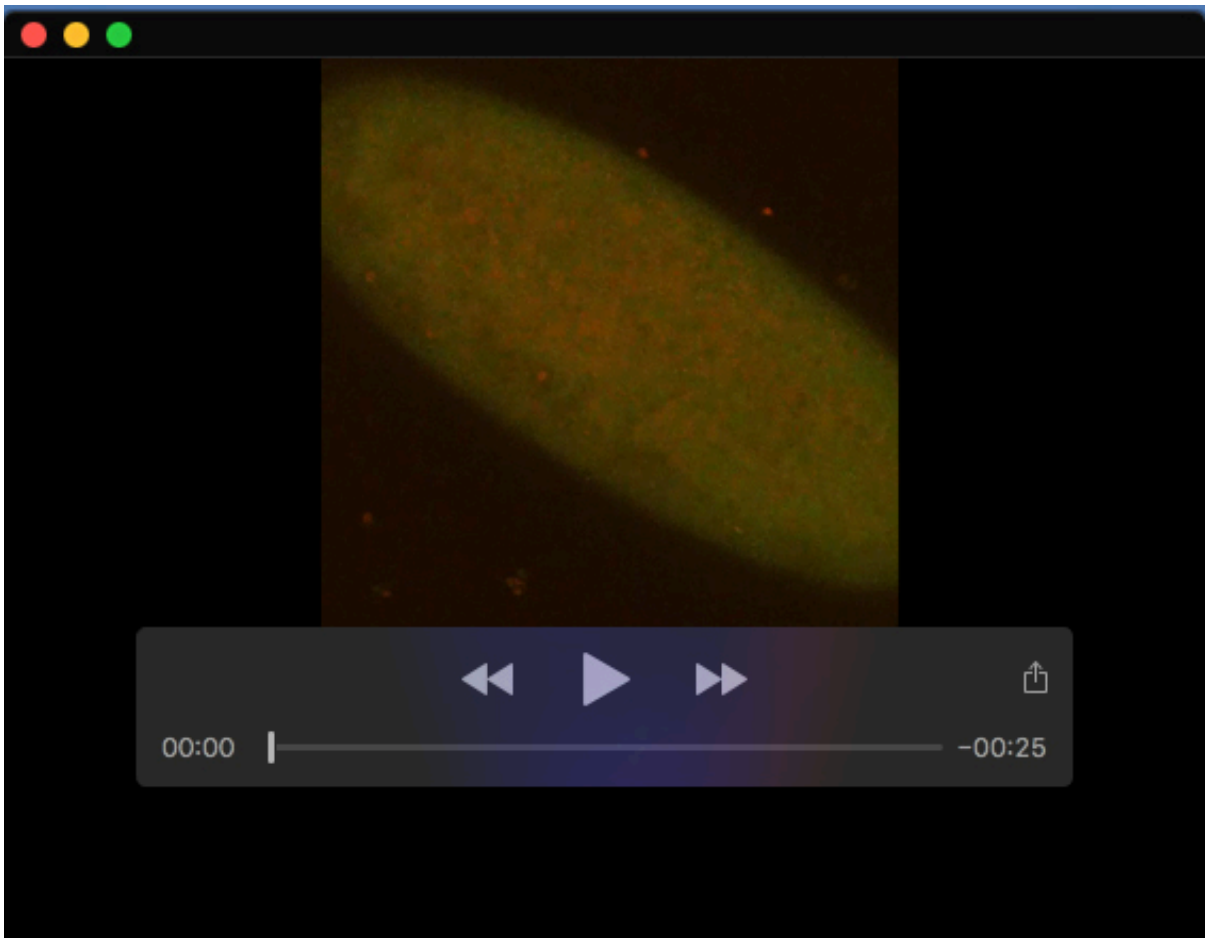


**Movie 1.** Live imaging of embryos expressing Jupiter::GFP to visualize the microtubules and Histone::RFP to visualize the chromatin. Control embryo laid by a *BicD* heterozygous mother (*BicD*$^{null}$/+) expressing the reporter constructs and subjected to the same experimental conditions as *BicD*$^{mom}$ females. After embryo collection and preparation for live imaging, control embryos were always found to be already in the first mitotic divisions and they proceeded through the mitotic divisions normally.

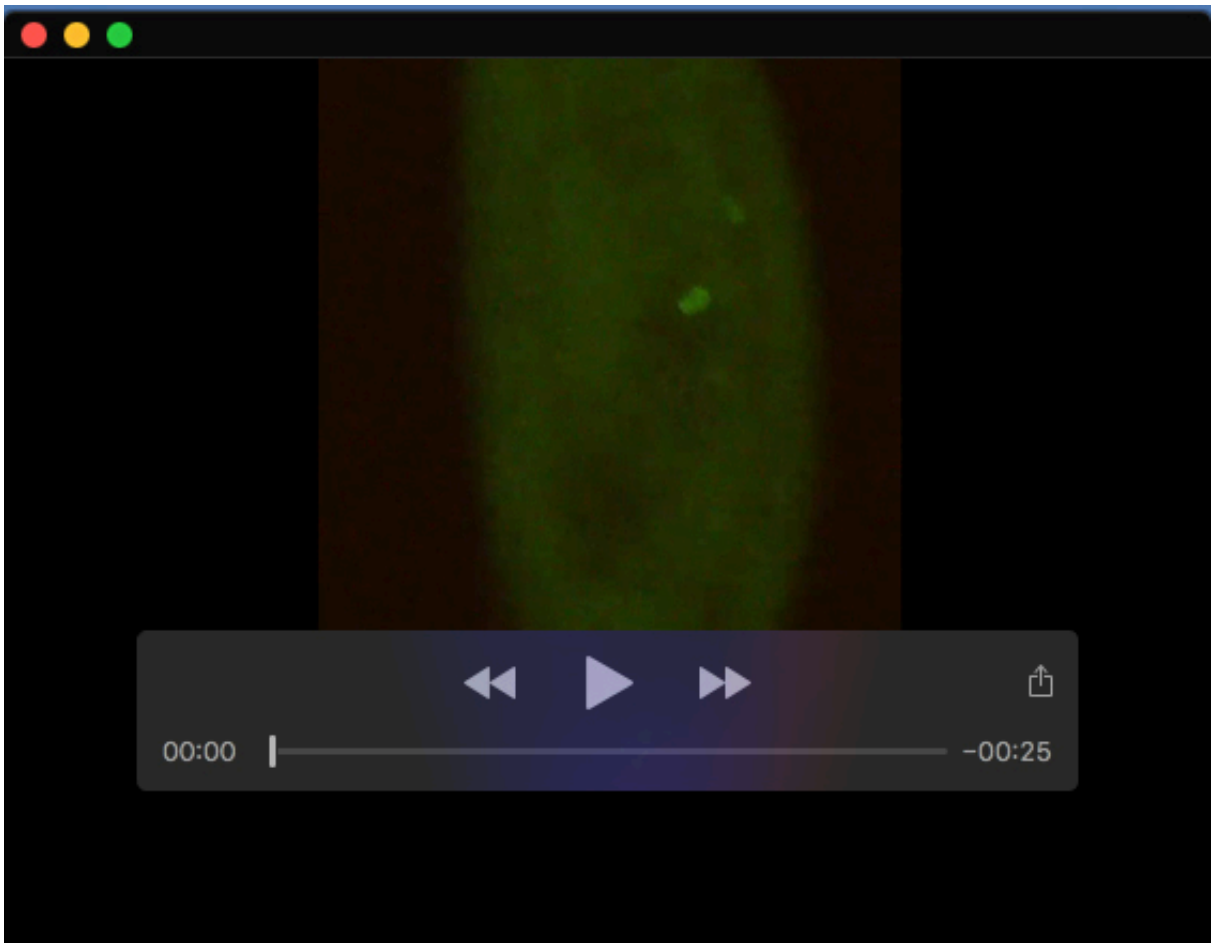


**Movie 2.** Live imaging of an embryo laid by a *BicD*$^{mom}$ mother 3 days after stopping the induction of *BicD* expression. The embryo express also Jupiter::GFP to visualize the microtubules and Histone::RFP to visualize the chromatin. *BicD*$^{mom}$ embryos are arrested with few abnormal spindles that they were unable to resolve. This embryo seems to have arrested in meiosis II with abnormal spindles that failed to separate.

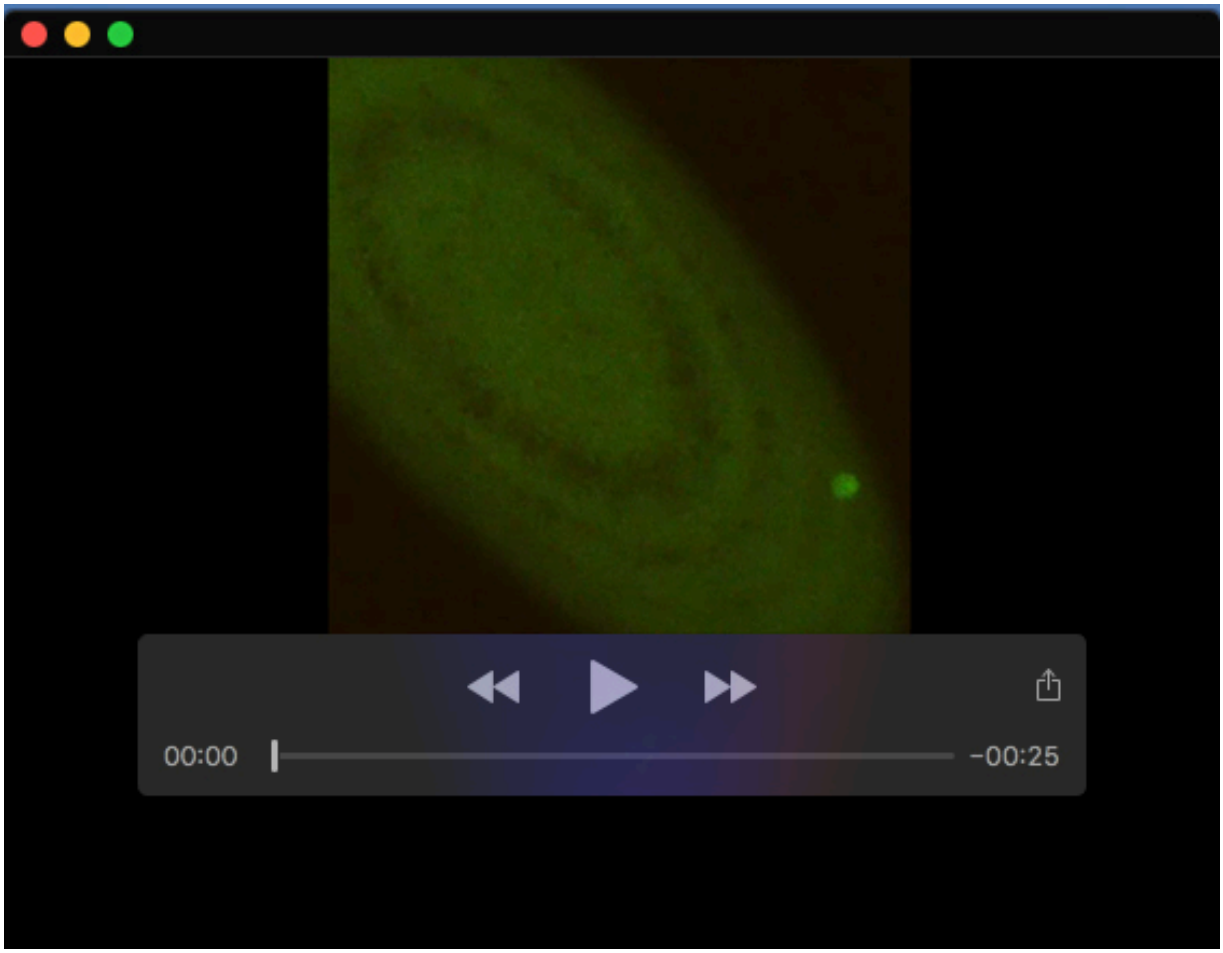


**Movie 3.** Live imaging of an embryo laid by a *BicD*$^{mom}$ mother 4 days after stopping the induction of *BicD* expression and expressing Jupiter::GFP to visualize the microtubules and Histone::RFP to visualize the chromatin. This embryo seems to have arrested in meiosis II with abnormal spindles that failed to separate.

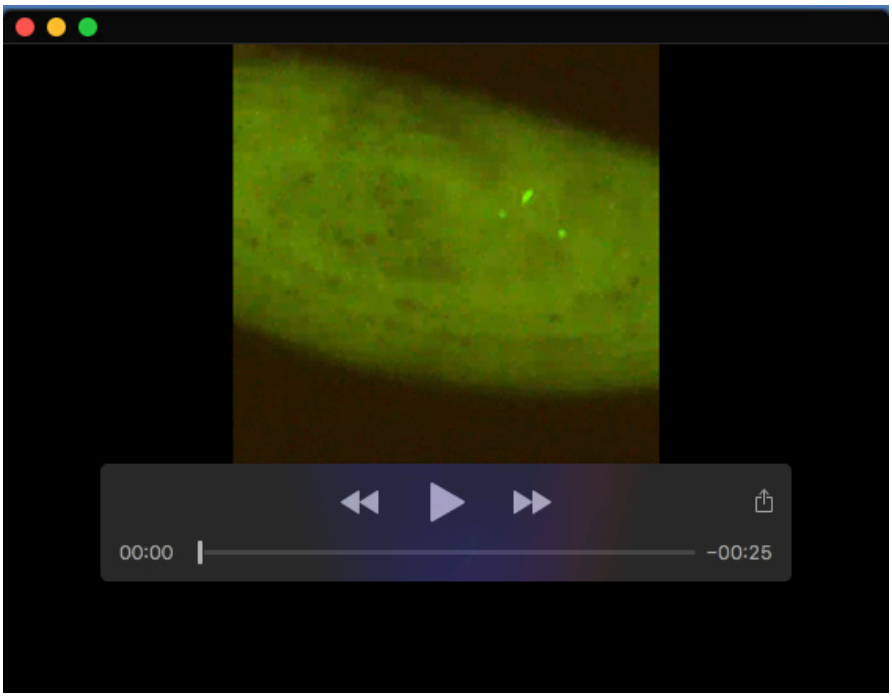


**Movie 4**. Live imaging of an embryo laid by a *BicD*$^{mom}$ mother 5 days after stopping the induction of *BicD* expression and expressing Jupiter::GFP to visualize the microtubules and Histone::RFP to visualize the chromatin. This embryo arrested, containing several more abnormal nuclei that were also unable to divide properly. At the end of the movie, free centrosomes were observed that replicated and populated the embryo.

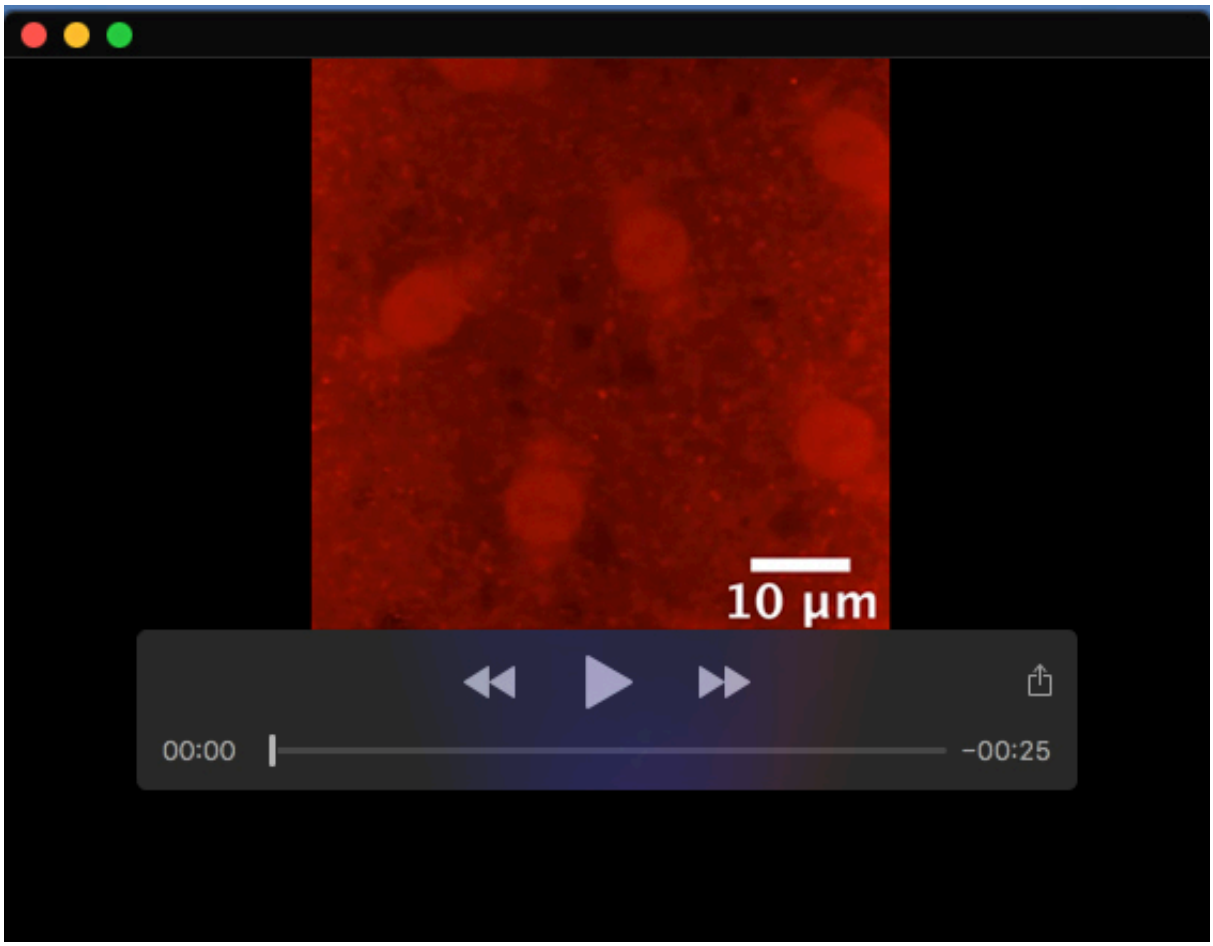


**Movie 5.** Live imaging of embryos expressing a Chc::mCherry fusion protein. *Nanos-Gal4Vp16* drives the expression of a *UASP-Chc:mCherry* construct in a wild-type background. Chc is present at the spindles and centrosomes throughout the cell cycle.

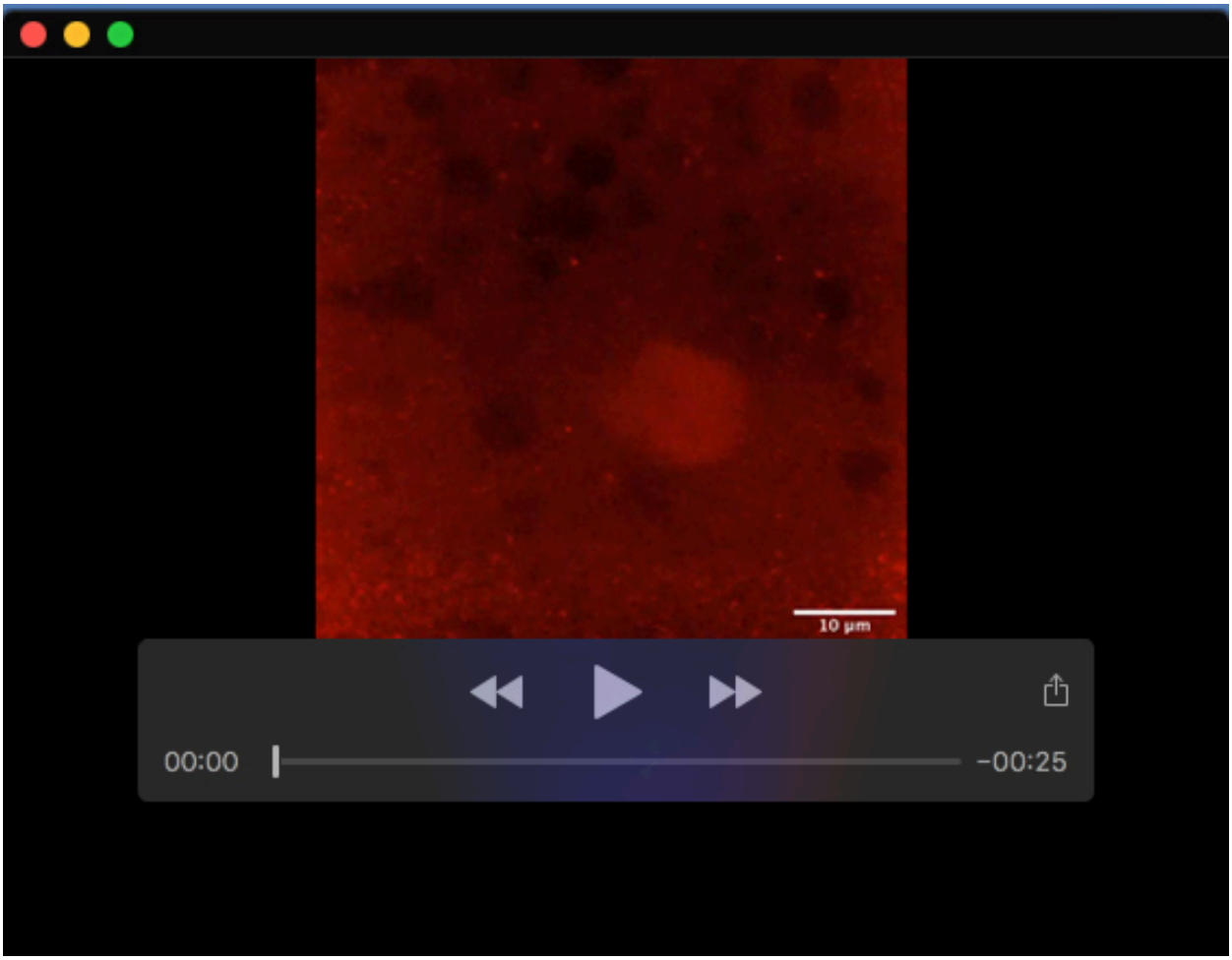


**Movie 6.** Embryos laid by *BicD::GFP, BicD$^{null}$/BicD::GFP, BicD$^{null}$; hb-deGradFP, UASP-Chc::mCherry/hb-deGradFP, Nanos-Gal4Vp16* females were imaged. This embryo is arrested in or soon after meiosis II, displaying few abnormal spindles that remained unresolved.

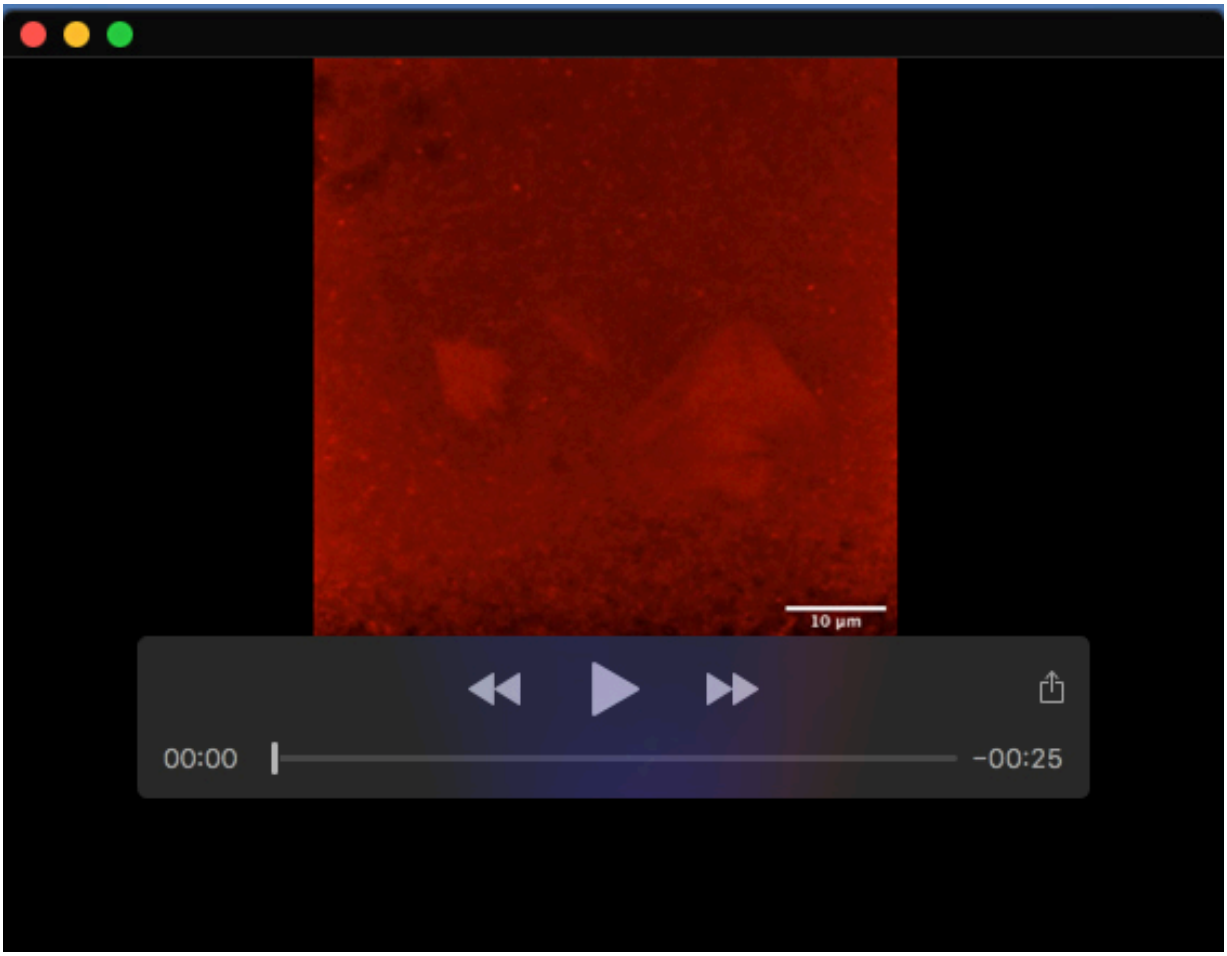


**Movie 7.** Embryos laid by *BicD::GFP, BicD$^{null}$/BicD::GFP, BicD$^{null}$*; *hb-deGradFP, UASP-Chc::mCherry/hb-deGradFP, Nanos-Gal4Vp16* females were imaged. This movie shows an embryo arrested in or soon after meiosis II, displaying few abnormal spindles that remained unresolved.

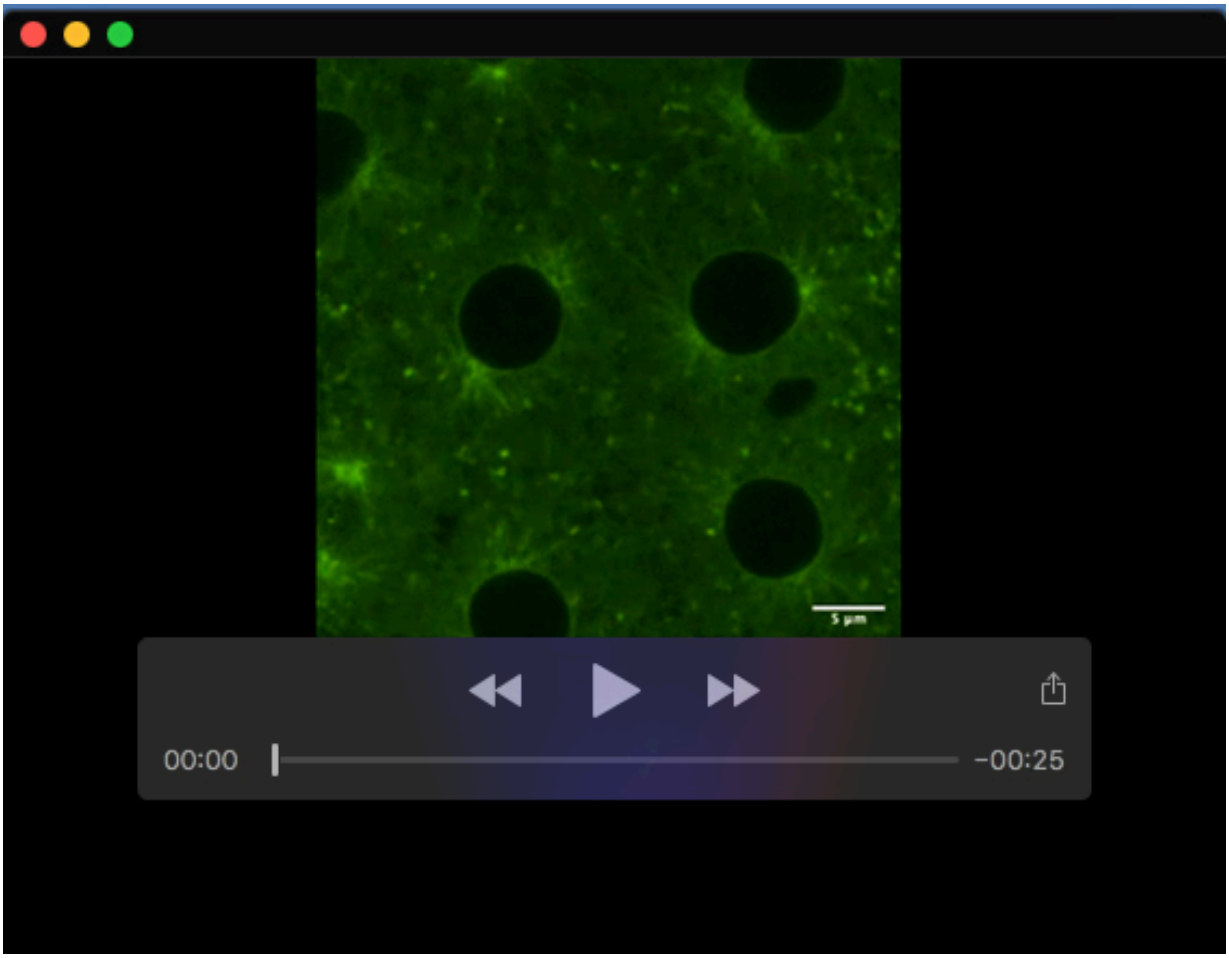


**Movie 8.** Live imaging of embryos expressing a Chc::mCherry fusion protein were imaged to detect Chc particle movements. An embryo laid by *BicD::GFP, BicD$^{null}$/+; hb-deGradFP, UASP-Chc::mCherry/hb-deGradFP, Nanos-Gal4Vp16* was imaged as control. Images were taken every 0.5 seconds over 75 seconds.

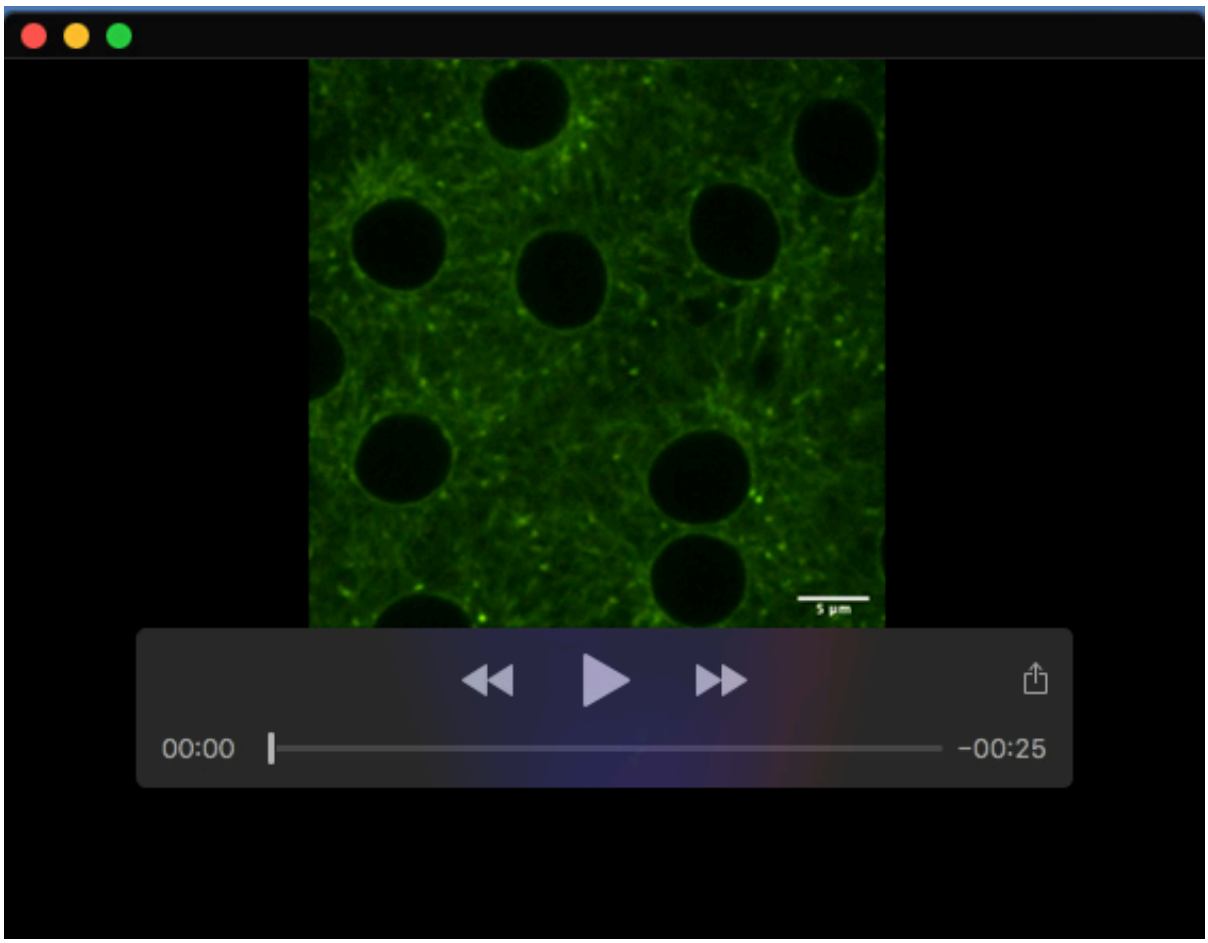


**Movies 9.** Embryos laid by *BicD::GFP, BicD$^{null}$/BicD::GFP, BicD$^{null}$; hb-deGradFP, UASP-Chc::mCherry/hb-deGradFP, Nanos-Gal4Vp16* females were imaged to detect Chc::mCherry particles in a *BicD$^{hb\text{-}deGradFP}$* background. Images were taken every 0.5 seconds over 75 seconds.

**Gergely, F., Kidd, D., Jeffers, K., Wakefield, J. G. and Raff, J. W.** (2000). D-TACC: a novel centrosomal protein required for normal spindle function in the early *Drosophila* embryo. *EMBO J.* **19**, 241–252.

**Kasprowicz, J., Kuenen, S., Miskiewicz, K., Habets, R. L. P., Smitz, L. and Verstreken, P.** (2008). Inactivation of clathrin heavy chain inhibits synaptic recycling but allows bulk membrane uptake. *J Cell Biol* **182**, 1007–1016.

**Kao, L.-R. and Megraw, T. L.** (2009). Centrocortin Cooperates with Centrosomin to Organize *Drosophila* Embryonic Cleavage Furrows. *Curr. Biol.* **19**, 937–942.

**Santel A., Winhauer T., Blümer N. and Renkawitz-Pohl R.** (1997). The *Drosophila don juan (dj)* gene encodes a novel sperm specific protein component characterized by an unusual domain of a repetitive amino acid motif. *Mech Dev*. **64**, 19–30.